Novel Inorganic/Polymer Composite Membranes for CO_2 Capture

Final Project Report
Updated August 30, 2016

Reporting Period Start Date: October 1, 2011

Reporting Period End Date: December 31, 2015

PI: W.S. Winston Ho, Professor*
Co-PI: Prabir K. Dutta, Professor*
Subcontractor: Steve J. Schmit, Director of Research and Development†

Date Report was Issued: October 2016

DOE Award Number: DE-FE0007632

*The Ohio State University
Colleges of Engineering, and Mathematical and Physical Sciences
Departments of Chemical and Biomolecular Engineering, Chemistry, and Materials Science and Engineering
151 West Woodruff Avenue
Columbus, OH 43210-1350

†Gradient Technology
Gradient Technology
11080 Industrial Circle NW
Elk River, MN 55330

Disclaimer

This report was prepared as an account of work sponsored by an agency of the United States Government. Neither the United States Government nor any agency thereof, nor any of their employees, makes any warranty, express or implied, or assumes any legal liability or responsibility for the accuracy, completeness, or usefulness of any information, apparatus, product, or process disclosed, or represents that its use would not infringe privately owned rights. Reference herein to any specific commercial product, process, or service by trade name, trademark, manufacturer, or otherwise does not necessarily constitute or imply its endorsement, recommendation, or favoring by the United States Government or any agency thereof. The views and opinions of authors expressed herein do not necessarily state or reflect those of the United States Government or any agency thereof.

Abstract

The objective of this project is to develop a cost-effective design and manufacturing process for new membrane modules that capture CO_2 from flue gas in coal-fired power plants. The membrane consisted of a thin selective layer including inorganic (zeolite) embedded in a polymer structure so that it can be made in a continuous manufacturing process. The membrane was incorporated in spiral-wound modules for the field test with actual flue gas at the National Carbon Capture Center (NCCC) in Wilsonville, AL and bench scale tests with simulated flue gas at the Ohio State University (OSU). Using the modules for post-combustion CO_2 capture is expected to achieve the DOE target of $40/tonne CO_2 captured (in 2007 dollar) for 2025.

Membranes with the amine-containing polymer cover layer on zeolite-Y (ZY) nanoparticles deposited on the polyethersulfone (PES) substrate were successfully synthesized. The membranes showed a high CO_2 permeance of about 1100 GPU (gas permeation unit, 1 GPU = 10^{-6} cm^3 (STP)/($cm^2 \bullet s \bullet$ cm Hg), 3000 GPU = 10^{-6} mol/($m^2 \bullet s \bullet$ Pa)) with a high CO_2/N_2 selectivity of > 200 at the typical flue gas conditions at 57ºC (about 17% water vapor in feed gas) and > 1400 GPU CO_2 permeance with > 500 CO_2/N_2 selectivity at 102ºC (~ 80% water vapor).

The synthesis of ZY nanoparticles was successfully scaled up, and the pilot-scale membranes were also successfully fabricated using the continuous membrane machine at OSU. The transport performance of the pilot-scale membranes agreed reasonably well with the lab-scale membranes. The results from both the lab-scale and scale-up membranes were used for the techno-economic analysis. The scale-up membranes were fabricated into prototype spiral-wound membrane modules for continuous testing with simulated or real flue gas. For real flue gas testing, we worked with NCCC, in consultation with TriSep Corporation, Gradient Technology and American Electric Power (AEP). The membrane module demonstrated > 800 GPU of CO_2 permeance and > 150 CO_2/N_2 selectivity when tested with real flue gas at NCCC. The results obtained were used to update the techno-economic analysis. In addition, the EH&S assessment of the membranes for post-combustion CO_2 capture was conducted.

Table of Contents

1 Executive Summary

The objective of this project is to develop a cost-effective design and manufacturing process for new membrane modules that capture CO_2 from flue gas in coal-fired power plants. Two approaches were investigated. In Approach 1, the membrane consisted of a thin selective polymer layer on inorganic nanoparticles embedded in a polymer substrate so that it can be made in a continuous manufacturing process. Approach 2 involved rapid synthesis of a continuous zeolite membrane on a polymer support.

For Approach 1 with an amine-containing polymer cover layer on top of the zeolite-Y (ZY) nanoparticles embedded in porous polyethersulfone (PES) substrate, ZY nanoparticles were deposited on top of the PES substrate first, and a polymer selective layer containing amines was coated on top of the ZY seed layer. The PES substrates were fabricated both at a lab scale and a pilot scale. The developed PES was cost-effective and affordable, and it was characterized to have a similar pore size and surface morphology with the commercial PES substrate. ZY nanoparticles with an average particle size of 40 nm were synthesized successfully and were deposited onto the nanoporous polymer support using a vacuum-assisted dip-coating method developed at The Ohio State University (OSU). For the amine-containing polymer cover layer on ZY composite membrane, a high molecular weight polyamine was synthesized and incorporated with different kinds of mobile carriers. The lab-scale CO_2 permeance reached up to 1100 GPU with a CO_2/N_2 selectivity of > 200 at 57°C. The continuous fabrication machine for the development of prototype membranes was used to fabricate pilot scale membranes. The amine-containing polymer cover layer was coated on 14 inches wide, scale-up ZY/scale-up PES substrate using the continuous membrane fabrication machine at OSU. The scale-up composite membrane showed a CO_2 permeance of 870 GPU and a CO_2/N_2 selectivity of 218 at 57°C. At 102°C, the scale-up composite membrane showed a CO_2 permeance of 1800 GPU and a CO_2/N_2 selectivity of 160.

The amine-containing composite membranes were successfully rolled into spiral-wound membrane modules for the testing with simulated and actual flue gas. The spiral-wound membrane modules demonstrated up to 820 GPU of CO_2 permeance and > 150 CO_2/N_2 selectivity with simulated flue gas. The membrane modules showed > 800 GPU of CO_2 permeance and > 150 CO_2/N_2 selectivity when tested with real flue gas at the National Carbon Capture Center (NCCC) in Wilsonville, AL. The influence of SO_2 on membranes was characterized by in-situ infrared spectroscopy.

Gradient Technology conducted the techno-economic analysis of the proposed 2-stage membrane process for CO_2 capture from flue gas in conjunction with the membrane transport model developed by OSU. The techno-economic analysis was carried out for a cost-sensitivity study with respect to membrane performance and operating conditions. The costs for the SO_2 polishing step, membrane installation, and process contingency were included in order to be consistent with the NETL cost estimation guideline. For the membrane performance with a CO_2 permeance of 1100 GPU and a CO_2/N_2 selectivity of > 200 based on the present ZY/polymer composite membrane with the amine-containing polymer cover layer on the ZY seed layer/PES substrate (Approach 1) synthesized in the lab, the preliminary techno-economic analysis showed a capture cost of about \$50.4/tonne CO_2 captured (in 2007 dollar), which was not optimized. The optimized result by OSU gave a capture cost of about \$40.1/tonne CO_2 captured (in 2007 dollar),

which nearly meets the DOE target of \$40/tonne CO_2 captured. This DOE target can be met or even a lower capture cost of less than \$40/tonne CO_2 can be achieved with further membrane improvements including higher CO_2 permeance, thinner membrane thickness, and higher performance membrane material. The proposed technology will become available for the cost-effective capture of CO_2 from coal-fired power plants. The developed membrane modules can be applied in the existing and new coal-fired power plants.

For Approach 2, a continuous zeolite Y membrane of about 250 nm thickness was synthesized on the PES polymer support within 60 minutes. Intercrystalline defects on the membrane were sealed with polydimethylsiloxane (PDMS), and transport properties of such membranes were examined. The performance of these membranes using dry feed gas was comparable to zeolite membranes grown on ceramic supports, which typically take much longer to form.

An Environmental Health and Safety (EH&S) assessment was conducted by Gradient Technology to assess the EH&S issues, including air and particulate emissions and solid and liquid waste streams. Compared to the baseline pulverized coal power plant, the CO_2 and SOx emissions were largely mitigated, and the other gas contaminants were not affected. The primary liquid wastes were the captured water from the flue gas and the spent NaOH-SO_2 solution, i.e., Na_2SO_3, from the SO_2 polishing step. Na_2SO_3 is a common commercially chemical. The replaced membrane modules were treated as a solid waste, which itself is not toxic and reactive. Other than the membrane modules, no other solid waste was generated in the membrane process.

2 Membrane Approaches

Two membrane approaches were investigated. In Approach 1, the membrane consisted of a thin selective polymer layer on inorganic nanoparticles embedded in a polymer substrate so that it can be made in a continuous manufacturing process. Approach 2 involved rapid synthesis of a continuous zeolite membrane on a polymer support. Fig. 1 shows the schematic of Membrane Approach 1 consisting of a selective amine-containing polymer cover layer on zeolite nanoparticles embedded in polymer support. The selective amine-containing polymer cover layer provides the facilitated transport of CO_2 via reaction with amine in the following reaction [1-23]:

$$CO_2 + R\text{-}NH_2 + H_2O \rightleftharpoons R\text{-}NH_3^+ + HCO_3^-$$

The layer of the zeolite-Y nanoparticles increases porosity and reduces pore size so that a thinner selective amine-containing polymer cover layer can be fabricated, leading to higher CO_2 permeance. This, together with the facilitated transport of CO_2, renders the membrane to have high CO_2 permeance and CO_2/N_2 selectivity.

Fig. 2 depicts the schematic of Membrane Approach 2 comprising a polymer caulking layer on the selective zeolite membrane grown on polymer support. This can provide high inorganic performance and low-cost polymer processing benefits. The rapid zeolite growth process developed in this project can synthesize the zeolite membrane for competitive cost.

3 Experimental Methods

3.1 All Inorganic Composite Membrane Synthesis

A highly permeable inorganic ceramic membrane supports were prepared as substrates for membrane deposition and heat treatment experiments as well as membrane characterization. These supports were prepared from high-purity α-Al_2O_3 powder with a narrow size distribution, allowing for well-packed and homogenous structures. The support was produced with a two-layer structure: a highly permeable AA3 carrier layer with ~1 μm pores, and a thin (~10 μm) AKP30 support coating with a smoother surface and ~100 nm pore size. Two types of inorganic selective layers including alumina and ZY were investigated, and alumina selective layers on both ceramic and polymer supports were prepared. Moreover, mesoporous γ-Al_2O_3 membranes on AKP30 supports were modified by interfacial polymerization (IP) inside the pores between an aqueous solution of PEO (polyethyleneoxide)-diamine and an organic solution of trimesoyl chloride (TMC). Table 1 summarizes the gas permeation results measurements for mesoporous and modified supported γ-alumina membranes using the dry gas as the feed gas.

Table 1. Transport measurements for meso-porous and modified supported γ-alumina membranes.

Membrane	T (°C)	CO_2 Permeance (GPU)	CO_2/N_2 selectivity
γ-alumina/AKP30	57	1100	0.88
γ-alumina + IPLC/AKP30	57	750	1.19
γ-alumina + IPHC/AKP30	22	120	29
	57	290	14.05
γ-alumina/AKP30AA3	22	7500	0.85
	57	1100	1.13
	100	280	1.04
	22	150	1

AKP30/γ-Al_2O_3 samples modified by deposition of a diamine PEO layer and subsequent interfacial polymerization exhibited two types of gas transport behavior. Sample IPLC was prepared with low reactant concentration, and it showed a low CO_2 permeance (750 GPU) and a low selectivity (1.19). A sample prepared with a higher reactant concentration (IPHC) showed a much higher selectivity of 14 at 57°C, but a lower permeance of 290 GPU. The low selectivity observed for these samples were probably due to the surface defects or incomplete coverage. A thicker modification layer ensures better coverage and increases the selectivity, but at the cost of permeance.

A structure with a mesoporous γ-alumina layer on AKP30/AA3 support had a high CO_2 permeance. However, after heating, the permeance dropped significantly and did not return to its initial value after cooling back to room temperature (Table 1). The irreversible change was probably due to pore blocking during the deposition process. However, modifying the step of

rapid thermal processing of γ-alumina precursor to conventional thermal processing did not appear to improve the performance.

Moreover, gas separation measurements with a humidified CO_2/N_2 mixture were performed for a mesoporous AKP30/γ-Al_2O_3 layer at 57ºC. The membrane demonstrated poor and unstable performances during the 24-hour test period. The CO_2/N_2 selectivity was observed to drop from 19.9 to 1.2. The drop in selectivity was believed to be due to the absolute drop in the CO_2 permeance in presence of water in the feed gas. Moreover, the selectivity was believed to be low due to uncovered or defect areas on the membrane surface.

In summary, the rapid thermal processing method of alumina did not show adequate performance (the separation factors were less than 10). Besides, all inorganic composite membranes had a low selectivity due to the defects and cracks in the membranes. It was also very difficult to scale up the synthesis processes for the inorganic support and composite membrane. The continuous fabrication of the all inorganic composite membrane was not available or suitable either. Hence, the membrane scale-up is costly. All these factors led to down selection of ZY/polymer composite membranes.

3.2 Synthesis of Zeolite-Y Nanoparticles

Nanocrystalline zeolite particles of 40 nm diameter were synthesized by the following procedure [24-29]. The gel composition was: 0.048 Na_2O : 2.40 $(TMA)_2O(2OH)$: 1.2 $(TMA)_2O(2Br)$: 4.35 SiO_2 : 1.0 Al_2O_3 : 249 H_2O, where TMA^+ is tetramethylammonium cations. Typically, in the silicon source, 26.2 g Ludox HS-30 and 10.46 g TMAOH were mixed in a polypropylene (PP) or Teflon bottle, sealed with parafilm and stirred at room temperature for 30 min. For the alumina source, 12.5 g aluminum isopropoxide was dissolved in 76.5 g H_2O and 52.3 g TMAOH. This solution was sealed, kept being stirred and heated in a water bath at 70ºC until the suspension became clear. The clear sol was aged at room temperature with stirring for 3 days, followed by heating at 100°C in an oil bath with stirring for 4 days. In the synthesis process, the nanocrystalline zeolite particles remained suspended in solution with no precipitate observed. The product was isolated by dialysis and ultracentrifugation from its mother solution until pH of supernatant was 7 and ion exchanged by stirring the zeolite suspension in 0.2 M NaCl solution for 2 hours. The ion exchanged product was washed with DI water and stored in 2 wt.% aqueous stock solution.

3.3 Rapid Synthesis and Characterization of Nano ZY

By the end of the project, an efficient and continuous nano zeolite synthesis method was developed. The composition used for nano zeolite synthesis was 0.048 Na_2O : 2.40 $(TMA)_2O(2OH)$: 1.2 $(TMA)_2O(2Br)$: 4.35 SiO_2 : 1.0 Al_2O_3 : 249 H_2O (Comp A, Fig. 3). This composition was aged at room temperature for 3 days before hydrothermal treatment.

Aged Comp A (agCompA) was moved to a dehydration-rehydration hydrothermal (DRHT) apparatus as shown in Fig. 3b and heated by a heating mantle at the bottom. In the first 30 min, 25% (v/v) of water was evaporated from agCompA and collected in the funnel. Then, concentrated agCompA was refluxed for 19 hours. At the same time, the proper amount of NaOH was added to the collected water (0.06 g NaOH per 100 g of agCompA). After 19-hour reflux, water collected in funnel was dropped back to the composition in 30 min. agCompA started to turn turbid. Then, a 9-hour DRHT process was applied to the mixture. The 9-hour DRHT process comprised 6 cycles with each cycle consisting of 30 min for dehydration + 30 min for reflux + 30 min for rehydration. In the dehydration process, 40% (v/v) of water was collected in the funnel by evaporation and condensation. In reflux, the same amount of NaOH was dissolved in the collected water (0.06 g NaOH per 100 g of agCompA). After the 9-hour DRHT process, the final product was isolated from the mixture and washed with centrifugation.

The final product of continuous nano zeolite synthesis had a yield of 93% with 29 hours in total of hydrothermal treatment. The synthesis rate was 3.2% per hour. The X-ray diffraction (XRD) pattern as shown in Fig. 4 indicated complete crystallization of pure zeolite Y. The particle size of the final product was studied with both dynamic light scattering (DLS) and transmission electron microscopy (TEM). With DLS, the final product had an average particle size of 89 nm, and TEM resulted in an average particle size of 29±7 nm. Typically, DLS provides a larger particle size value than TEM. From TEM images (Fig. 5), it could also be learnt that the final product was colloidal nano zeolite single crystals without aggregation. For each particle, the octahedral shape of faujasite was confirmed. The Si/Al ratio of the final product was studied with ^{29}Si NMR as shown in Fig. 6. Based on the calculation, the final nano zeolite product had a Si/Al ratio of 1.76.

Thus, a continuous synthesis strategy was developed which optimized the synthesis rate of colloidal nano zeolite Y. After 29 hours of heating, 93% yield was reached, which ensured enough supply of nano zeolite particle in this project.

3.4 Fabrication of PES Substrates

The commercial polyethersulfone (PES) was used for polymer support preparation. First, PES was dissolved in an appropriate amount of solvent under magnetic stirring at 80°C for 3 hours until the solution was clear and homogeneous. Then, the solution was cooled down to room temperature, and a pore former was added dropwise to minimize phase separation. The solution was continuously kept under magnetic stirring overnight. All the procedures were carried out under a N_2 shower. Then, the solution was cast on a flattened non-woven fabric by using the GARDCO stainless steel film applicator in the laboratory. The wet film was exposed to a certain relative humidity (RH) for a period of time and then immersed into a water bath at a particular temperature. Eventually, the solid PES layer was formed on the non-woven fabric.

In a similar way to the abovementioned lab-scale PES preparation, for the pilot-scale fabrication, the solution was continuously cast on the non-woven fabric moving at a particular speed using a stationary stainless-steel knife (for 14 inches in width) with the pre-determined gap setting. A proper tension was applied to ensure the flatness of the fabric. The trough holding the casting solution was purged with N_2 at a sufficient flow rate to prevent the casting solution from

phase separation. A humidity chamber was installed after the casting knife, and the rolling speed of the fabric controlled the exposure time in the humidity chamber. Subsequently, the cast film was immersed into the water tank to form PES support. Pore size and porosity of the pilot-scale PES support were controlled by adjusting the polymer concentration and coagulant bath temperature.

By the end of the project period, a total of > 2000-feet long and 14-inch wide PES substrates were fabricated by the continuous casting machine for the subsequent ZY deposition and amine-containing polymer cover layer coating. The conditions that could achieve an average pore size of ~ 69 nm and a porosity of ~ 17% were successfully reproduced.

3.5 Deposition of ZY Particles on Polymer Support

In this project, the deposition of 40-nm ZY particles on a polyethersulfone support (PES) was successfully achieved by the vacuum-assisted dip-coating technique developed at OSU in lab scale and pilot scale. In lab scale, a 0.09 wt.% ZY aqueous dispersion was used for the vacuum-assisted dip coating. The ZY dispersion was diluted from the original dispersion prepared with deionized water and then sonicated for 30 minutes. The deposition was carried out under vacuum for 5 seconds. After the deposition, the sample was dried in a humidity chamber (70 — 80% RH) at room temperature for 24 hours.

The deposition technique was successfully scaled up for the scale-up ZY deposition on the scale-up PES supports via the pilot-scale vacuum-assisted dip coating assembly with appropriate operation conditions to simulate the deposition conditions in lab scale. A total of > 400 feet long and 14-inch wide ZY-PES substrates were fabricated. As shown in Fig. 7, the coverage of ZY nanoparticles was uniform with a thickness of ~240 nm.

An alternative pore-filling method was developed in the pilot-scale to obtain a ZY layer with minimum cracks. The pore-filling method that could reduce the surface pore size of the PES support was applied for minimizing the penetration of the amine-containing polymer cover layer, resulting in improving the membrane performance results. Fig. 8 shows the representative images of the surfaces of the ZY deposited samples by the pore-filling method. For low ZY concentration, PES surface pore size/porosity reduced by 0.5% – 1.8%, and there were individual zeolite particles on the PES surface as shown in Fig. 6a. For very low ZY concentration, PES surface pore size/porosity reduced by ~ 0.2%, merely no individual zeolite particles were observed on the PES surface as shown in Fig. 6b. About > 100 feet of the pore-filling zeolite deposition substrate was fabricated with the large-batch synthesized ZY nanoparticles to eliminate the potential defects, including protruded surface spots and large cracks.

For this project, two kinds of substrates were used sequentially. One was prepared by depositing 40 nm ZY particles onto the commercial PES support initially, and another was the ZY/pilot-fabricated PES.

3.6 Amine-Containing Polymer Cover Layer Synthesis for 57°C

High molecular weight polyamine was synthesized by the following procedure. The polymerization was carried out under nitrogen purge at around 50°C for 3 h. The initiator was 2,2'-azobis(2-methylpropionamide) dihydrochloride (AIBA), and the solvent was water. After that, HCl was used to carry out the acidic hydrolysis at 70°C for 5 h. After the hydrolysis, the solution was poured into ethanol to precipitate the polymer. The polymer was dissolved in water and ion-exchanged until pH = 10. Different synthesis conditions of the free-radical polymerization were used to obtain polyamine with higher molecular weights. The purpose for obtaining polyamine with a higher molecular weight was to obtain a high coating solution viscosity, and further minimize the penetration of the amine-containing coating solution into the porous substrate. This could reduce the mass transfer resistance and improve the CO_2 permeance. The synthesis conditions including monomer concentration, initiator/monomer ratio, temperature, and reaction time along with the resultant 3 wt.% polymer solution viscosity of polyamine are shown in Table 2. In general, increasing the monomer concentration and the reaction duration will lead to polyamines with higher molecular weights. As shown in this table, a very high viscosity of more than 2000 cp was obtained for the 3 wt.% solution of the polyamine synthesized.

Table 2. Synthesis conditions and 3 wt.% polymer solution viscosity of polyamine.

Monomer Concentration (wt.%)	Initiator/ Monomer Ratio (by weight)	Temperature (°C)	Reaction Time (h)	Gel formation	3 wt.% Polymer Solution Viscosity (cp)
50	0.09/100	40	5	No	1932
55	0.11/100	40	5	Yes	1975
53	0.11/100	40	5	No	1948
45	0.11/100	35	6.5	No	530
45	0.1/100	40	5.5	No	1941
50	0.11/100	40	4.5	No	1952
45	0.1/100	45	5.5	Yes	1860
45	0.1/100	45	5	No	1922
45	0.11/100	40	5.5	No	1945
45	0.1/100	45	4.5	No	1566
45	0.12/100	45	4	No	1912

45	0.11/100	45	4	No	1935
50	0.14/100	45	3.5	Yes	1450
48	0.14/100	45	3.5	No	1682
46.5	0.14/100	45	4	No	1843
43	0.14/100	45	5	No	1254
45	0.14/100	45	4.5	Yes	1868
45	0.14/100	45	4	No	1795
45	0.14/100	50	3	Yes	413
43	0.14/100	50	3	Yes	938
43	0.14/100	45	4	No	1215
38	0.14/100	50	3.8	No	2170

Mobile carrier was then incorporated into the polyamine solution to prepare the coating solution. Different substrates were employed for membrane preparation, including scale-up PES support and scale-up ZY/scale-up PES substrate. The solution was coated on the aforementioned substrates either by using the GARDCO stainless-steel film applicator in lab-scale fabrication or by using the continuous membrane fabrication machine for pilot-scale fabrication with pre-determined gap settings to control the thickness of the amine-containing polymer cover layer. The fabricated membranes were then dried at ambient conditions for overnight. The amine-containing composite membranes were used for achieving higher CO_2 permeance and higher CO_2/N_2 selectivity based on the facilitated transport of CO_2 via reversible reaction with amines [1-23].

3.7 Amine-Containing Polymer Cover Layer Synthesis for 102°C

Initially, the coating solution for the amine-containing polymer cover layer was prepared with the following method. First, polyvinylalcohol (PVA) was cross-linked by glutaraldehyde using potassium hydroxide (KOH) as the catalyst. After the crosslinking reaction, a viscous and homogeneous brownish solution was obtained. The crosslinked polyvinylalcohol (XL-PVA) solution was then mixed with fixed and mobile carriers to make a very viscous casting solution. During this process, room temperature gelling and also solvent evaporation both contributed to increase the viscosity of the casting solution. In the lab-scale, the solution was then coated on the substrate flattened on a glass plate using the GARDCO stainless steel film applicator. The membrane was then cured in a convective oven to evaporate the solvent completely and finish the crosslinking reaction. Later, the amine-containing polymer cover layer synthesized for 57°C described above was used for 102^{o}C to obtain improved membrane performance.

3.8 PES/Grown-ZY/PDMS Membrane Synthesis

ZY seed layers on top of PES supports were prepared with vacuum dip-coating. The commercial PES support was chosen for this synthesis. Before dip-coating, ZY stock dispersion was put in ultrasonic bath for 1 hour and then diluted with DI water to the required concentration. The nanocrystalline ZY suspension was used for vacuum dip-coating. A crystal dish was filled with 10 – 15 mL of the prepared nanocrystalline ZY suspension to be used for dip-coating. In the dip-coating process, one end of PES support surface was first soaked in the ZY seed dispersion, and the whole support was moved slowly to the other end with each part of the sample staying in the ZY suspension for 5 seconds. The same procedure would be repeated if multiple-time depositions were needed. The deposited support was stored in a humidity chamber.

The seed support was secondary grown following the rapid ZY synthesis procedure as shown in Fig. 9. The gel composition was 17 Na_2O : 1 Al_2O_3 : 21.80 SiO_2 : 975 H_2O, which was prepared by mixing and stirring the clear solution of 85.24 g H_2O, 2.208 g of $Al(OH)_3$ and 7.29 g NaOH with 13.85 g Ludox SM-30, followed by aging for 4 hours at room temperature. Then, the opaque gel was moved to the round bottom flask to dehydrate, in which 40 mL of H_2O was removed from the gel in 1 hour of heating. The seed deposited support was anchored in a holder and put into the flask. The 40 mL of H_2O was dripped back into the concentrated gel in 1 hour of rehydration, and the synthesis process was completed. The secondary grown membrane was cooled to room temperature and washed with a hair brush.

The grown zeolite membrane was spin coated with 3.5 wt.% polydimethylsiloxane (PDMS) monomer solution. After being taped on the round plate for spin coating, the membrane was first filled with water for three times to prevent the penetration of PDMS into the pore of membrane. Then, PDMS was dropped to cover the whole surface area of the membrane, followed by 2000 rpm spin for 5 s to remove the extra PDMS and 6000 rpm spin for 1 min to spread the PDMS and make the PDMS cover layer as thin as possible. After the spin coating, the membrane was kept at room temperature overnight or kept at 100°C for 1 hour for PDMS to crosslink.

3.9 Development of Prototype Membranes by Continuous Fabrication

The continuous fabrication machine for the development of prototype membranes in roll-to-roll continuous operation was successfully upgraded and operated. The pilot-scale coating machine with the thin-film casting (TFC) assembly is shown in Fig. 10. The TFC assembly was used to coat the amine-containing polymer cover layer. This coating machine was successfully modified and used for the ZY deposition on the PES substrate by pilot-scale ZY vacuum-assisted dip coating. The casting machine as shown in Figs. 11 and 12 was successfully installed and operated for the fabrication of the pilot-scale PES substrate.

PES substrates with desirable pore size, porosity, and morphology were fabricated using the pilot-scale continuous casting machine. PES substrates of 14 inches in width and a total length of > 2000 ft. were successfully fabricated; Fig. 13 shows a sample. The casting solution

composition along with the web-speed, coagulation bath temperature and casting solution temperature was optimized to obtain the PES substrate layer with a desired morphology.

As mentioned before, > 400 feet long and 14 inches ZY-PES substrates were successfully fabricated using the modified coating machine. The deposition of scale-up ZY nanoparticles on the scale-up PES supports was performed by using a pilot-scale vacuum-assisted dip coating assembly as shown in Fig. 14. For the scale-up ZY deposition, the lab-scale ZY deposition operating conditions were simulated and employed successfully. Experiments with different vacuum degrees and web speeds were carried out to optimize the operating parameters. Uniform coverage of ZY nanoparticles with a thickness of < 250 nm were obtained from experiments carried out at optimized operating conditions for the 14-inch wide ZY deposition on scale-up PES substrates. The pore-filling method that could reduce the surface pore size was developed for improving the results.

For the fabrication of Approach 1 composite membranes, the amine-containing polymer cover layer was fabricated using the TFC assembly of the continuous coating machine on the scale-up PES substrates including the scale-up ZY/scale-up PES substrates. For the fabrication of the scale-up amine-containing polymer cover layer, the coating solution containing the mixture of polyamine and small mobile carriers was used. The thin amine coatings (< 200 nm) on the scale-up PES substrates were successfully obtained. Different operating parameters were optimized to obtain desirable amine-layer coating, resulting in the amine-containing composite membranes with desirable transport performance. A total of > 1500 feet long and 14 inch wide composite membranes were fabricated using the TFC assembly.

3.10 Fabrication of Spiral-Wound Module of Composite Membrane

Spiral-wound membrane modules were successfully fabricated at OSU with the counter-current configuration and by TriSep Corporation with the crossflow configuration. The physical impact of the feed spacer on the selective layer during the initial element preparation, resulting in indentations, was believed to be the main reason for the poor selectivity. Thus, a layer of a fine, smooth polymer spacer was incorporated between the feed spacer and the selective polymer layer to minimize/eliminate the indentations. The indentations were successfully eliminated in the elements prepared by OSU, resulting in improved performance with good CO_2/N_2 selectivity. However, there were 2 major drawbacks of the initial spiral-wound module design, including the feed gas bypass and the glue line failure. The issue of the glue line failure was successfully resolved by optimizing the glue application procedure including sufficient glue curing. Moreover, the ineffective sealing of the end-cap flanges with the spiral-wound membrane in the initial membrane module design led to significant “bypass” of the feed gas to the outlet (retentate) without even flowing between the wrapped membrane layers. This resulted in low CO_2 permeance (lower than the lab-scale performance). In principle, if the issues of the feed gas bypass and the glue-line failure are resolved, the performance and quality of element fabrication should be improved.

The quality of the spiral-wound membrane element fabrication was improved by optimizing the glue-line procedure including sufficient glue curing. The new procedure aided in adequate

sealing of the nonwoven fabric in the membrane leaf and sealing between the membrane leaf and the central tube. The quality of fabrication was successfully improved as the new elements during testing demonstrated essentially no leakage. The image of the fabricated spiral-wound membrane element is shown in Fig. 15.

The spiral-wound membrane element was eventually loaded in the housing to become the membrane module. Fig. 16 shows the fabricated membrane module. The membrane module was used for testing the transport performance of CO_2/N_2 separation. The new membrane module design along with the improved glue application procedure successfully helped in enhancing the transport performance by demonstrating about 800 GPU of CO_2 permeance and greater than 200 CO_2/N_2 selectivity using the scale-up composite membrane of the thin-film amine-containing polymer cover layer on the ZY/PES substrate for the membrane element (Approach 1).

4 Results and Discussions

4.1 Morphology of PES Substrates

In order to further reduce the fabrication cost of the inorganic/polymer composite membrane for CO_2 capture, PES supports were synthesized in both lab scale and pilot scale and were investigated for their potentials as the alternative low-cost substrate. A hydrophilic polymer support with a relatively large average pore size and a high porosity along with a smooth surface was important for both ZY deposition and gas transport for the CO_2 separation process. Therefore, scanning electron microscopy (SEM) and atomic force microscopy (AFM) were used to characterize the surface morphology and roughness of the synthesized PES supports with different preparation conditions.

Lab-fabricated PES Support

As shown in Figs. 17 and 18, both the pore size and porosity increased with the increase of relative humidity for the exposure of the cast film, because the vapor-induced phase inversion during the exposure was enhanced before the non-solvent induced phase inversion. In addition to pore size and porosity, the surface roughness of the supports was characterized by atomic force microscopy (AFM). According to the AFM, the roughness was around 10 – 12 nm, which showed a relatively good smoothness of the substrate.

Scale-up PES Support

The casting solution composition and operation conditions were further optimized to obtain good surface morphologies which should be close to those of the commercial PES support. As shown in Figs. 19 – 21, both the pore size and porosity increased with the decrease of PES concentration in the casting solution. One reason was that the lower PES concentration resulted in larger free volume generated during the solvent/non-solvent exchange process. The other reason was that the lower PES concentration led to a lower casting solution viscosity, which increased the solvent/non-solvent exchange rate. However, the PES concentration could not be reduced below

a critical level. Otherwise, the viscosity of the casting solution became too low to prevent severe penetration into the underneath non-woven fabric during the fabrication process.

The conditions that could achieve an average pore size of ~ 65 nm with a porosity of ~ 16.8% and an average pore size of ~ 69 nm with a porosity of ~ 17% are summarized in Table 3. Fig. 22 shows the surface morphology of the representative PES fabricated. A total of > 2000 feet PES substrates were successfully fabricated during the Budget Period 3 of this project. The thickness and morphology were successfully reproduced.

Table 3. Summary of the pilot-scale PES support surface morphology.

PES category	Average pore size (nm)	Surface porosity (%)
Low MW PES	~ 65	~ 16.8
Low MW PES	~ 69	~ 17.2
High MW PES	~ 69	~ 17.3

4.2 Amine-Containing Polymer Cover Layer Performance at 57°C

The membranes with an amine-containing polymer cover layer on different ZY/PES substrates (Approach 1) were tested at the typical flue gas temperature of 57°C and near ambient pressure. The feed gas composition was 20% of CO_2 and 80% of N_2 (on dry basis), and the sweep gas was argon. The gas flow rates for the feed side and sweep side were 60 cc/min and 30 cc/min, respectively. Water was also pumped into the system to make the water contents on the feed and sweep sides to be 17% (saturation water vapor level at 57°C). The transport performance results of scale-up and lab-scale membranes are included in Fig. 23. As shown in this figure, the lab-scale membranes reached a high CO_2 permeance of about 1100 GPU with a very high CO_2/N_2 selectivity of greater than 150. The scale-up membranes attained a high CO_2 permeance of about 870 GPU with a very high CO_2/N_2 selectivity of greater than 200. This figure also includes the transport performances of the prototype spiral-wound membrane modules with a high CO_2 permeance of about 820 GPU with a very high CO_2/N_2 selectivity of greater than 250.

4.3 Amine-Containing Polymer Cover Layer Performance at 102°C

Unless mentioned differently, all the transport characterization was carried out at 102˚C with 80% water in the feed gas (20 – 25% CO_2 and 75% N_2 on dry basis) and 57% water in the sweep gas (argon). Fig. 24 shows the transport performances of membranes with an amine-containing polymer cover layer with the XL-PVA/commercial polyamine/mobile carrier composition on different substrates at 102°C. The membrane performances were improved significantly at the high temperature due to the enhanced CO_2-amine reaction rate for the facilitated transport. A CO_2 permeance of 1460 GPU with extremely high CO_2/N_2 selectivity was obtained from the commercial PES substrate with ZY deposition on top of it. On lab-fabricated substrates,

reasonably good membrane performance was also obtained, which had a CO_2 permeance of 1325 GPU and CO_2/N_2 selectivity of 235. Further improvements may be obtained by seeking for other efficient fixed and mobile carriers. Besides the results from the XL-PVA/commercial polyamine/mobile carrier composition, the polymer cover layer with the high molecular weight polyamine/mobile carrier composition in the scale-up membrane was also tested at 102°C. The scale-up membrane showed a CO_2 permeance of 1800 GPU and a CO_2/N_2 selectivity of 160.

4.4 PES/Grown-ZY/PDMS Membrane Performance

Zeolite Membrane Synthesis

About eighty PES/grown-ZY/PDMS membranes (Approach 2) were synthesized and their transport properties were examined. Fig. 25 shows the cross-section view SEM of (A) grown zeolite membrane and (B) PDMS coated grown zeolite membrane. Fig. 26 depicts the effects of CO_2 concentration and temperature on the transport properties of the PES/ZY/PDMS membrane. With increasing CO_2 concentration, the permeance increased up to by about 40%, and then remained constant. The selectivity exhibited a gradual increase with CO_2 concentration. With increasing temperature, CO_2 permeance increased and the selectivity reduced, which is expected.

The CO_2 permeance vs. the CO_2/N_2 selectivity is plotted in Fig. 27. All the membranes were tested at room temperature with dry feed and sweep gas. The best membrane showed a CO_2 permeance of 789 GPU with a CO_2/N_2 selectivity of 72. There was a wide variation in performance, with the majority of specimens performing poorly (separation factor < 20). This arose because of large cracks that developed in the membrane if there was any flexing of the support. These cracks could be several microns wide and the PDMS cover layer did fill these cracks and the membrane performance was similar to PDMS on the bare support. These cracks ripped through the zeolite layer and the PES support. The cracking was extensive because the zeolite layer also grew within the PES support. The rigidity of the inorganic membrane and the elasticity of the PES support were mismatched giving rise to the cracks. However, with very careful manipulation of the membrane, high quality transport data were obtained, but even then, the reproducibility was not optimal, though in many cases, the transport properties were satisfactory. The issue of reproducible manufacture of zeolite membranes on conventional alumina supports has been addressed. There is a wide variability in performance. In the present study, the major issue with reproducibility was due to cracking and the performance of these membranes was poor. Even with the membranes that were carefully handled, there was a variation in the performance.

Zeolite Membrane Fabrication with Roller Assembly

In this study, an innovative roll-to-roll synthesis setup for the fabrication of zeolite membranes was built as shown in Fig. 28. Gel composition used in the reactor was: 8.3 Na_2O : 1 Al_2O_3 : 6.4 SiO_2 : 483.9 H_2O. After dissolving 4.416 g of $Al(OH)_3$ and 14.58 g NaOH in 170.48 g H_2O, 27.7 g Ludox SM-30 was added to the gel. The mixed gel was sealed in polypropylene bottle and aged at room temperature for 4 hours. The aged gel was transferred to a dehydration/rehydration hydrothermal setup for removal of half the water in 1 hour. This partially dehydrated hot gel was

then immediately transferred to the reactor and heated to 100°C. Seeded PES support was stapled onto the outer side of the rolling nonwoven fabric band. The convex membrane was stapled with the PES side facing out whereas the concave membrane was stapled with the PES side of membrane facing in. The entire PES support was immersed into the gel in the beginning of zeolite growth. During 1 hour of the zeolite growth process, water was added to the gel, diluting the gel from 120 mL to 200 mL. At the same time, the PES support moved through the gel due to the movement of the rolling non-woven fabric via the rollers. After zeolite growth, the membrane sample was washed with flowing water and fur brush, soaked in water to remove residual surface species and dried for further study.

Fig. 29 illustrates the detailed geometry. In the first case (convex), the seeded PES side of the support was directly exposed to the hot aluminosilicate gel. As growth occurred over one hour and the membrane moved from position 1 to 2, the flattening of the membrane would lead to compressive stress, as shown in Fig. 29a and b. Two different nano zeolite seed loading levels of the PES were examined in this particular geometry (10 and 14 µg/ml). In the second geometry (concave), the seeded PES layer (10 µg/ml) was faced towards the fixed column, being separated from it by the highly porous nonwoven fabric band (which acted as the moving support, as well as letting reactants through). In this case, as the membrane moved from position 1 to 2, upon flattening, the membrane would be subject to tensile stress, as shown in Fig. 29c and d.

Zeolite/PES membranes fabricated by roll-to-roll synthesis were coated with a PDMS cover layer (200 – 300 nm) before examining for CO_2/N_2 separation. Five membrane samples were prepared with concave geometries with the low seed loading. The CO_2/N_2 separation performance using the dry feed gas are shown in Fig. 30, with CO_2 permeance 1881 ± 182 GPU and CO_2/N_2 selectivity 34 ± 3. Five samples were prepared with the convex geometry, with CO_2 permeance of 1841 ± 181 GPU and CO_2/N_2 selectivity of 35 ± 4. For two samples prepared in the convex geometry with the high seed loading, the transport properties were CO_2 permeance of 275 ± 14 GPU and CO_2/N_2 selectivity of 7 ± 2.

4.5 Analysis of SO_2 Absorption by In-situ FTIR

A Perkin-Elmer Spectrum 400 FT-IR/FT-NIR spectrometer was used for analysis with 256 scans taken with a resolution of 8 cm^{-1}. A custom gas cell incorporated in the spectrometer is shown in Fig. 31. The spectrum for KBr was used as background. About 50 mg of liquid sample was placed on the KBr window and pretreated in flowing Ar at 102°C for 30 min. The adsorption of CO_2 was carried out by switching the inlet flow from the inert gas stream (argon) to the adsorbing gas stream (10% CO_2) when the gas cell was heated to 102°C. The gas stream was bubbled through hot water corresponding to 100% humidity during absorption. In-situ FTIR spectra were then recorded at 102°C. The SO_2 absorption was carried out in a similar way with 45 ppm SO_2 in N_2. In order to study the SO_2 effect on CO_2 absorption, the sample was exposed to a mixed gas stream containing 10% CO_2 and 45 ppm SO_2. Two sets of membrane samples were studied in attenuated total reflectance (ATR) infrared spectroscopy. Sample A consisted of high molecular weight polyamine and mobile carrier, and Sample B comprised XL-PVA, KOH, mobile carrier, and commercial polyamine. Sample A was treated with 0.7 ppm SO_2 at 57°C while Sample B was treated with 0.7 ppm SO_2 at 102°C before ATR measurement.

CO_2 Absorption at 102°C in Commercial Polyamine and Mobile Carrier A

Fig. 32 shows the FTIR spectra during CO_2 absorption in commercial polyamine (Fig. 32a) and Mobile Carrier A (Fig. 32b). Before exposure to CO_2, the sample was exposed to Ar. The exposure to CO_2 produced carbamate species at 1525 cm^{-1} and bicarbonate species at 1470 and 1458 cm^{-1} by the following reactions:

$$2\ R\text{-}NH_2 + CO_2 \rightarrow R\text{-}NH_2^+ + R\text{-}NHCOO^- \text{ (carbamate)}$$

$$R\text{-}NH_2 + H_2O + CO_2 \rightarrow RNH_2^+ + HCO_3^- \text{ (bicarbonate)}$$

SO_2 Absorption at 102°C in Commercial Polyamine and Mobile Carrier A

The FTIR spectra during 45 ppm SO_2/N_2 absorption are shown in Fig. 33. The adsorption of SO_2 in commercial polyamine (Fig. 33a) and Mobile Carrier A (Fig. 33b) led to a peak at 960 cm^{-1} which can be assigned to the S=O stretching vibrations of sulfites formed on the surface of amine carriers by the following reactions:

$$R\text{-}NH_2 + SO_2 + H_2O \rightarrow R\text{-}NH_3^+ + HSO_3^-$$

$$HSO_3^- + H_2O \rightarrow H_3O^+ + SO_3^{2-} \text{ (sulfite)}$$

In-situ FTIR Measurement of Gas Absorption at 102°C in Commercial Polyamine and Mobile Carrier A

The growth of IR peak intensities as a function of time was plotted during CO_2, SO_2 exposure and the mixture of both gases on the amine carriers. A typical plot of the normalized IR peak intensities of carbonate and sulfite species versus time for commercial polyamine is shown in Fig. 34. From the growth of sulfite peak at 960 cm^{-1} in Fig. 34a, the SO_2 reaction with commercial polyamine in 45 ppm SO_2 started from 180 min and reached steady state at 220 min. Fig. 34b shows that the reaction in 10% CO_2 started from 240 min and reached equilibrium at 300 min. In the presence of mixed gases (Fig. 34c), the growth of sulfite peak started from 270 min and reached equilibrium at 330 min. However, no peak of carbonate species was observed during the reaction.

The reaction of Mobile Carrier A was carried out in a similar way and a typical plot of the normalized IR peak intensities versus time is shown in Fig. 35. In 45 ppm SO_2 (Fig. 35a), the growth of sulfite peak started from 60 min and reached steady state at 120 min. In 10% CO_2 (Fig. 35b), the reaction started from 10 min and reached steady state at 240 min. When the sample was exposed to the mixed gases, the growth of sulfite peak started from 40 min and reached steady state at 80 min (Fig. 35c), while the growth of carbonate peak started from 10 min and reached steady state at 80 min (Fig. 35d). The slope of the intensity profile versus the time profile reflects the rate of formation of these new species. The peak height of produced carbonates/bicarbonates and sulfites increased with the increase in exposure time of the amine carriers to CO_2 and SO_2, respectively. Most absorption reactions reached steady state within an hour, which indicates the

absorption capacity on both samples was about the same. However, the beginning of formation of new species in Mobile Carrier A was much faster than the commercial polyamine, which proves that Mobile Carrier A is an effective mobile carrier in the membrane. The plots of Mobile Carrier A also show that the formation of sulfites is slower than the formation of carbonates, reflecting higher activation energy for the formation of stable sulfite species. These species require the use of a significantly higher temperature to decompose than that for the absorbed carbonates and bicarbonates.

In-situ FTIR Measurement of Gas Absorption at 102°C in Mobile Carrier B

The absorption of SO_2 and CO_2 in Mobile Carrier B was studied and the results were compared with Mobile Carrier A. The exposure to CO_2 produced bicarbonate species at 1460 cm^{-1}. The absorption of SO_2 led to a peak at 960 cm^{-1} which can be assigned to the S=O stretching vibrations of sulfites. The growth of IR peak intensities as a function of time was plotted during CO_2, SO_2 and the mixture of both gases exposure to Mobile Carrier B. A typical plot of the normalized IR peak intensities of bicarbonate and sulfite species versus time for Mobile Carrier B is shown in Fig. 36. From the growth of sulfite peak at 960 cm^{-1} in Fig. 36a, the SO_2 reaction with Mobile Carrier B in 45 ppm SO_2 started from 30 min and reached steady state at 50 min. Fig. 36b shows the CO_2 reaction in 10% CO_2 started from 10 min and reached steady state at 60 min. In the presence of mixed gases, the growth of sulfite peak started from 10 min and reached steady state at 60 min (Fig. 36c) while the growth of bicarbonate peak started from 40 min and reached steady state at 60 min (Fig. 36d). Both reaction rates of CO_2 and SO_2 in Mobile Carrier B were faster than those in Mobile Carrier A, which were reported previously. According to literature reports, the secondary amines adsorbed more SO_2 than the primary and tertiary amines with comparable amine loadings and exhibited more stability after SO_2 treatment by displaying higher normalized CO_2 capacities. The compiled data for the SO_2 absorption experiments suggest that Mobile Carrier B is not only a potential efficient mobile carrier for CO_2 transport, but also could be acting as a SO_2 sponge, freeing up the other mobile carriers for transport. Mobile Carrier B exhibited potentially higher affinity to SO_2 in comparison with Mobile Carrier A, indicating that more SO_2 will be released during the facilitated transport, which implies the CO_2 capacity loss of the fixed amine carrier after exposure to SO_2 is lower. This suggests that Mobile Carrier B might be promising in the mobile amine carrier system for the SO_2 mitigation; this mobile amine carrier was used in the optimized composite membrane (Approach 1) for this project.

Analysis of Mixture of Mobile Carrier A and Mobile Carrier B by in-situ FTIR at 102°C

The mixture of Mobile Carrier A and Mobile Carrier B were exposed to 45 ppm SO_2 at 102°C. A weak peak at 960 cm^{-1} was assigned to S=O stretch of sulfite (SO_3^{2-}) and could not be removed by nitrogen purging (Fig. 37). In addition, a strong peak at 960 cm^{-1} was generated when Mobile Carrier A and Mobile Carrier B were exposed to the mixture of 10% CO_2 and 45 ppm SO_2 (Fig. 38). The intensity of sulfite peak in the gas mixture was apparently stronger than that of sulfite peak in 45 ppm SO_2, which indicated that CO_2 was promoting SO_2 reaction to sulfite in the mobile amine carriers. The chemical basis of this promotion is not yet well understood.

Analysis of Mixture of Mobile Carrier A and Mobile Carrier B by in-situ FTIR at 57°C

In 45 ppm SO_2 at 57°C, there was no 960 cm^{-1} generated but only a weak peak at 950 cm^{-1} after 2-hour exposure (Fig. 39), which was assigned to symmetric stretching of adsorbed SO_2. This result showed a weak SO_2 absorption in the mobile amine carriers at low temperature. The 950 cm^{-1} peak could be removed by dry nitrogen purging at 102°C, indicating the mobile amine carriers could be regenerated. When switching to the mixture of 10% CO_2 and 45 ppm SO_2 (Fig. 40), the 950 cm^{-1} peak became much stronger but still could be removed by dry nitrogen purging at 102°C. There were two weak peaks appeared at 970 cm^{-1} and 925 cm^{-1}, which were also assigned to reacted sulfite and could not be removed by nitrogen purging. According to the intensity of those two peaks, there was only a small amount of sulfite generated. This result proved that CO_2 could promote SO_2 reaction even at low temperature, and adsorbed SO_2 was the main species at 57°C. The compiled data for the SO_2 absorption experiments suggest that applying a lower temperature in the mobile amine carriers is promising for the mitigation of SO_2 effect. The explanation for the promotion of CO_2 on SO_2 reaction is still unknown and needs further investigation.

ATR Measurement of Membrane

The mixture of Mobile Carrier A and Mobile Carrier B was used as the mobile amine carrier in membrane sample A. The membrane was treated with 0.7 ppm SO_2 at 57°C and there was no significant change detected by FTIR (Fig. 41), only a very weak band at 960 cm^{-1}, which could be assigned to sulfite species. The membrane performance in SO_2 was also improved according to the membrane transport data. However, using Mobile Carrier A as the mobile amine carrier in membrane sample B showed a strong band at ~1000 cm^{-1} after exposure to 0.7 ppm SO_2 102°C (Fig. 42).

The products generated by reaction of CO_2 and SO_2 with mixed and mobile amine carriers were identified by infrared spectroscopy. The exposure to CO_2 produced carbonate and bicarbonate species at 1475 and 1440 cm^{-1}. The absorption of SO_2 led to a peak at 960 cm^{-1} which could be assigned to sulfites. The rate of formation of these new species was studied by the plot of peak intensity as a function of time. Both reaction rates of CO_2 and SO_2 absorbed in Mobile Carrier B were faster than those absorbed in Mobile Carrier A, which suggest that Mobile Carrier B is not only a potential efficient mobile carrier for CO_2 transport, but also could be acting as a SO_2 sponge. The mixed mobile carriers were studied in the presence of SO_2 at different temperatures, and 57°C was found to be a better temperature for SO_2 mitigation. The ATR measurements of the membrane containing the mixed mobile carriers provided further evidence on our previous conclusions. On the basis of our experimental results, it can be inferred that applying the mixed, mobile amine carriers as the mobile amine carrier system as well as a lower temperature for gas absorption is promising for SO_2 mitigation. To assess the tolerance of the membrane to SO_2, a series of quantitative experiments were conducted and are discussed in the following paragraphs.

Influence of SO_2 on Membrane: Characterization by In-situ IR

The instrumentation and experimental procedures of the HATR sampling were described before. By locating the absorbance of each species on the vertical axis of the standard graph, the corresponding concentration can be found on the horizontal axis and plotted as a function of time for reaction of 10% CO_2 with 30 wt.% aqueous amine at 57°C as depicted in Fig. 43. As shown

in Fig. 43a, the concentration of a primary amine keeps dropping during CO_2 exposure with a steady rate. By comparing Fig. 43b and c, there was more carbamate produced than carbonate.

The protonation of a primary amine results in C-N stretching shifts from 1076 cm^{-1} to 1069 cm^{-1} as shown in Fig. 44. The quantification of protonated amine concentration cannot be determined directly from Beer's Law graph. It is well known that the primary amine is involved in pH-dependent protonation equilibria: $Am + H^+ \overset{K}{\leftrightarrow} AmH^+$, where K is the equilibrium constant and $K = \frac{[AmH^+]}{[Am][H^+]}$ with a value of log K = 9.06. The standard primary amine solution was titrated with concentrated HCl, and the concentrations of primary amine and protonated primary amine at different pH were determined using the equilibrium constant.

By using the absorbance values of Am (amine) and AmH^+ (protonated amine), their proportionality constants ε at each pH were calculated, the average value of which were ε = 0.107 for Am and $\varepsilon^+ = 0.27$ for AmH^+. As shown in Fig. 44, the peak area at 1069 cm^{-1} (Abs_{UNK}) consists of the peak area of Am at 1076 cm^{-1} (Abs_{AM}) and the peak area of AmH^+ (Abs_{AMH+}):

$$Abs_{UKN} = Abs_{AM} + Abs_{AMH+} = [Am]\,\varepsilon + [AmH^+]\,\varepsilon^+$$

And finally, we can obtain:

$$[AmH^+] = \frac{Abs_{UNK} - 4.91\varepsilon}{\varepsilon^+ - \varepsilon}$$

The concentration of protonated primary amine has been calculated and plotted as a function of time in Fig. 45. There is a considerable amount of protonated primary amine produced during CO_2 absorption, which indicates that the pH effect plays an important role and the absorption ability of a primary amine will be affected by changing pH such as introducing acidic SO_2.

Influence of SO_2 on Membrane: The pH Effect of SO_2 on Aqueous Amine Solution

SO_2 can react with water to form sulfurous acid, which will dissociate to release protons and the sulfite ion. The pH effect of SO_2 absorbed into amine was investigated by an equilibrium and kinetic study with the HATR (horizontal attenuated total reflectance) spectrum. Quantitative analysis of CO_2 absorption by amine membrane samples was performed by in-situ FTIR measurements in the presence of SO_2.

The pH effect of SO_2 on aqueous amine solutions was also investigated during this project. The pH value of the solution during gas absorption was monitored by an Accumet AB15 pH meter (Fisher Scientific). As an acidic gas, SO_2 reacts with amine, which reduces the free amine concentration to generate sulfite.

$$SO_2 + H_2O + 2\,RNH_2 \rightarrow 2\,RNH_3^+ + SO_3^{2-}$$

The sulfite peak at 936 cm^{-1} was observed in the 2.5 M MEA (monoethanolamine) solution after five days in the presence of 151 ppm SO_2 and 6% O_2 (Fig. 46).

Infrared spectra of 30 wt.% aqueous MEA was recorded with 15% CO_2 in the presence of 45 ppm and 176 ppm SO_2, respectively. There was no sulfite or sulfate peak observed after 10 h. Therefore, it was possible that these types of reactions are very slow at low temperature and there was no observable direct interaction between SO_2 and MEA in a short experimental period. The remaining effect of accumulation of SO_2 in the MEA solution was the acid behavior of the sulfurous acid.

The pH value of the MEA solution was monitored during the absorption reactions. As shown in Fig. 47, there is a slight pH change from 11.93 to 11.76 induced by 151 ppm SO_2. Despite the significant pH change caused by CO_2 from 11.93 to 10.36, SO_2 showed a minor effect on the pH of the MEA solution with a further decrease to a value of 10.27.

As mentioned, SO_2 can react with water to form sulfurous acid, which will dissociate to release two protons and the sulfite ion, SO_3^{2-}. The sulfite ions will not play an important role (rather than formation of heat stable amine salts), but the released protons by lowering the pH will interfere in the equilibriums of the amine, hydroxide, and CO_2 in the formation of carbamate and carbonate species.

$$SO_2 + H_2O \leftrightarrow H^+ + HSO_3^- \text{ (bisulfite)}$$

$$HSO_3^- \leftrightarrow H^+ + SO_3^{2-} \text{ (sulfite)}$$

$$SO_2 + \frac{1}{2}O_2 + H_2O \leftrightarrow 2H^+ + SO_4^{2-} \text{ (sulfate)}$$

MEA and its carbamate are involved in pH-dependent protonation equilibria at the primary amine for MEA and the carboxylate group of the carbamate. As a consequence, the chemical shifts of the two species are pH-dependent. The released protons by lowering the pH will interfere in the following equilibria:

$$R\text{-}NH_2 + H^+ \leftrightarrow RNH_3^+$$

$$R\text{-}NHCOO^- \text{ (carbamate)} + H^+ \leftrightarrow R\text{-}NHCOOH \text{ (carbamic acid)}$$

$$CO_3^{2-} + H^+ \leftrightarrow HCO_3^-$$

There are several effects of lowering of the pH. The immediate kinetic effects include: (a) protonation of MEA and (b) lowering the hydroxide concentration, thus reducing the kinetics of carbonate formation. The equilibrium effects are more subtle and complex but generally there should be a reduction of the absorption capacity of the amine solution with increasing accumulation of SO_2.

From the quantitative results presented in Fig. 48, the growth of $MEAH^+$ formation matched the prediction well. However, we also observed the growth of CO_3^{2-} and $NCOO^-$ in the presence of SO_2. Briefly, there were more protonated amine, carbamate and carbonate species formed with SO_2 than the products with CO_2. The growth of carbamate formation could be attributed to the growth of carbonate. Thus, SO_2 induced-pH change can interfere in the equilibrium of amine and promotes the CO_2 reaction with amine to a small extent.

4.6 Spiral-Wound Module Performance at 57°C

The testing conditions for the spiral-wound membrane module were similar to the flat-sheet membrane test. However, higher feed and sweep flow rates (~ 1000 cc/min) were used for testing the transport performance of the spiral-wound membrane module. Table 4 and Fig. 23 show the transport results of the spiral-wound membrane modules. This table along with the figure shows a high CO_2 permeance of about 820 GPU with a very high CO_2/N_2 selectivity of greater than 200. This high transport performance was achieved after we solved the glue line failure, module leakage and membrane indentation issues encountered initially, which have been described before.

Table 4. Transport performances and pressure drops of spiral-wound membrane modules.

Module No.	Amine layer thickness (nm)	Feed/sweep flow rate (cc/min)	CO_2 permeance (GPU)	CO_2/N_2 selectivity	Pressure drop (feed/sweep, psi/m)
SW-35	200	500/500	300	130	1.48/1.48
		500/250	250	120	1.48/1.31
		1000/500	300	130	1.48/1.48
SW-36	200	1000/1000	350	120	1.48/1.48
		2000/1000	400	120	1.64/1.48
		3000/1000	400	120	1.97/1.64
SW-37	200	1000/1000	350	220	1.48/1.31
		2000/1000	350	220	1.64/1.48
SW-38	345	2000/1000	250	150	1.64/1.48
		3000/1000	250	150	1.97/1.48
SW-41	205	2000/1000	350	200	1.64/1.48
		3000/2000	350	200	1.97/1.48

		4000/2000	350	200	2.30/1.48
SW-50	200	1000/1000	200	110	1.48/1.48
		2000/1000	450	120	1.64/1.48
		3000/1000	450	120	1.97/1.48
SW-51	200	1000/1000	350	160	1.64/1.48
		2000/1000	450	200	1.97/1.48
		3000/1000	400	20	2.30/1.48
SW-61	230	1000/1000	580	150	1.48/1.48
		2000/1000	640	45	1.97/1.64
SW-62	230	1000/1000	450	210	1.48/1.97
		2000/1000	360	25	1.64/2.30
SW-63	240	1000/1000	430	350	1.64/1.64
		1500/1000	480	280	1.97/1.97
		2000/1000	480	250	2.30/1.97
		2000/1500	480	14	2.30/2.30
SW-64	240	1000/1000	470	210	1.64/1.97
		1500/1000	600	250	1.97/1.97
		2000/1000	400	50	2.30/2.30
SW-67	195	1000/1000	520	330	1.64/1.97
		1500/1000	620	330	1.97/2.30
SW-70	190	1000/1000	570	250	1.48/1.64
		1500/1000	600	200	1.64/1.97
		2000/1000	600	40	1.97/2.30
SW-72	190	1000/1000	600	200	1.48/1.64
		1500/1000	600	150	1.64/1.97
		2000/1000	590	30	1.97/2.30
SW-80	180	1000/1000	715	360	0.33/2.62
		1500/1000	720	250	0.66/2.95
SW-88	375	1000/1000	450	2500	0.66/1.97

		1500/1000	480	1000	0.98/1.97
SW-94	200	1000/1000	550	230	0.66/1.97
		1500/1000	720	200	1.48/1.97
SW-122	110	1000/1000	720	300	1.48/1.48
		1500/1000	580	23	1.64/1.64
SW-132	145	1000/1000	715	180	1.48/1.48
SW-133	150	1000/1000	725	300	0.98/0.98
SW-138	155	1000/1000	670	500	1.48/1.48
	155	1500/1000	680	500	1.48/1.97
SW-152	165	1000/1000	800	160	2.30/0.66
SW-156	130	1000/1000	750	200	1.48/1.31
SW-154	165	1000/1000	800	220	1.31/1.31
SW-158	130	1000/1000	950	65	1.48/1.31
SW-159	175	1000/1000	770	200	1.48/1.31
SW-162	145	1000/1000	820	270	1.48/1.48
SW-171	175	1000/1000	800	200	1.48/1.48
SW-174	155	1000/1000	820	200	1.48/1.48

4.7 Pressure Drop Measurements of Membrane Modules

The pressure drop measurements of the spiral-wound membrane elements were performed. The pressure drop was measured by using 4 pressure gauges with two on each side of the feed and sweep/permeate streams. The positions of the pressure gauges were as follows: before the module feed inlet (position 1), after the module retentate outlet (position 2), before the module sweep inlet (position 3), and after the module permeate outlet (position 4). The pressures at the module feed and sweep outlets were set to be 1.5 psig and 1.0 psig, respectively, using a near-ambient pressure regulator. The pressure difference between position 1 and position 2 was considered as the pressure drop on the feed side of the module. The pressure difference between position 3 and position 4 was considered as the pressure drop on the sweep side of the module. The results are summarized in Table 4. As shown in this table, a low pressure drop of less than 1.5 psi/m (meter of the membrane length) was obtained for the membrane modules with good transport performance after we solved the glue line failure, module leakage and membrane indentation issues encountered initially, which have been described before. This low pressure drop value is highly desirable.

4.8 Spiral-Wound Module Testing at NCCC

To investigate the membrane module performance with the real flue gas, three spiral-wound modules were tested at NCCC (National Carbon Capture Center in Wilsonville, AL) for a total test period of one month. The flue gas composition provided by NCCC contained approximately 12% (± 1%) CO_2, 7% (± 1%) O_2, 81% (± 1%) N_2, 0.5 – 5 ppm SO_2, and 1.5 – 4 ppm NO_2. Among those components, the oxygen concentration was much higher than the typical average of 2.3% in coal-fired power plants. Our gas chromatograph (GC) settings, including the GC column, were incapable of separating the oxygen concentration from the nitrogen concentration in the permeate stream sample. However, we were able to solve this problem with the great help from the analytical lab team of NCCC by using an oxygen analyzer to measure the oxygen concentration in the retentate stream. By using this concentration, we were able to determine the permeate oxygen concentration from the mass balance, and further obtain the accurate CO_2/N_2 selectivity of our membrane modules.

Membrane Module Test Results at OSU

For comparison with the NCCC field test results, the spiral wound membrane modules SW-173 and SW-67 were tested at OSU with a simulated flue gas. The membrane transport performance of the membrane modules are summarized in Table 5. Figs. 49 and 50 include the stability test results of the models SW-173 and SW-67, respectively, as a comparison to the spiral-wound modules tested at NCCC.

Table 5. Transport performances of spiral-wound membrane elements at 57°C tested at OSU.

Module No.	Selective layer thickness (nm)	Feed/sweep flow rate (cc/min)	CO_2 permeance (GPU)	CO_2/N_2 selectivity	Feed/sweep pressure drop (psi/m)
SW-173	180	1000/1000	700	210 → 160	1.48/1.48
SW-67	195	1500/1000	585	205	1.97/2.30

The membrane module SW-173 stability was tested with the simulated flue gas consisting of 20% CO_2, 7% O_2, 3 ppm SO_2, and balance of N_2 (on dry basis) before humidification. After humidification, as mentioned earlier, the water vapor was at 17% at 57°C. As can be seen from Fig. 49, the subject module (SW-173) showed a CO_2 permeance of around 700 GPU throughout the test. The CO_2/N_2 selectivity fluctuated around 210 until the 150th hour of test, then dropped to 160.

The membrane module SW-67 stability was tested with the simulated flue gas consisting of 20% CO_2, 3% O_2, 1 – 3 ppm SO_2, and balance of N_2 (on dry basis) before humidification. After humidification, as mentioned earlier, the water vapor was at 17% at 57°C. As can be seen from Fig. 50, the subject module (SW-67) showed a CO_2 permeance of around 590 GPU and a CO_2/N_2 selectivity of about 205 for a total test time of about 200 hours. This result indicated that the

module was reasonably stable to 3% O_2 and 1 – 3 ppm SO_2, which were the key impurities in the flue gas.

Membrane Module Field Test Results at NCCC

OSU membrane module testing at NCCC lasted from May 28th, 2015 to June 22nd, 2015. During this period, three spiral-wound modules were tested, after passing the leak test. As shown in Table 6, the three modules tested at NCCC showed repeatable results with ~ 800 GPU CO_2 permeance and ~ 200 CO_2/N_2 selectivity. Those results agreed well with the modules tested in our OSU lab. The first module (SW-154) was tested for 96 hours and showed a stable result at 820 GPU and 150 CO_2/N_2 selectivity. This module exhibited a promising 96-hour stability of performance as shown in Fig. 51; however, we stopped the test since we believed the other modules could exhibit higher CO_2/N_2 selectivity.

Table 6. Transport performances of spiral-wound membrane modules at 57°C tested at NCCC.

Module No.	Selective layer thickness (nm)	Feed/sweep flow rate (cc/min)	CO_2 permeance (GPU)	CO_2/N_2 selectivity	Feed/sweep pressure drop (psi/m)
SW-154	165	1000/1000	820	150	0.98/1.31
SW-162	145	1000/1000	800	170 → 60	0.98/1.48
SW-161	145	1000/1000	800 → 630	270 → 180	1.31/1.48

The second module (SW-162) was tested for 208 hours, and there was a flue gas shutdown for a period of 60 hours in the middle of the test. The SW-162 showed an initial CO_2 permeance of around 800 GPU and a CO_2/N_2 selectivity of 170 before the flue gas shutdown; however, the selectivity dropped to around 60 after the restart of the test following the flue gas return. Fig. 49 shows the stability plot of the membrane module SW-162 and the comparison to the membrane element SW-173 that was tested at OSU. Both the membrane modules showed a reasonably stable CO_2 permeance throughout the test and a drop of CO_2/N_2 selectivity. We believe that the insufficient curing of the glue used and the membrane indentations caused by the rough surface of the feed spacer might have introduced the leakage of the module and resulted in the CO_2/N_2 selectivity drop. The membrane indentations caused by the rough surface of the feed spacer are shown in Fig. 52 for the module SW-162. Also shown in this figure were no such indentations for the original membrane before rolling into the spiral-wound module configuration.

The third module (SW-161) was tested for 200 hours, and there was a flue gas shutdown for a period of 48 hours in the middle of the test. The SW-161 with a longer glue curing time showed reasonably stable selectivity of 180 – 270 for 200 hours. Fig. 50 shows the stability plot of the membrane module SW-161 and the comparison to the membrane module SW-67 that had a similar longer glue curing and was tested at OSU. Both the membrane modules showed a reasonably

stable CO_2/N_2 selectivity throughout the test, with the exception of the drop of CO_2/N_2 selectivity after the restart of the test following the flue gas return (after its shutdown) for the module SW-161 at NCCC. However, this selectivity after the flue gas shutdown was stabilized at about 180, which is still very high. This module showed an initial CO_2 permeance of around 800 GPU; however, the CO_2 permeance dropped to ~ 630 GPU after the restart of the test following the flue gas return. This permeance drop was presumably due to the feed gas bypass caused by the glue failure, which was indicated by the change of epoxy glue color from gray to green-yellowish after 208 hours of test. After the NCCC testing, we further improved glue curing with a longer curing time and eliminated membrane indentations using a layer of a fine, smooth polymer spacer incorporated between the feed spacer and the selective polymer layer.

Table 6 also shows the results of the pressure drops for the feed and sweep sides measured from the three spiral-wound membrane modules tested at NCCC. As shown in this table, all the pressure drops measured were lower than 1.5 psi/m, which is very desirable.

Overall, the membrane module results obtained at NCCC achieved the same level of performance as compared to our OSU lab test results with the simulated flue gas. The modules showed about 800 GPU permeance and about 200 selectivity as well as a pressure drop of less than 1.5 psi/m. In other words, the results showed that the modules tested at NCCC behaved similarly to those in the OSU lab, indicating a great potential of the membrane modules for CO_2 capture from flue gas in power plants.

4.9 System and Cost Analysis

Refining of system and cost analysis was carried out by Gradient Technology with the collaboration of two Ph.D. students from our OSU team. Gradient Technology essentially focused on refining the techno-economic analysis by incorporating SO_2 removal equipment for the SO_2 polishing step, membrane installation cost and process contingency. The overall techno-economic analysis was updated using the new quotes obtained from the vendors and membrane results obtained at OSU. Comprehensive cost sensitivity studies were carried out.

Cost sensitivity studies were carried out based on the updated economic model and the NETL report [30]. "Cost (in 2007 dollar)/tonne of CO_2 removed" along with "Increase in the Cost of Electricity (COE)" was used as the economic indicative unit for the techno-economic evaluations. Fig. 53 shows the economic sensitivity of our system with CO_2 permeance at 1.5 atm as the Stage 1 feed gas pressure and 150 torr as the Stage 1 permeate pressure. The increase in the COE (%) and $ (2007)/tonne of CO_2 removed were estimated. Fig. 54 depicts the cost sensitivity in terms of $ (2007)/tonne of CO_2 removed vs. the CO_2/N_2 selectivity at the Stage 1 feed gas pressure of 1.5 atm and the Stage 1 permeate pressure of 150 torr. Stage 1 feed pressure and Stage 1 permeate pressure were required to be optimized to reach a globally optimized Stage 1 pressure. Figs. 55 and 56 show the effect of Stage 1 feed pressure and Stage 1 permeate pressure on the overall cost, respectively, with 1100 GPU of CO_2 permeance and 140 CO_2/N_2 selectivity. It should be noted that the membrane installation labor cost and process contingency were not included in the costs as shown in Figs. 53 and 54.

Gradient Technology executed a total of ten cases utilizing the Aspen Plus model. These case studies included the membrane installation cost, process contingency (20%), and other minor items as recommended by NETL. The results of these ten cases in 2007 dollar are summarized below in Table 7. It should be noted that although the membrane installation labor and process contingency (20%) as well as the cost of the SO_2 polishing step were included, but the costs were not fully optimized.

	Case A	**Case B**	**Case C**	**Case D**	**Case E**	**Case F**	**Case G**	**Case H**	**Case I**	**Case J**
Flue Gas Pressure (atm)	1.5	1.5	1.5	1.5	1.5	1.5	1.5	1.5	1.75	2.0
Membrane 1										
Permeate Pressure (torr)	150	150	150	150	150	150	150	150	150	150
CO_2 Permeance (GPU)	800	820	850	800	820	850	900	1100	1100	1100
H_2O:CO_2 Selectivity	1	1	1	1	1	1	1	1	1	1
CO_2:N_2 Selectivity	170	170	170	140	140	140	170	170	170	170
H_2O Permeance (GPU)	800	820	850	800	820	850	900	1100	1100	1100
N_2 Permeance (GPU)	4.7	4.8	5.0	5.7	5.9	6.1	5.3	6.5	6.5	6.5
SO_x and NO_x Permeance (GPU)	0	0	0	0	0	0	0	0	0	0
Membrane 2										
Air Sweep (%)	80	80	80	80	80	80	80	80	80	80
Air Sweep Gas Pressure (atm)	1.05	1.05	1.05	1.05	1.05	1.05	1.05	1.05	1.05	1.05
CO_2 Permeance (GPU)	800	820	850	2000	2000	2000	900	1100	1100	1100
H_2O:CO_2 Selectivity	1	1	1	1	1	1	1	1	1	1
CO_2:N_2 Selectivity	170	170	170	25	25	25	170	170	170	170
H_2O Permeance (GPU)	800	820	850	2000	2000	2000	900	1100	1100	1100
N_2 Permeance (GPU)	4.7	4.8	5.0	80.0	80.0	80.0	5.3	6.5	6.5	6.5
SO_x and NO_x Permeance (GPU)	0	0	0	0	0	0	0	0	0	0
Turboexpander	Yes	Yes	Yes	Yes	Yes	Yes	Yes	Yes	Yes	Yes
COE Increase (%)	76.0%	75.5%	74.9%	71.9%	71.8%	71.6%	73.9%	70.8%	71.9%	72.2%
Capture cost ($/tonne)	54.1	53.7	53.3	50.9	50.8	50.6	52.6	50.4	50.5	51.5

Table 7. The summary of the case studies incorporating the cost of the SO_2 polishing step, membrane installation cost, and process contingency in 2007 dollar.

To compare the capture cost to the $40/tonne target in 2007 dollar set by DOE, the capture costs in 2007 dollar were calculated and optimized by OSU. The costs for the SO_2 polishing, membrane installation, and process contingency were included in the cost calculations. Two types of membrane were employed: (1) amine-containing membrane with a CO_2 permeance of 1100 GPU and a CO_2/N_2 selectivity of 140 and (2) polyethyleneoxide-containing membrane with a permeance of 2000 GPU and a selectivity of 20. The calculation results are shown in Table 8 [31]. When the amine-containing membrane was used for both membrane stages (Case C in Table 8), the capture cost was $41.6/tonne. If the second membrane stage was replaced by the

polyethyleneoxide-containing membrane (Case F in Table 8), the optimized capture cost could be reduced to $40.1/tonne, which is very close to the DOE target in 2007 dollar. This DOE target can be met or even a lower capture cost of less than $40/tonne CO_2 (in 2007 dollar) can be achieved with further membrane improvements including higher CO_2 permeance, thinner membrane thickness, and higher performance membrane material.

	Case A	Case B	Case C	Case D	Case E	Case F
Flue Gas Pressure (atm)	1.5	1.7	2.1	1.5	1.7	2.1
Membrane 1						
Permeate Pressure (torr)	150	150	150	150	150	150
CO_2 Permeance (GPU)	1100	1100	1100	1100	1100	1100
CO_2:N_2 Selectivity	170	170	170	170	170	170
Membrane 2						
Air Sweep (%)	80	80	80	80	80	80
Air Sweep Gas Pressure (atm)	1.05	1.05	1.05	1.05	1.05	1.05
CO_2 Permeance (GPU)	1100	1100	1100	2000	2000	2000
CO_2:N_2 Selectivity	170	170	170	25	25	25
Turboexpander	Yes	Yes	Yes	Yes	Yes	Yes
Capture cost ($/tonne)	50.1	44.7	41.6	46.7	42.5	40.1

Table 8. The summary of the case studies calculated by OSU in 2007 dollar.

Gradient Technology completed the conversion of the economic model to the June 2011 basis and was based on the NETL report, *Updated Costs (June 2011 Basis) for Selected Bituminous Baseline Cases*, August 2012, DOE/NETL-341/082312 [32]. Gradient Technology recalculated the capture costs of the cases listed in Table 7 (in 2007 basis). The results in 2011 dollar are summarized in Table 9. It should be noted that the membrane installation labor and process contingency as well as the cost of the SO_2 polishing step were included, but the capture cost could be further optimized by adjusting the feed and vacuum pressures. OSU calculated a parallel techno-economic analysis for the membrane system in subject. Although the capture cost was evaluated in 2007 dollar, the results showed that a higher feed-to-permeate pressure ratio could reduce the capture cost when the membrane installation cost was added. For instance, increasing the feed pressure from 1.5 atm to 1.6 atm could reduce the capture cost by $1/tonne CO_2 for 1100 GPU membrane (see Table 8). Such effect was more significant when the permeance was lower (i.e., the total membrane area was larger). An elevated feed pressure reduced the capture costs for 700 and 900 GPU membranes by $3.5 and $2/tonne CO_2, respectively. Therefore, the optimal capture cost incorporated with the membrane installation cost should be further studied. Regarding the 20% process contingency, it is recommended by NETL, but could be overestimated for a membrane process. In taking the mature membrane technologies, for example, reverse osmosis plants with a membrane area of > 1 million m^2 have been constructed [33], and an average 4 – 5 years of membrane life has been demonstrated also in natural gas sweetening [34]. These membrane plants are typically designed in service for 15 – 20 years, and a 5% – 8%

contingency is assigned [35]. Consequently, the CO_2 capture cost with the 20% process contingency could be a very conservative estimation.

	Case A	Case B	Case C	Case D	Case E	Case F	Case G	Case H	Case I	Case J
Flue Gas Pressure (atm)	1.5	1.5	1.5	1.5	1.5	1.5	1.5	1.5	1.75	2.0
Membrane 1										
Permeate Pressure (torr)	150	150	150	150	150	150	150	150	150	150
CO_2 Permeance (GPU)	800	820	850	800	820	850	900	1100	1100	1100
H_2O:CO_2 Selectivity	1	1	1	1	1	1	1	1	1	1
CO_2:N_2 Selectivity	170	170	170	140	140	140	170	170	170	170
H_2O Permeance (GPU)	800	820	850	800	820	850	900	1100	1100	1100
N_2 Permeance (GPU)	4.7	4.8	5.0	5.7	5.9	6.1	5.3	6.5	6.5	6.5
SO_x and NO_x Permeance (GPU)	0	0	0	0	0	0	0	0	0	0
Membrane 2										
Air Sweep (%)	80	80	80	80	80	80	80	80	80	80
Air Sweep Gas Pressure (atm)	1.05	1.05	1.05	1.05	1.05	1.05	1.05	1.05	1.05	1.05
CO_2 Permeance (GPU)	800	820	850	2000	2000	2000	900	1100	1100	1100
H_2O:CO_2 Selectivity	1	1	1	1	1	1	1	1	1	1
CO_2:N_2 Selectivity	170	170	170	25	25	25	170	170	170	170
H_2O Permeance (GPU)	800	820	850	2000	2000	2000	900	1100	1100	1100
N_2 Permeance (GPU)	4.7	4.8	5.0	80.0	80.0	80.0	5.3	6.5	6.5	6.5
SO_x and NO_x Permeance (GPU)	0	0	0	0	0	0	0	0	0	0
Turboexpander	Yes	Yes	Yes	Yes	Yes	Yes	Yes	Yes	Yes	Yes
COE Increase (%)	64.9%	64.6%	64.1%	62%	62%	62%	63%	61%	63%	65%
Capture cost ($/tonne)	63.3	63.0	62.5	60.4	60.3	60.2	61.8	59.7	60.3	61.7

Table 9. The summary of the case studies after incorporating SO_2 polishing step, membrane installation cost, and process contingency in 2011 dollar.

Furthermore, Gradient Technology and OSU compiled a response summary to the NETL comments on the techno-economic analysis (TEA) report of Budget Period 2. Gradient Technology has taken all of the NETL comments into account for the final report of the TEA.

In addition, a new membrane process was designed by the OSU team without using air sweep for the second membrane stage. The process is sketched in Fig. 57. The two membrane stages form an enriching cascade. The CO_2 is separated from the flue gas sequentially by the first and second membrane stages, and is eventually enriched to > 95%. The highlight of this process design is that a portion of the retentate (mainly N_2) of the first stage is recycled as its own sweep gas. This increases the transmembrane driving force of the first stage and reduces the N_2 loss from the feed to the sweep side. Consequently, the membrane area and energy consumption are reduced.

Initial techno-economic analysis shows that the optimal operation conditions are reached at 20% retentate recycle. The effect of CO_2 permeance on the capture cost of this process is shown in Fig. 58. A CO_2/N_2 selectivity of 140 was used in the calculations, and the equipment was cost in 2007 dollar. Also shown in this figure are the capture costs of the air sweep process. As seen, the retentate recycle process performs slightly better than the air sweep process when the CO_2 permeance is lower than 900 GPU. At a higher permeance, the air sweep process shows a lower capture cost, but the difference between these two processes is not huge. For instance, the air sweep process gives a capture cost of \$37.5/tonne CO_2 at 1100 GPU, while \$38.5/tonne CO_2 for the retentate recycle process. More importantly, the retentate recycle process avoids some shortcomings of using air sweep in a membrane process. Firstly, there is no need to modify the combustion air system of the existing power plant, by which the capital cost of retrofitting the existing ductwork is avoided. Secondly, the restriction of using only the secondary air as sweep gas is removed. Therefore, the flow rate of the sweep gas does not affect the power plant operation. Lastly, the reduced O_2 content encountered in the CO_2 laden air is avoided, thus the boiler efficiency is not affected.

4.10 Environmental Health and Safety Assessment (EH&S)

An Environmental Health and Safety (EH&S) assessment was conducted by Gradient Technology to assess the environmental friendliness and safety of any future process based on the materials and process being researched in this project. The proposed 2-stage membrane process was evaluated for EH&S issues, including air and particulate emissions and solid and liquid waste streams.

Compared to a 550 MW pulverized coal power plant without carbon capture, the CO_2 emissions were reduced by 90%. The particulate emissions were either not affected or slightly reduced by the addition of the carbon capture system. The SOx and NOx emissions were mitigated to a level of <10 ppm because of the SO_2 polishing step associated with the carbon capture system. Other contaminants, including mercury, arsenic, and selenium, etc., were not affected by the carbon capture system.

The liquid waste primarily comprises the capture combustion water from the flue gas, which was estimated as 1.357×10^6 tonne/year. In addition, the hazardous liquid waste generated by the SO_2 polishing system was estimated to be 10,865 tonnes/year, and it is disposed of using a licensed hazardous waste treatment facility. The key component in the hazardous liquid waste generated is the reaction product of NaOH and SO_2, i.e., Na_2SO_3. Na_2SO_3 is a common commercially chemical. The cooling water was not treated as a liquid effluent since it was fully recycled.

No solid waste is generally disposed of in this membrane process. At some point in the life cycle of the process, the CO_2 separation membrane modules will be removed and replaced. The constituents of the membrane modules in themselves are not toxic or reactive.

5 Accomplishments

The accomplishments of the project are summarized below:

Approach 1: Composite Membrane Scaled up and Prototype Membrane Modules Fabricated and Tested

- PES polymer support scaled up to 14" wide for >2500 feet.
- 40 nm ZY particles successfully synthesized for scale-up deposition.
- ZY deposition scaled up to 14" wide for ~800 feet.
- Composite membrane scaled up to 14" wide for ~800 feet
- 870 GPU of CO_2 permeance with 218 CO_2/N_2 selectivity obtained in flat-sheet membrane at 57^oC from lab test
- About 100 of ~2" diameter by 14" long spiral-wound membrane elements / modules fabricated using the rolling machine
- 820 GPU of CO_2 permeance with ~200 CO_2/N_2 selectivity obtained from membrane modules at 57^oC from lab test
- Membrane module stable to 1 – 3 ppm SO_2, 3% O_2 and 17% H_2O for 200-h test conducted in the lab
- Effects of SO_2 and CO_2/SO_2 mixture on amine carriers studied by in-situ FTIR
- SO_2 permeated with CO_2 through the membrane
- Amines were regenerated by air sweep at 57^oC, which was confirmed by in-situ FTIR
- 810 GPU of CO_2 permeance with ~200 CO_2/N_2 selectivity obtained at 57^oC from membrane module testing with real flue gas at the National Carbon Capture Center (NCCC) in Wilsonville, AL; the flue gas contained 0.5 – 5 ppm SO_2, 1.5 – 4 ppm NO_2, 6.6 – 8% O_2 and 17% H_2O
- Membrane modules tested at NCCC behaved similarly to those in OSU Lab
- Repeatable results from 3 membrane modules tested at NCCC
- Good dissemination of the project results to communities of interest, including 2 issued U. S. patents, 5 U. S. patent applications, 17 journal papers, 9 plenary / keynote lectures, and 40 invited presentations

Approach 2: Rapid Zeolite Membrane Growth Achieved

- Bendable zeolite membrane synthesized within PES support and roll-to-roll processing shown in lab
- >2000 GPU CO_2 permeance with ~40 CO_2/N_2 selectivity achieved with dry gas mixture at 25^oC
- Two papers published in *Langmuir* and 3 other journal papers

In addition, techno-economic analyses were conducted in both 2007 dollar and 2011 dollar and an EH&S assessment was developed by Gradient Technology.

6 Conclusions

A cost-effective design and manufacturing process for new membrane modules that capture CO_2 from flue gas in coal-fired power plants was developed. The membrane consisted of a thin selective layer including zeolite-Y nanoparticles embedded in the nanoporous polyethersulfone (PES) structure so that it can be made in a continuous manufacturing process. The membrane was successfully incorporated in spiral-wound modules for the field test with actual flue gas at the National Carbon Capture Center (NCCC) in Wilsonville, AL and bench scale tests with simulated flue gas at the Ohio State University (OSU).

The PES substrates were fabricated both at the lab scale and the pilot scale. ZY nanoparticles with an average particle size of 40 nm were synthesized and deposited onto the nanoporous PES supports using the vacuum-assisted dip-coating technique developed at OSU in lab scale and pilot scale. For the amine-containing polymer cover layer, a high molecular weight polyamine was synthesized and incorporated with different kinds of mobile carriers. The lab-scale CO_2 permeance reached 1100 GPU with a CO_2/N_2 selectivity of > 200 at 57°C for the amine-containing polymer cover layer on ZY composite membrane (Approach 1). The scale-up amine-containing polymer cover layer on ZY composite membrane showed a CO_2 permeance of 870 GPU and a CO_2/N_2 selectivity of 218 at 57°C. At 102°C, the scale-up composite membrane showed a CO_2 permeance of 1800 GPU and a CO_2/N_2 selectivity of 160. Spiral-wound membrane modules were successfully prepared by using the scale-up composite membrane. The spiral-wound membrane modules demonstrated up to 820 GPU of CO_2 permeance and > 150 CO_2/N_2 selectivity with simulated flue gas. The membrane modules showed > 800 GPU of CO_2 permeance and > 150 CO_2/N_2 selectivity when tested with real flue gas at NCCC. The performance of the modules agreed reasonably well with the pilot-scale membranes. The influence of SO_2 on membranes was characterized extensively by in-situ infrared spectroscopy.

Gradient Technology conducted the techno-economic analysis of the proposed 2-stage membrane process for CO_2 capture from flue gas in conjunction with the membrane transport model developed by OSU. The techno-economic analysis was carried out for a cost-sensitivity study with respect to membrane performance and operating conditions. For the membrane performance with a CO_2 permeance of 1100 GPU and a CO_2/N_2 selectivity of > 200 based on the present ZY/polymer composite membrane with the amine-containing polymer cover layer on the ZY seed layer/PES substrate (Approach 1) synthesized in the lab, the preliminary techno-economic analysis showed a capture cost of about \$50.4/tonne CO_2 captured (in 2007 dollar), which was not optimized. The optimized result by OSU gave a capture cost of about \$40.1/tonne CO_2 captured (in 2007 dollar), which nearly meets the DOE target of \$40/tonne CO_2 captured. This DOE target can be met or even a lower capture cost of less than \$40/tonne CO_2 can be achieved with further membrane improvements including higher CO_2 permeance, thinner membrane thickness, and higher performance membrane material. The proposed technology will become available for the

cost-effective capture of CO_2 from coal-fired power plants. The developed membrane modules can be applied in the existing and new coal-fired power plants.

For Approach 2, a continuous zeolite Y membrane of about 250 nm thickness was synthesized on the PES polymer support within 60 minutes. Intercrystalline defects on the membrane were sealed with polydimethylsiloxane (PDMS), and transport properties of such membranes were examined. The performance of these membranes using dry feed gas was comparable to zeolite membranes grown on ceramic supports, which typically take much longer to form.

An Environmental Health and Safety (EH&S) assessment was conducted by Gradient Technology to assess the EH&S issues, including air and particulate emissions and solid and liquid waste streams. Compared to the baseline pulverized coal power plant, the CO_2 and SOx emissions were largely mitigated, and the other gas contaminants were not affected. The primary liquid wastes were the captured water from the flue gas and the spent NaOH-SO_2 solution, i.e., Na_2SO_3, from the SO_2 polishing step. Na_2SO_3 is a common commercially chemical. The replaced membrane modules were treated as a solid waste, which itself is not toxic and reactive. Other than the membrane modules, no other solid waste was generated in the membrane process.

7 Graphical Materials List

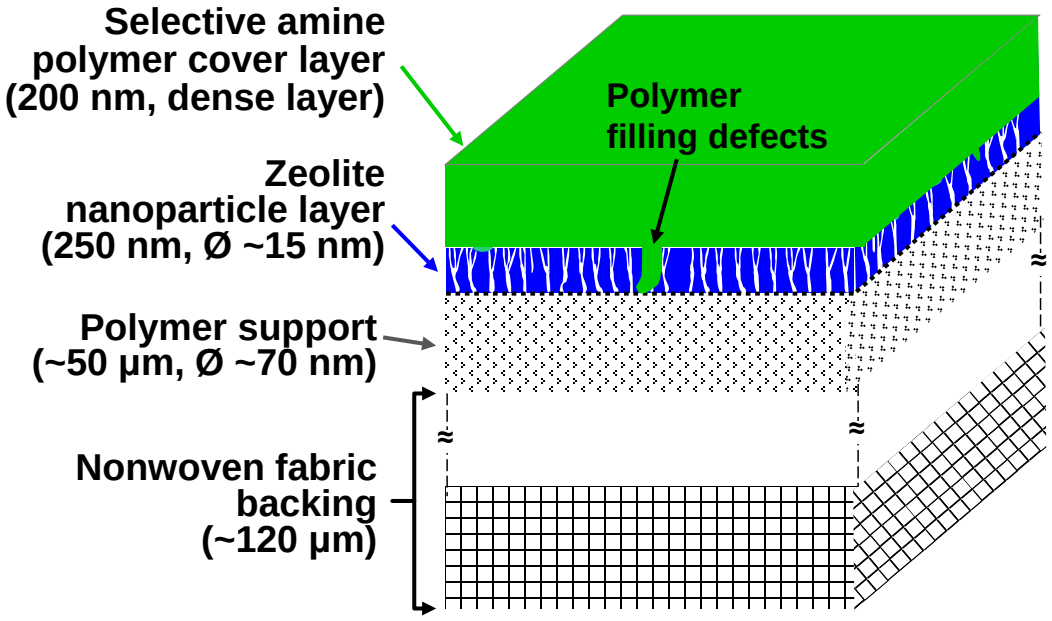

Fig. 1. Schematic of Membrane Approach 1 consisting of a selective amine-containing polymer cover layer on zeolite nanoparticles embedded in polymer support.

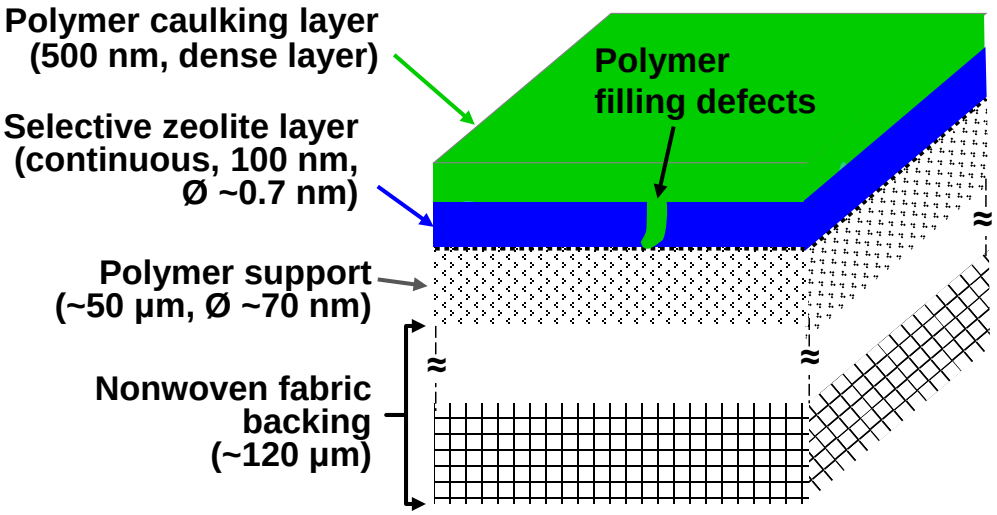

Fig. 2. Schematic of Membrane Approach 2 comprising a polymer caulking layer on the selective zeolite membrane grown on polymer support.

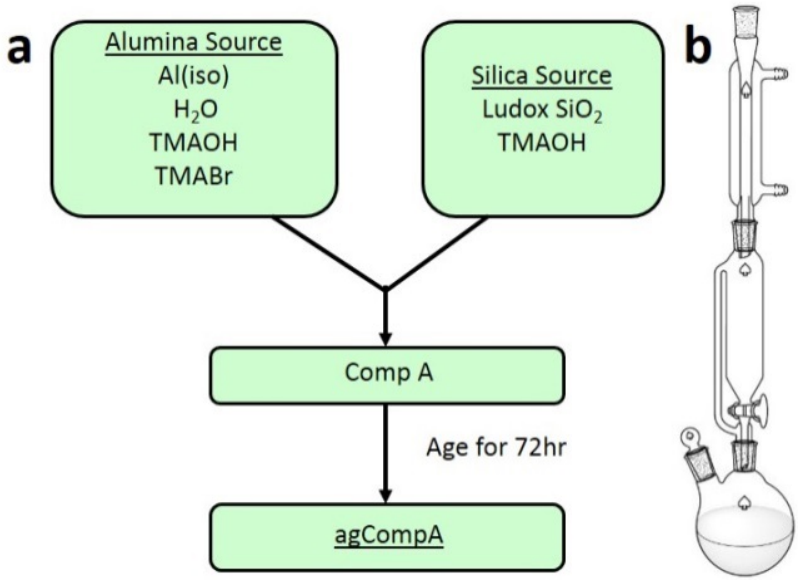

Fig. 3. (a) Flowchart illustration on composition preparation and (b) DRHT apparatus.

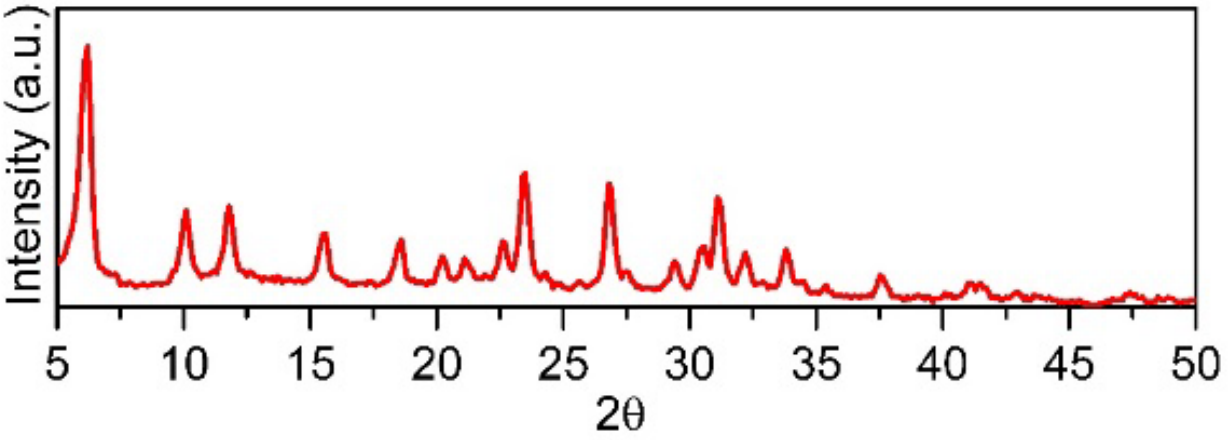

Fig. 4. XRD pattern of nano zeolite particles.

.

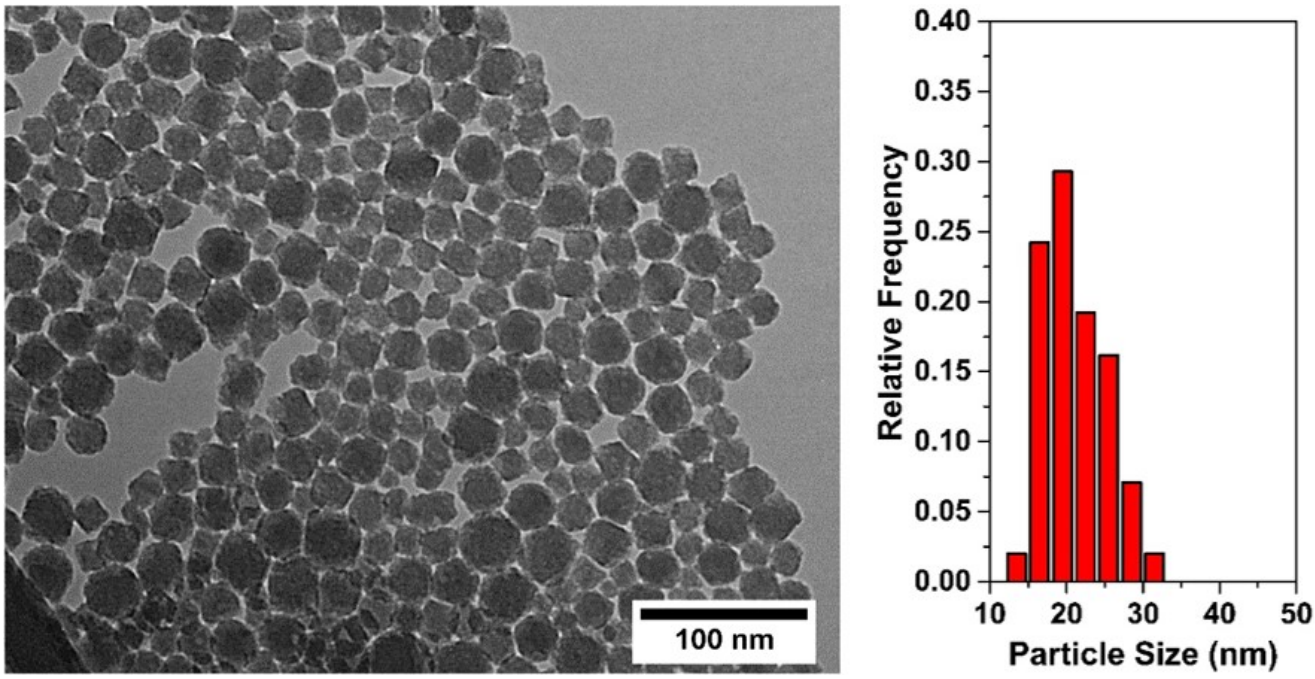

Fig. 5. TEM image and particle size distribution.

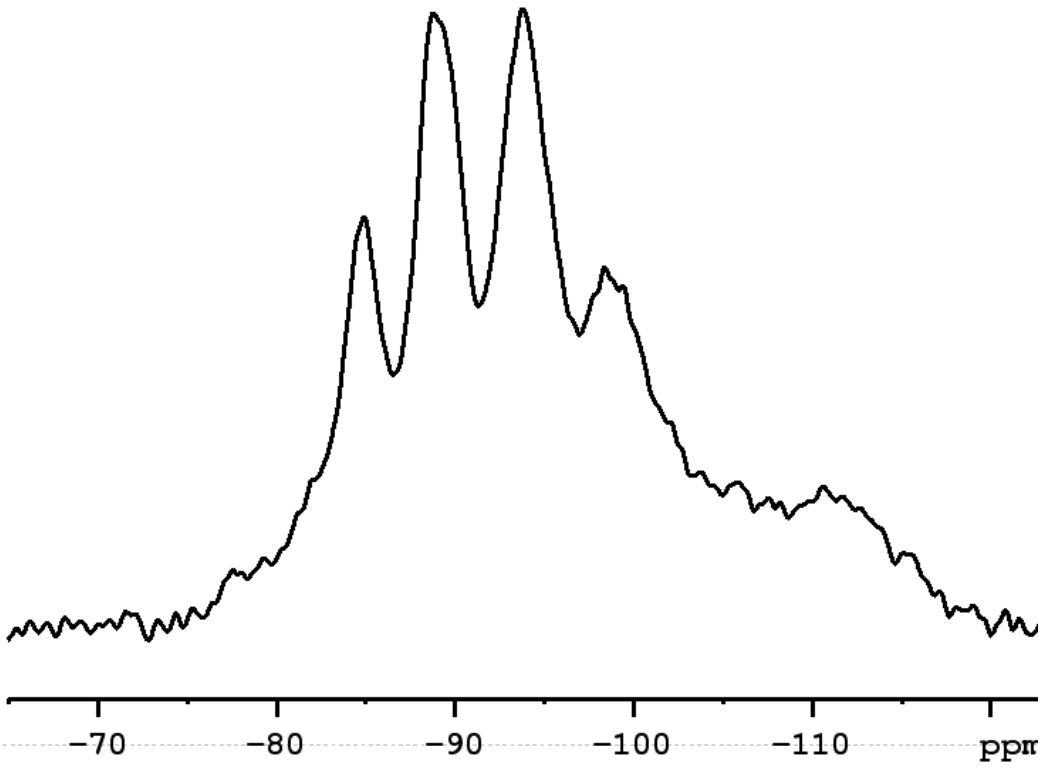

Fig. 6. ^{29}Si NMR spectra of nano zeolite final product.

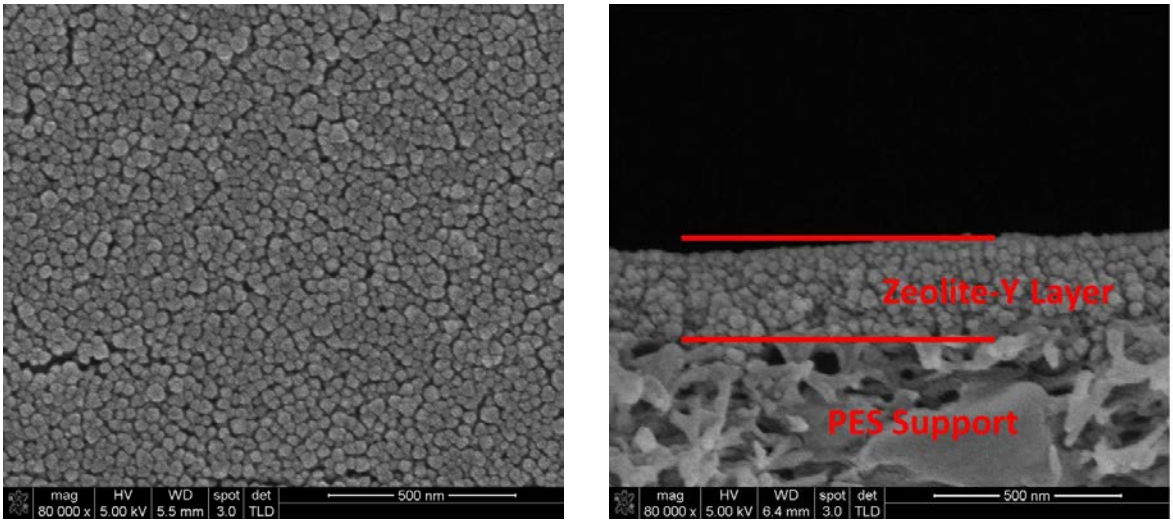

(a) (b)

Fig. 7. SEM images of scale-up ZY deposition on scale-up PES support: (a) surface and (b) cross section.

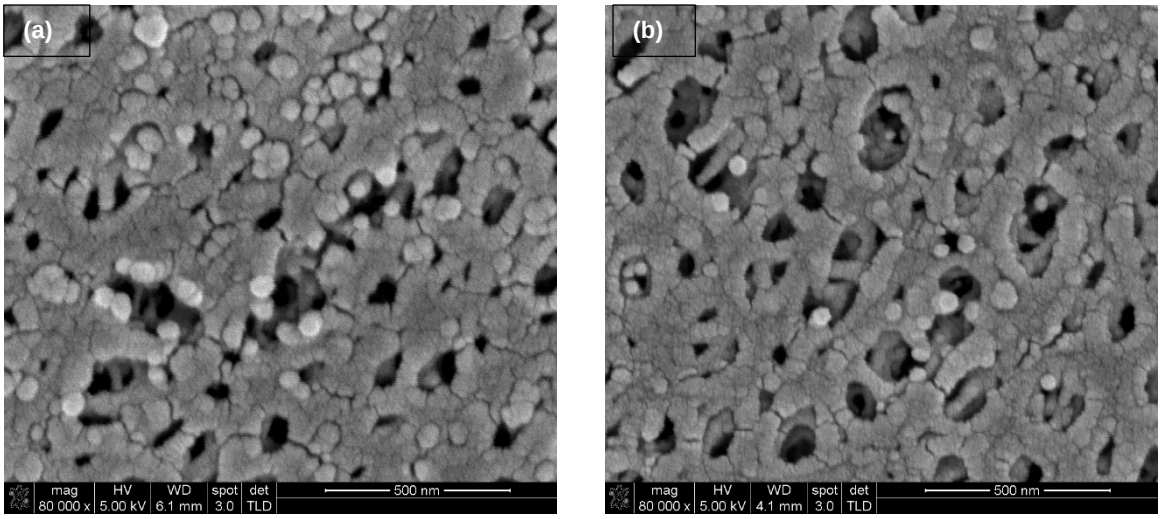

Fig. 8. SEM images of the surfaces of the pore-filling ZY deposition samples with two ZY dispersion concentrations: (a) low ZY dispersion concentration and (b) very low ZY dispersion concentration.

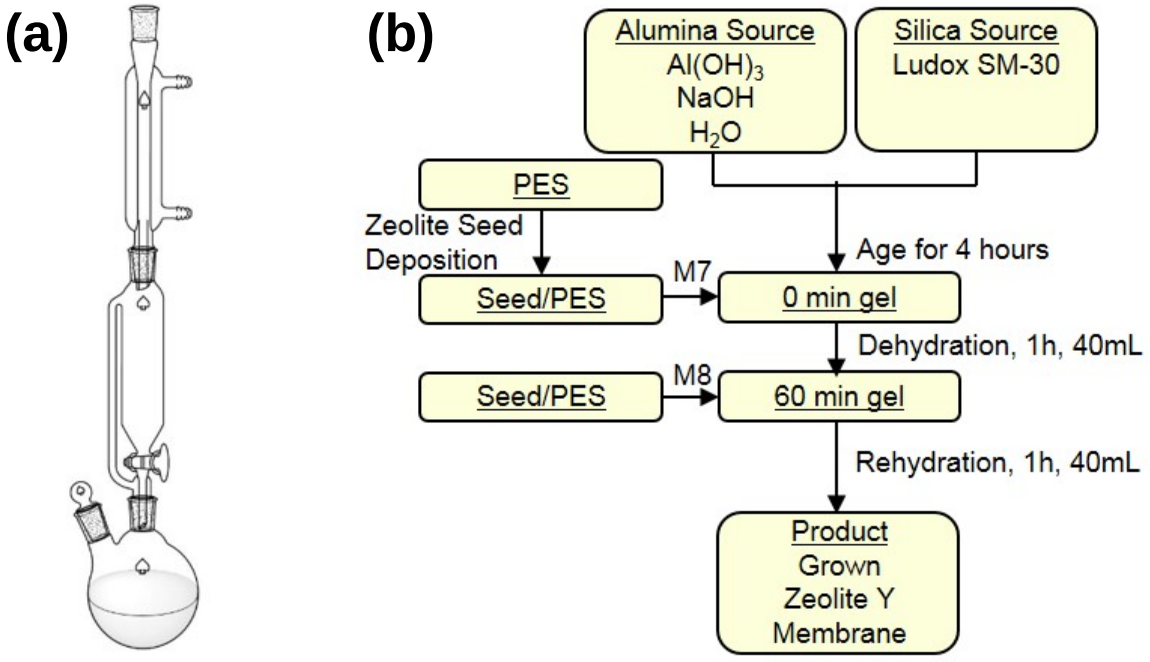

Fig. 9. (a) Reactor of zeolite membrane and (b) Schematic of secondary growth procedure.

Fig. 10. The continuous membrane coating machine with thin-film casting assembly at OSU.

Fig. 11. The continuous casting machine for the fabrication of nanoporous polymer supports at OSU.

Fig. 12. The continuous casting machine for the fabrication of nanoporous polymer supports at OSU (with fume hood curtains open to show the casting trough and knife).

Fig. 13. PES fabricated using the continuous casting machine.

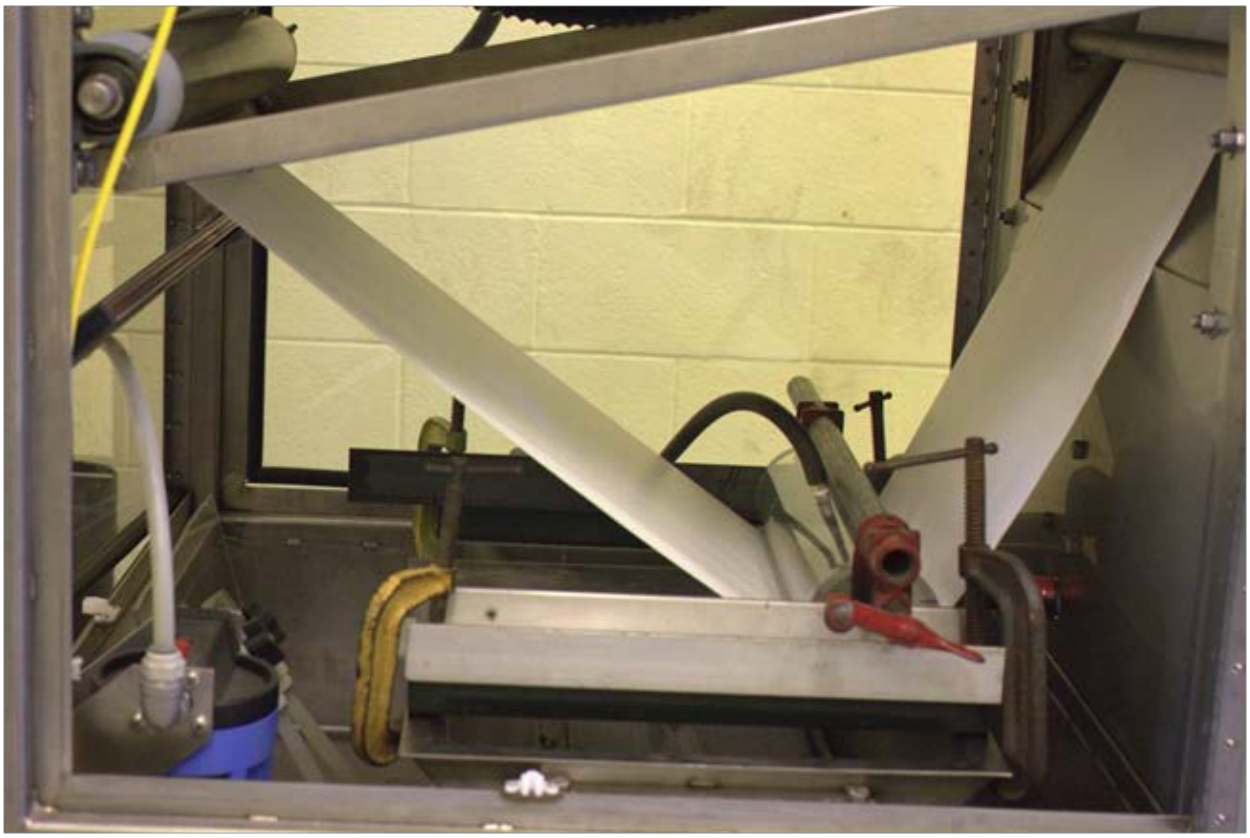

Fig. 14. Pilot-scale vacuum-dip coating for ZY deposition.

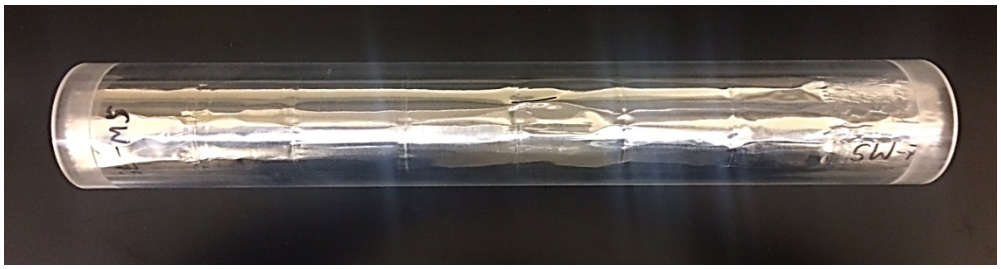

Fig. 15. Spiral-wound membrane element fabricated.

Fig. 16. Spiral-wound membrane module consisting of the membrane element inside a housing.

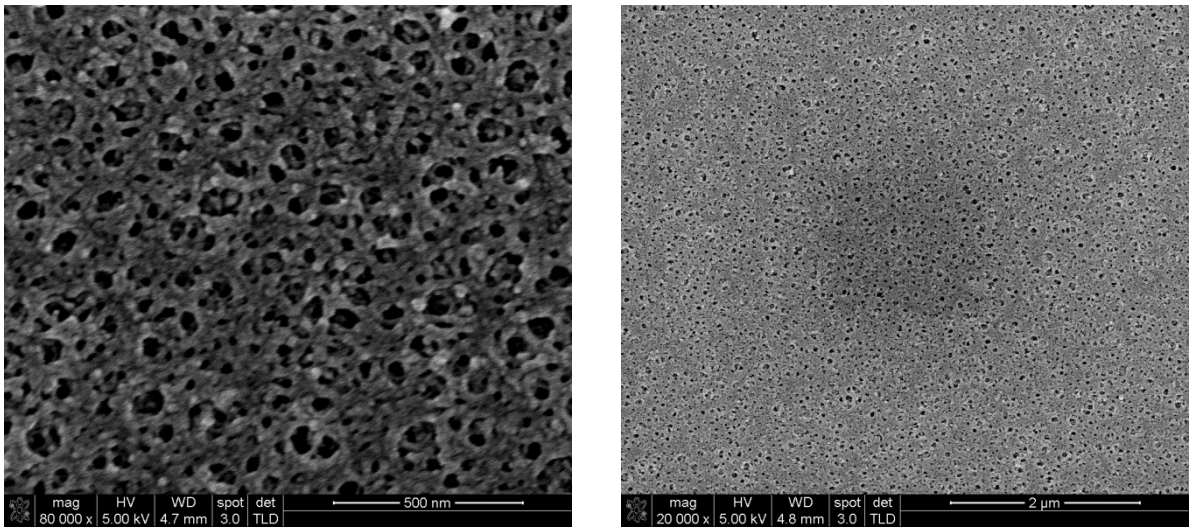

(a) (b)

Fig. 17. SEM images of lab-fabricated PES support prepared with exposure to 75% relative humidity: (a) large magnification and (b) small magnification.

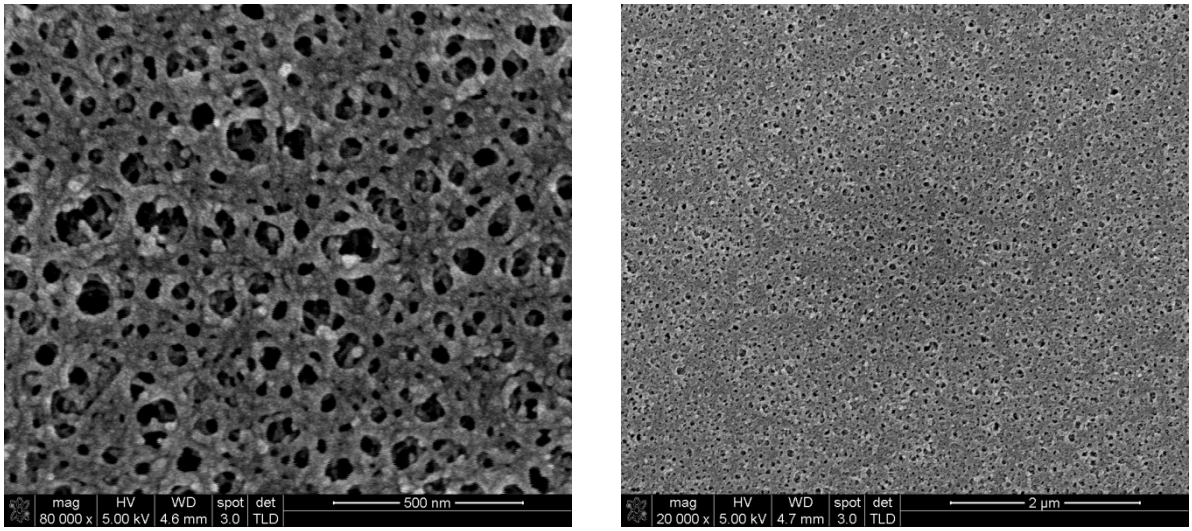

(a) (b)

Fig. 18. SEM images of lab-fabricated PES support prepared with exposure to 85% relative humidity: (a) large magnification and (b) small magnification.

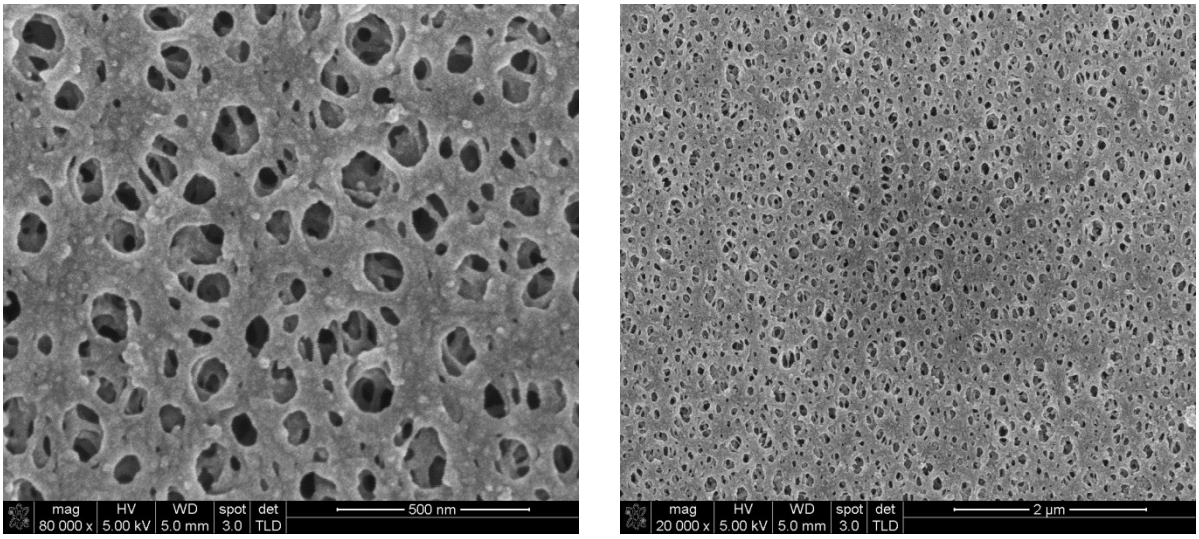

(a) (b)

Fig. 19. SEM images of scale-up PES support prepared with high PES concentration: (a) large magnification and (b) small magnification.

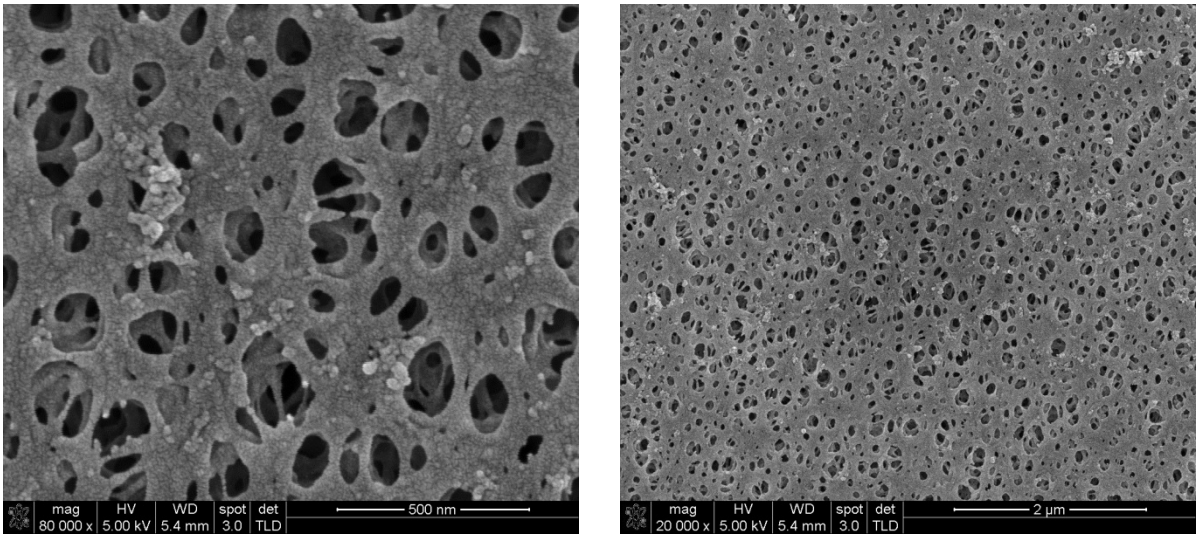

(a) (b)

Fig. 20. SEM images of scale-up PES support prepared with intermediate PES concentration: (a) large magnification and (b) small magnification.

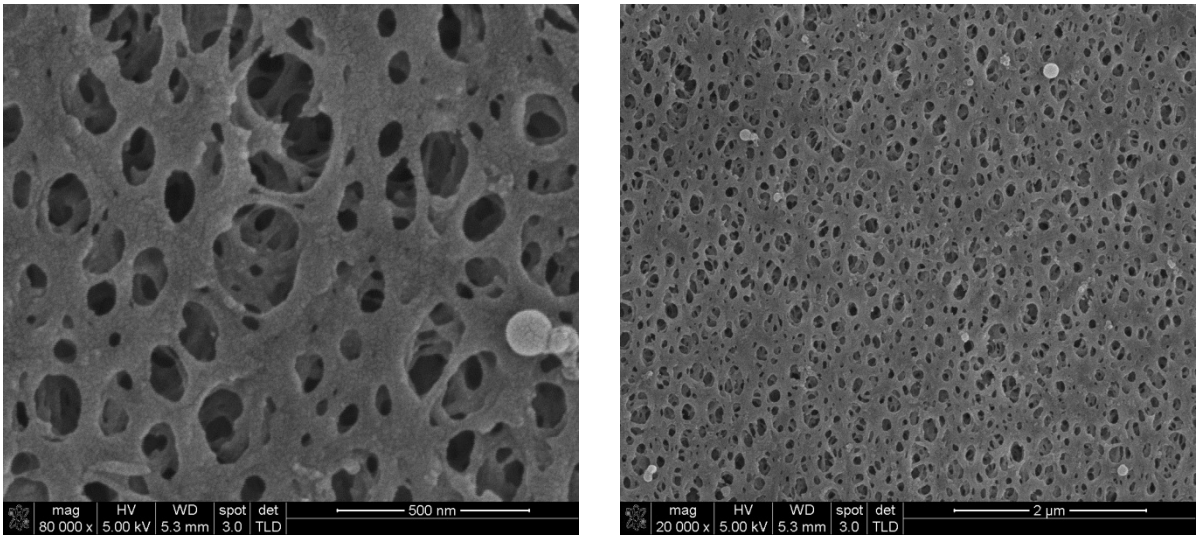

(a) (b)

Fig. 21. SEM images of scale-up PES support prepared with low PES concentration: (a) large magnification and (b) small magnification.

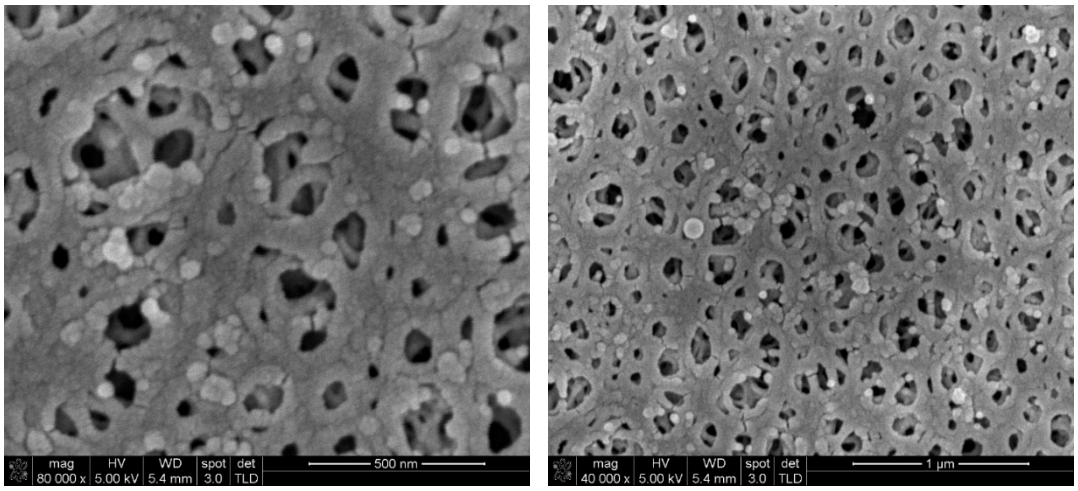

a) Surface morphology of PES substrate from Row 1 in Table 3 (~ 65.3 nm and 16.8%).

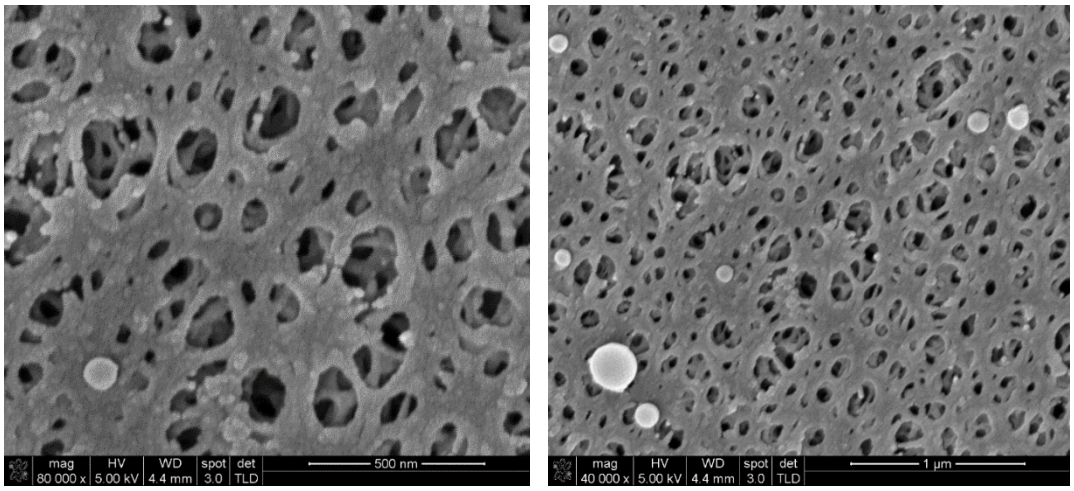

b) Surface morphology of PES substrate from Row 2 in Table 3 (~ 69.7 nm and 17.2%).

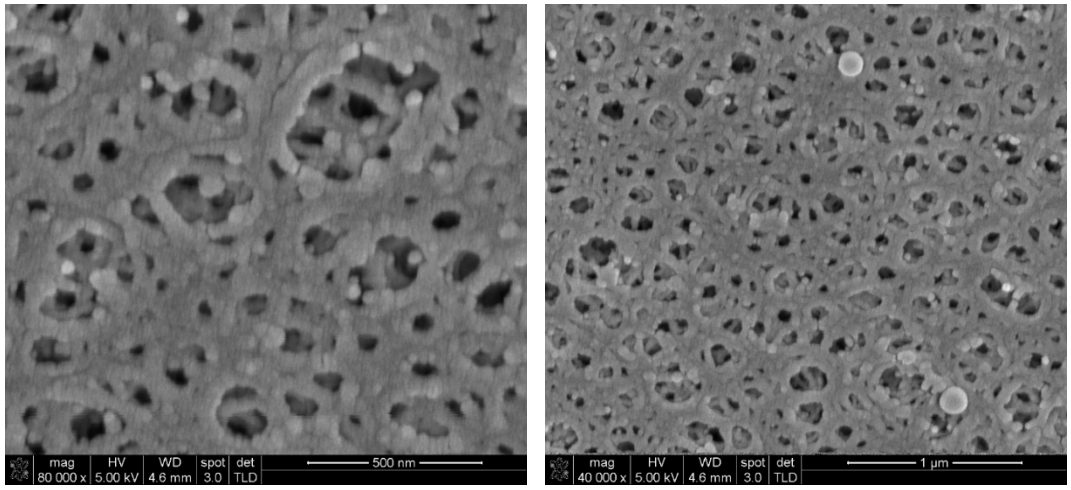

c) Surface morphology of PES substrate from Row 3 in Table 3 (~ 69.7 nm and 17.3%).

Fig. 22. Surface morphology of PES substrates.

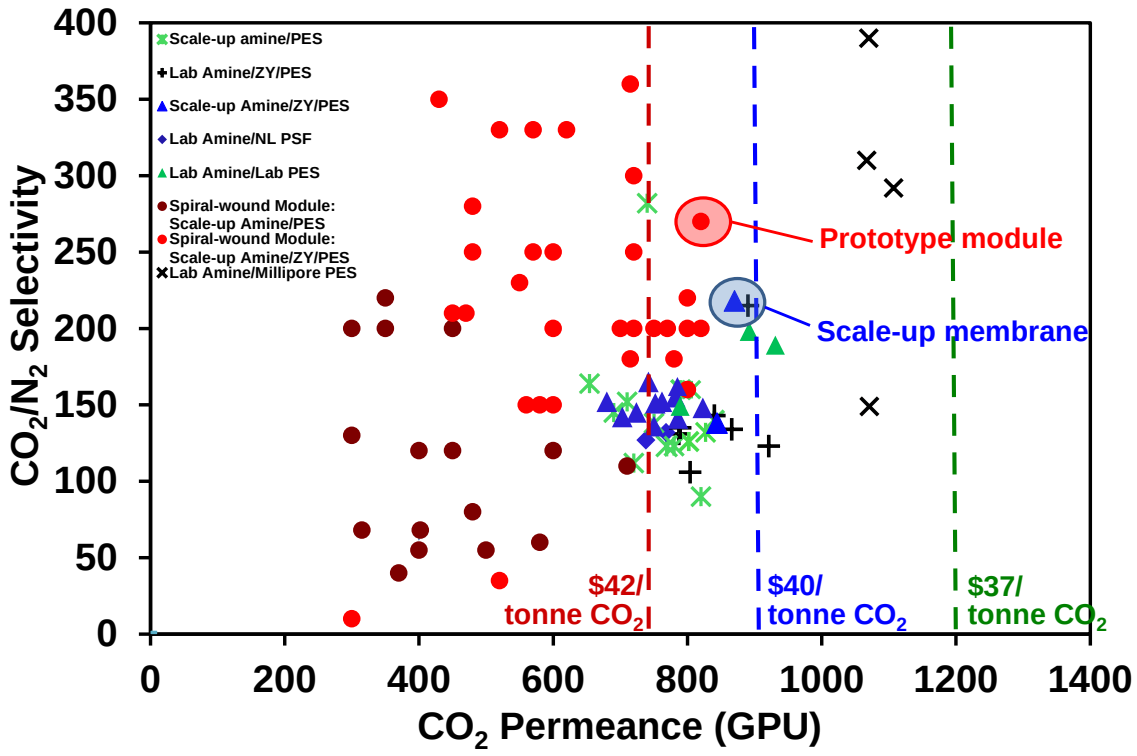

Fig. 23. Transport performances of scale-up and lab-scale flat-sheet membranes and spiral-wound membrane modules at 57°C.

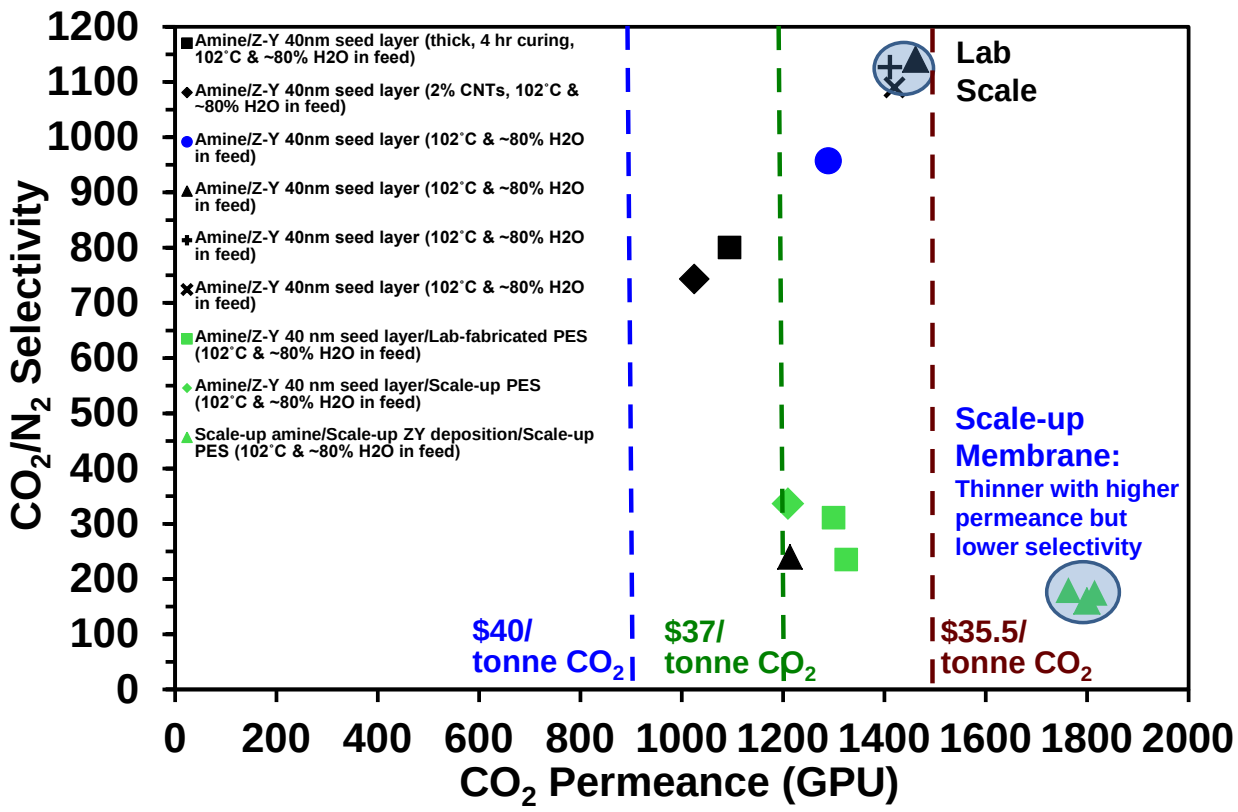

Fig. 24. Transport performances of membranes with the amine-containing polymer cover layer on different substrates at 102°C.

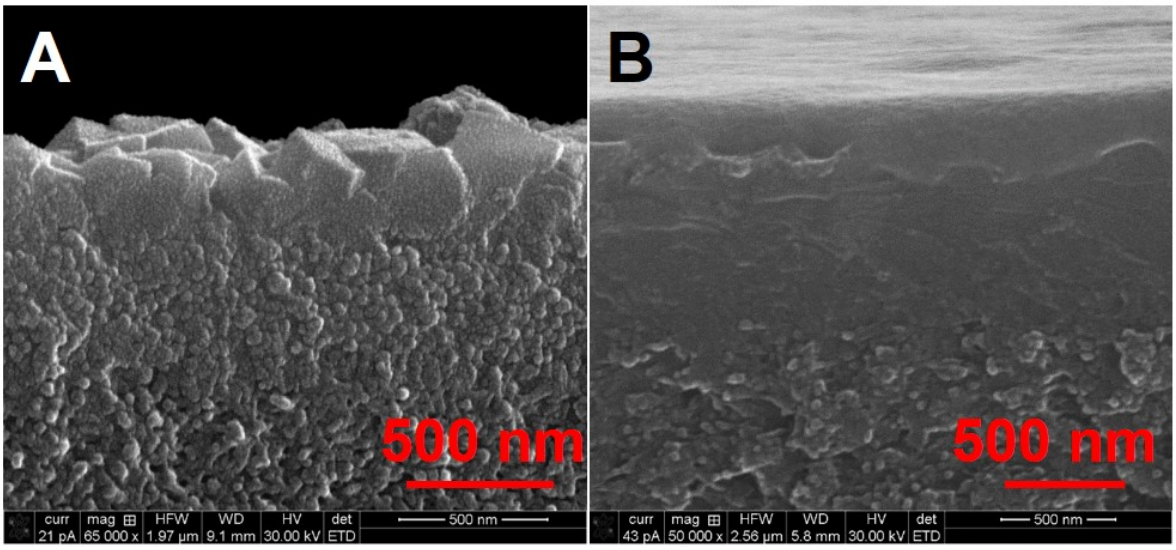

Fig. 25. Cross-section view SEM of (A) grown zeolite membrane and (B) PDMS coated grown zeolite membrane.

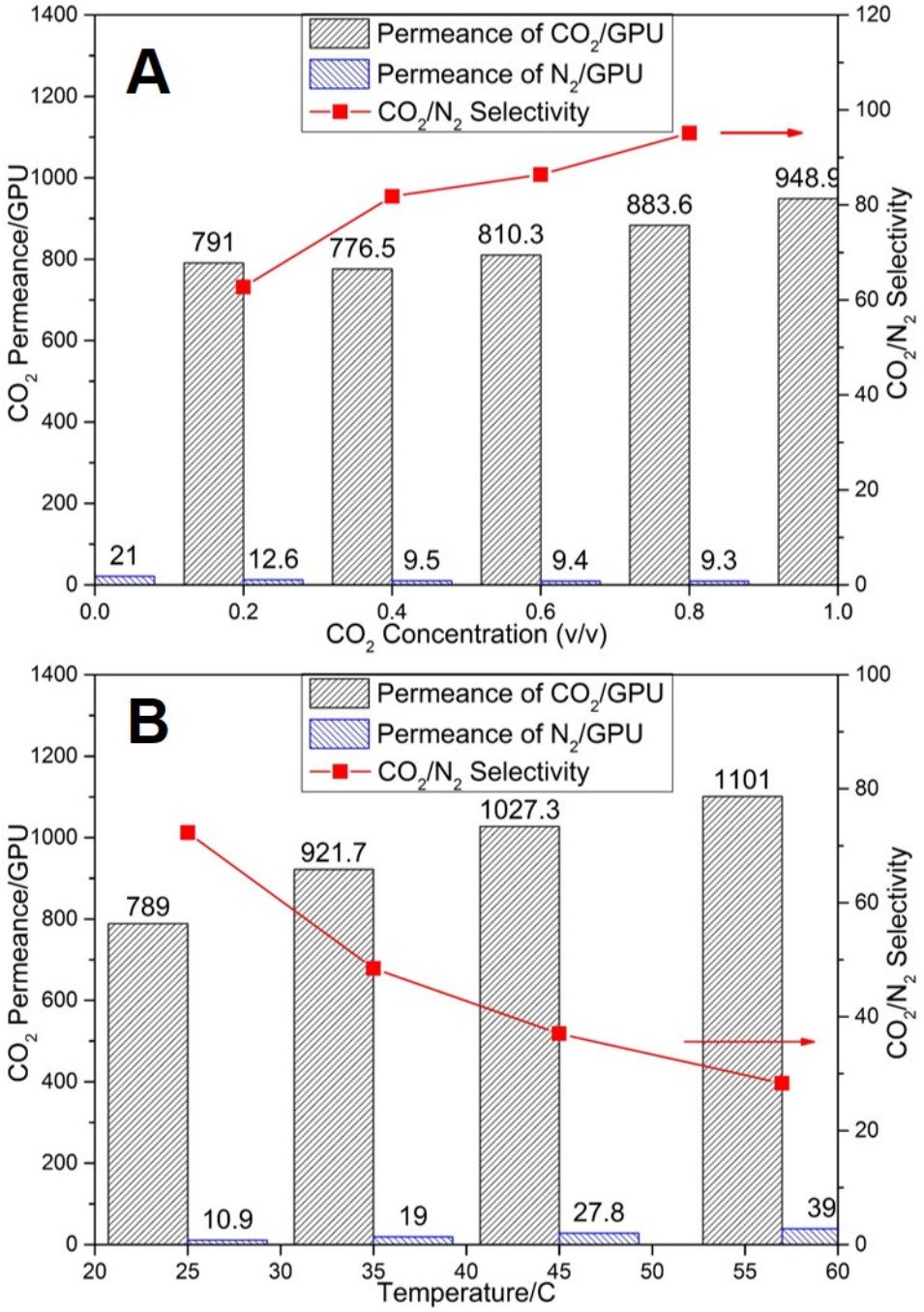

Fig. 26. The effects of CO_2 concentration and temperature on the transport properties of the PES/ZY/PDMS membrane.

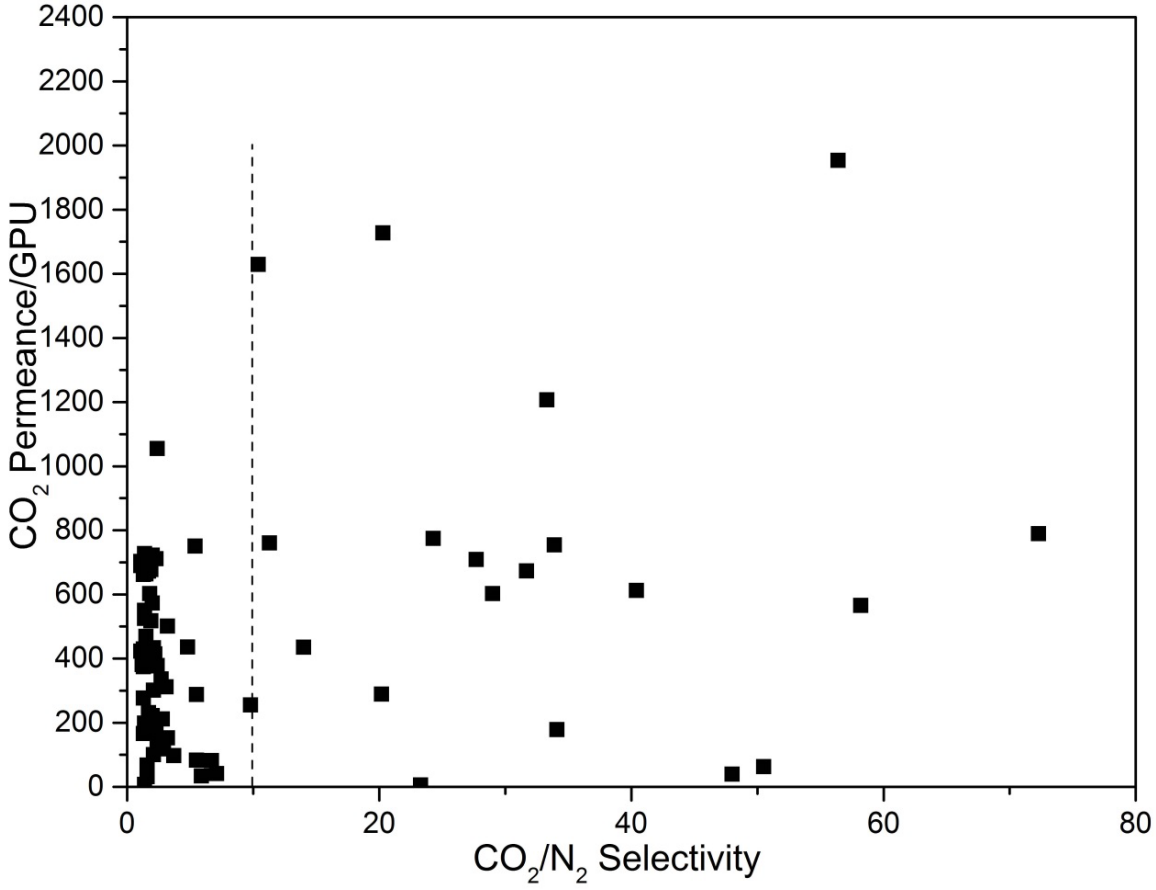

Fig. 27. Histogram of separation property of PES/ZY/PDMS membranes.

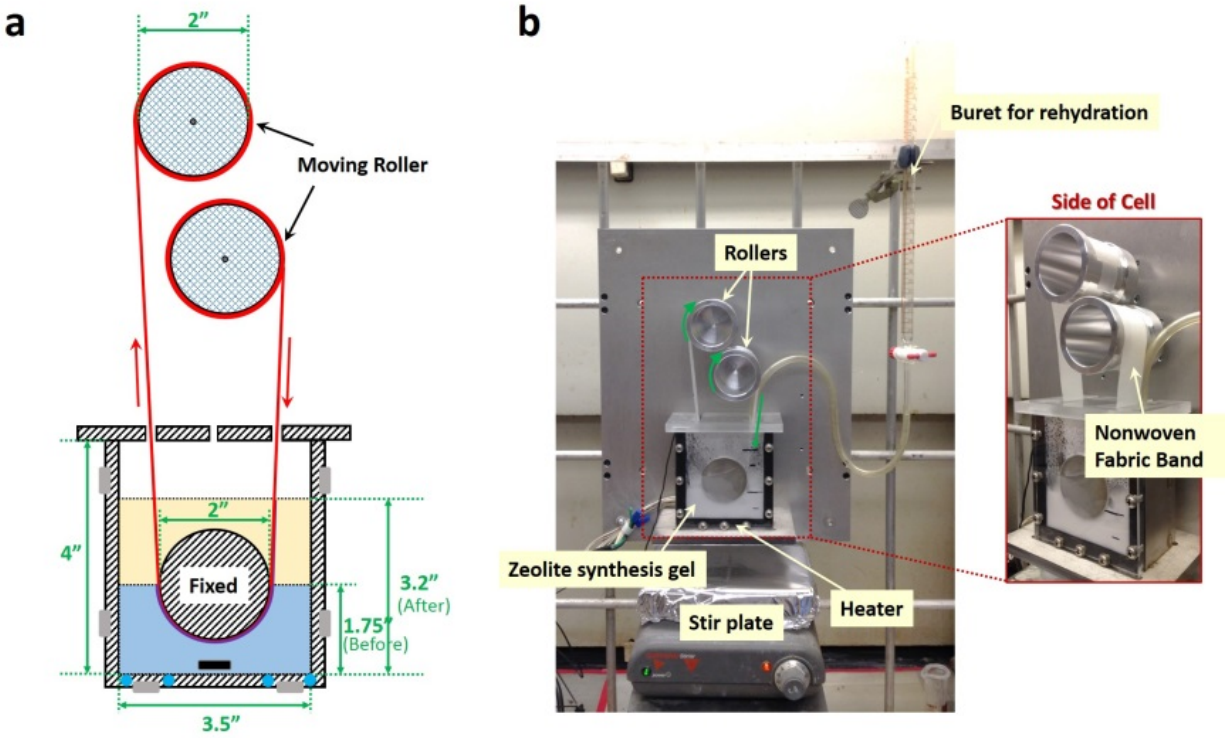

Fig. 28. (a) Scheme and (b) picture of roll-to-roll synthesis setup.

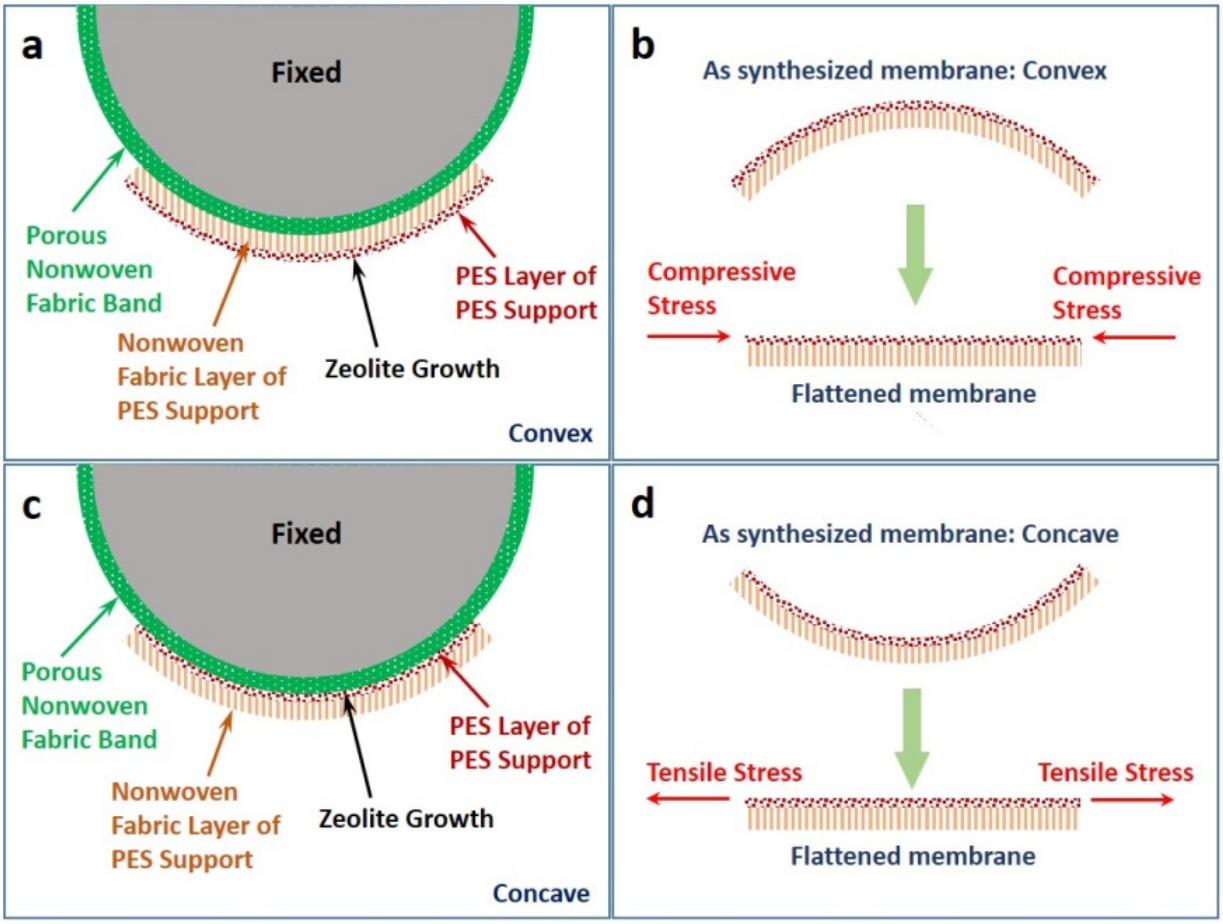

Fig. 29. Scheme of (a) convex and (c) concave synthesis geometries realized in the roll-to-roll reactor, and the type of stress experienced during (b) convex and (d) concave growth and eventual flattening of membrane.

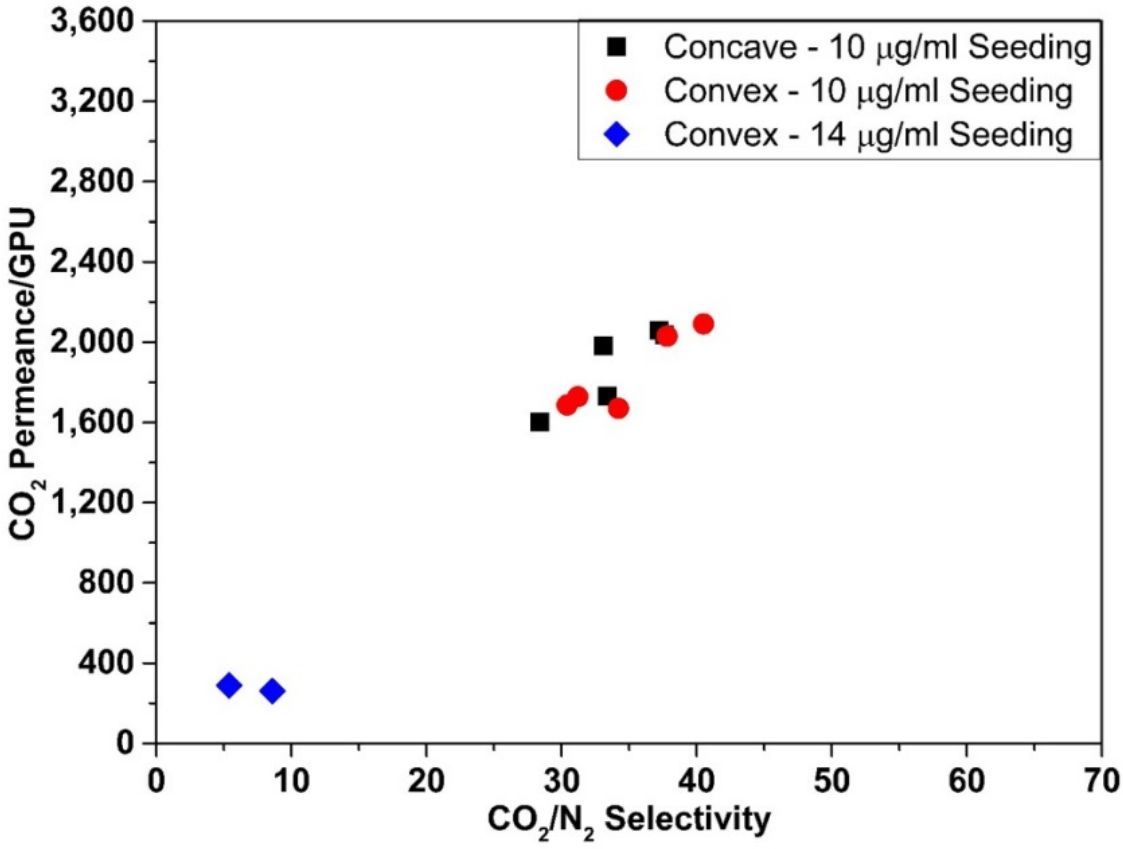

Fig. 30. CO_2/N_2 gas transport results of zeolite membranes fabricated from the roll-to-roll setup.

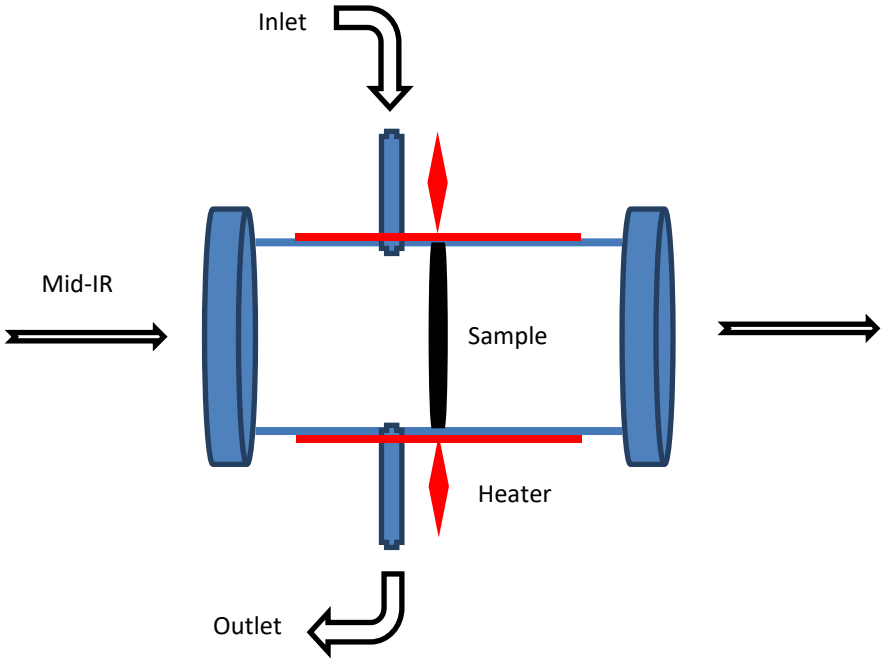

Fig. 31. Schematic of the gas cell for in-situ FTIR measurement.

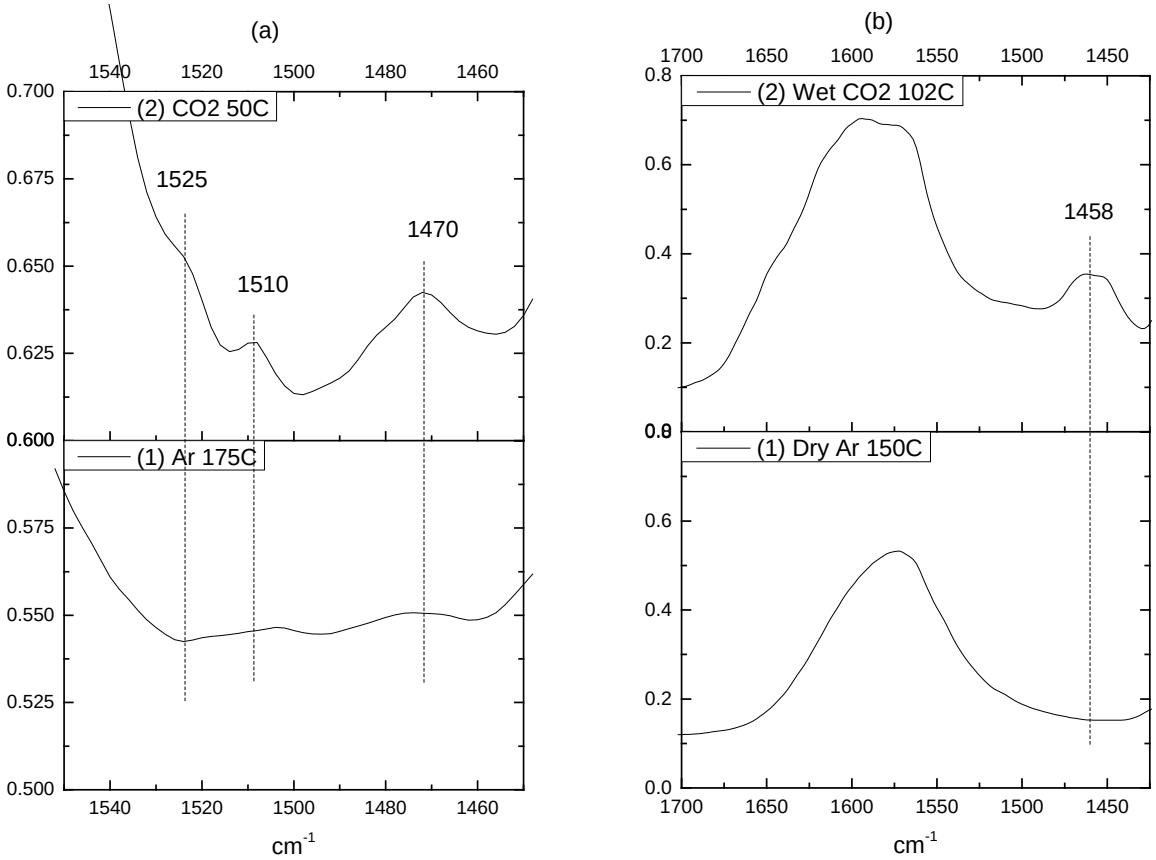

Fig. 32. FTIR spectra during CO_2 absorption at 102°C in (a) commercial polyamine and (b) Mobile Carrier A.

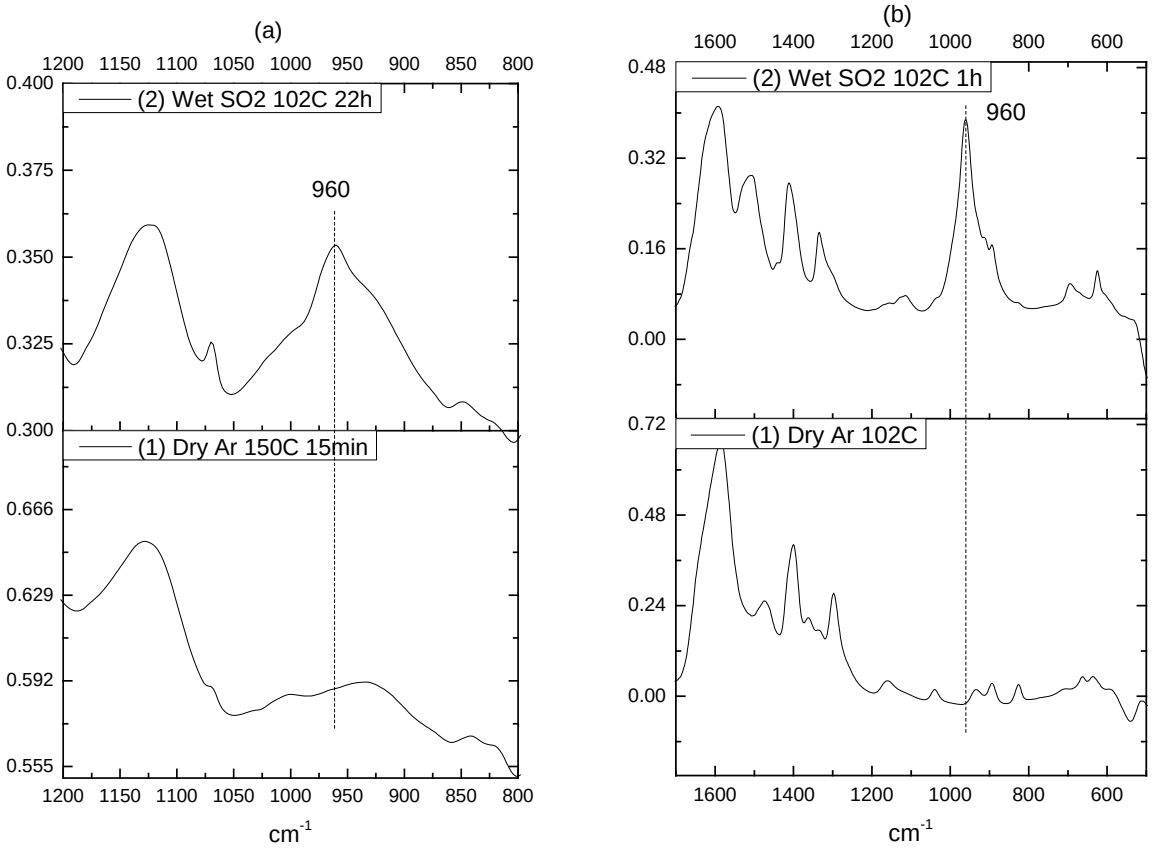

Fig. 33. FTIR spectra during SO_2 absorption at 102°C in (a) commercial polyamine and (b) Mobile Carrier A.

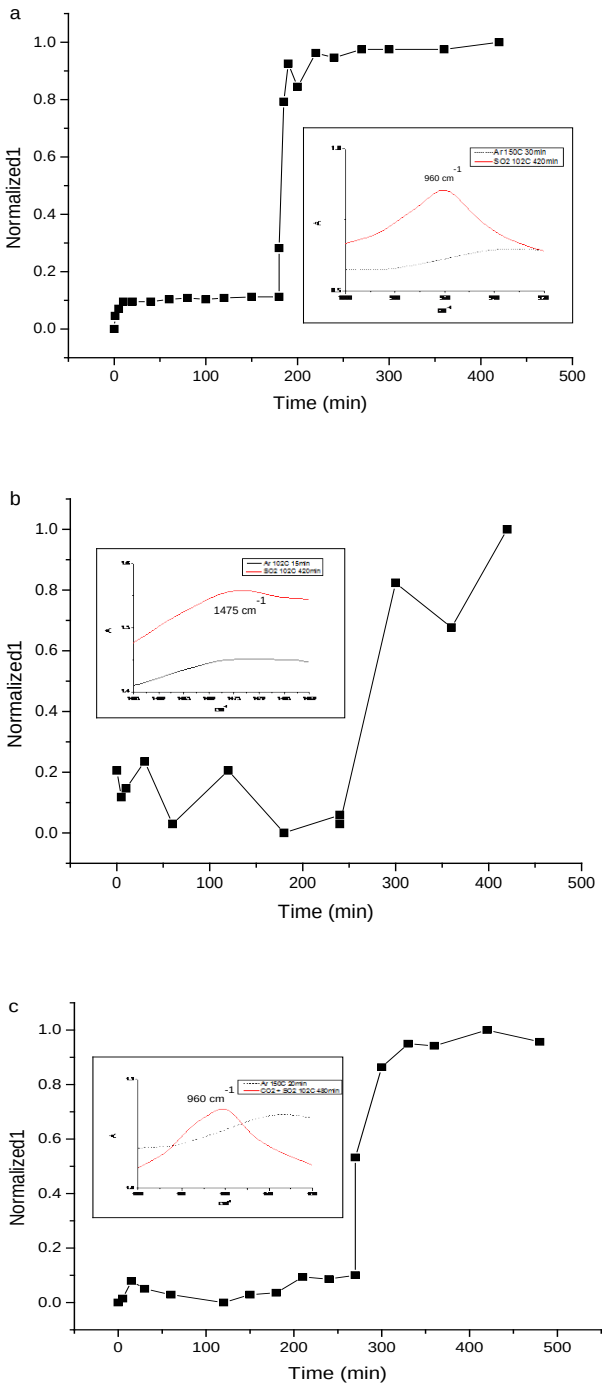

Fig. 34. The growth of IR peak intensity of commercial polyamine versus time at 102°C: (a) normalized IR peak intensity at 960 cm^{-1} during 45 ppm SO_2 absorption (Inset: infrared spectrum of commercial polyamine before and after SO_2 exposure); (b) normalized IR peak intensity at 1475 cm^{-1} during 10% CO_2 absorption (Inset: infrared spectrum of commercial polyamine before and after CO_2 exposure); (c) normalized IR peak intensity at 960 cm^{-1} during 10% CO_2 and 45 ppm SO_2 absorption (Inset: infrared spectrum of commercial polyamine before and after mixture exposure).

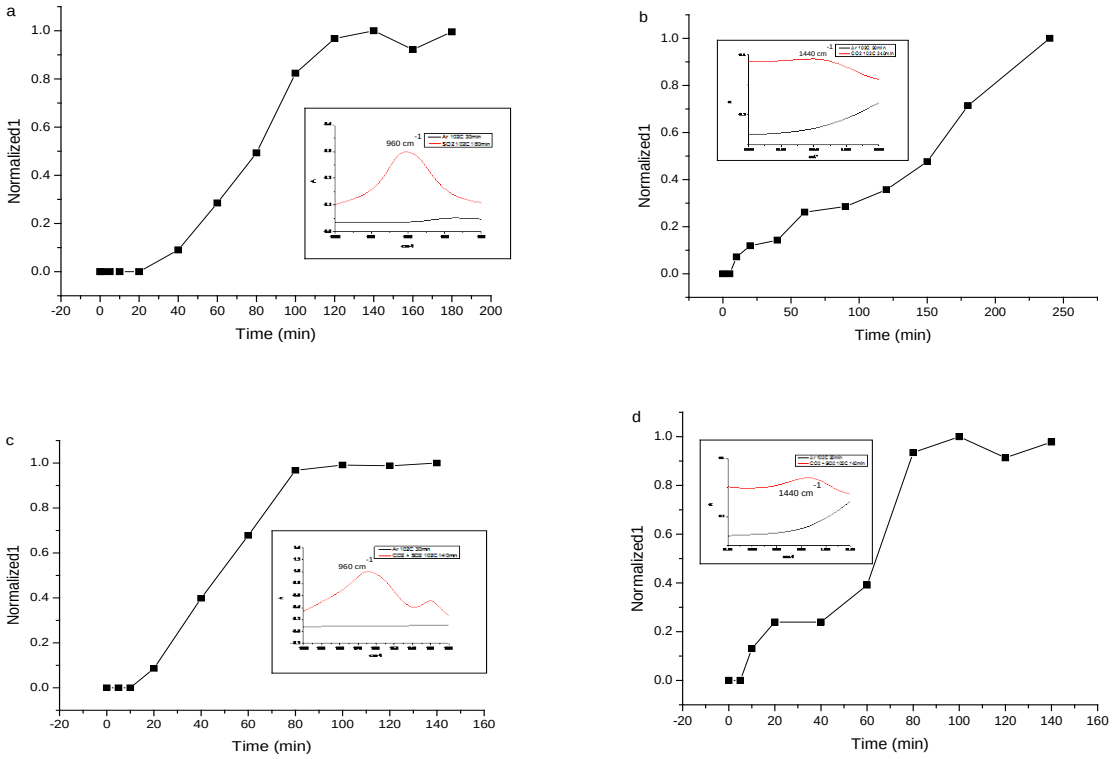

Fig. 35. The growth of IR peak intensity of Mobile Carrier A versus time at 102°C: (a) normalized IR peak intensity at 960 cm^{-1} during 45 ppm SO_2 absorption (Inset: infrared spectrum of Mobile Carrier A before and after SO_2 exposure); (b) normalized IR peak intensity at 1440 cm^{-1} during 10% CO_2 absorption (Inset: infrared spectrum of Mobile Carrier A before and after CO_2 exposure); (c) normalized IR peak intensity at 960 cm^{-1} during 10% CO_2 and 45 ppm SO_2 absorption (Inset: infrared spectrum of Mobile Carrier A before and after mixture exposure); (d) normalized IR peak intensity at 1440 cm^{-1} during 10% CO_2 and 45 ppm SO_2 absorption (Inset: infrared spectrum of Mobile Carrier A before and after mixture exposure).

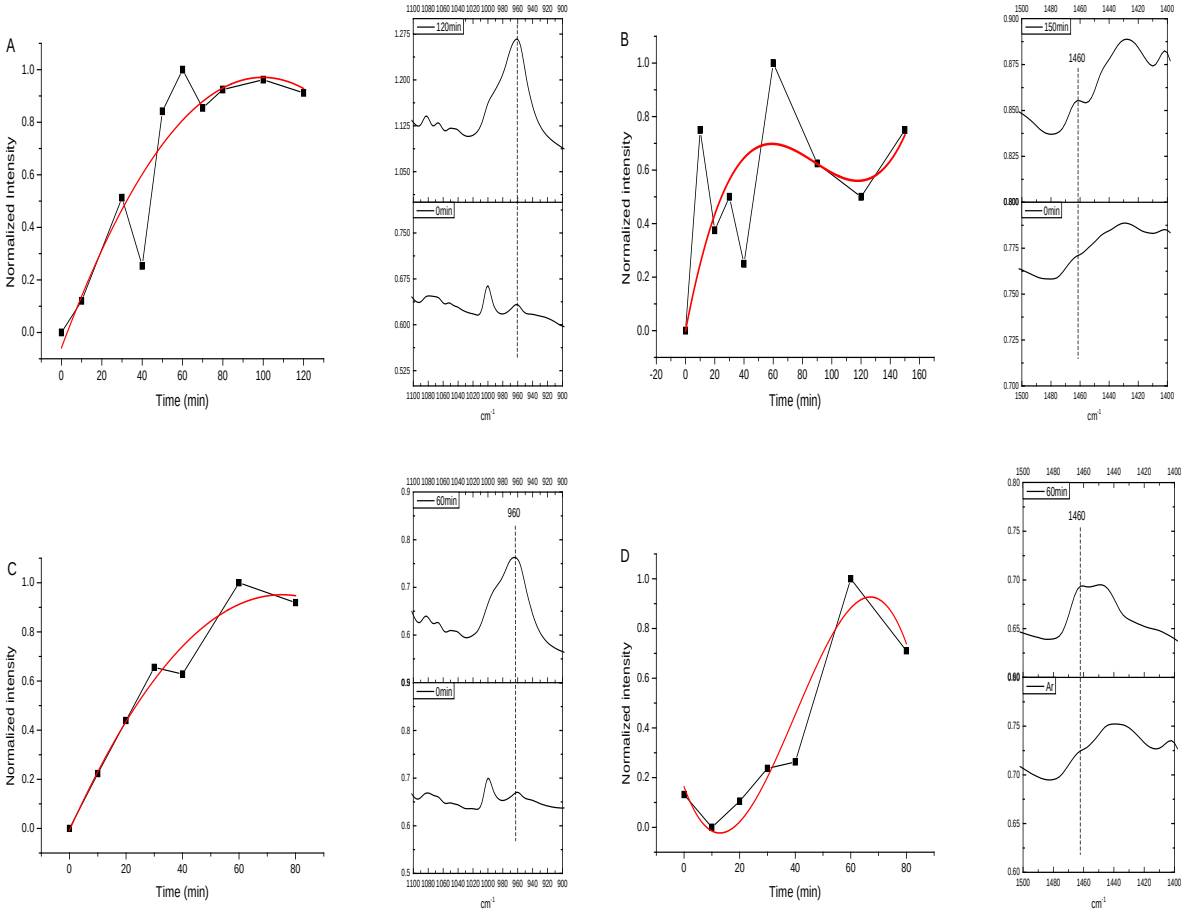

Fig. 36. The growth of IR peak intensity of Mobile Carrier B versus time at 102ºC: (a) Left: normalized IR peak intensity at 960 cm^{-1} during 45 ppm SO_2 absorption. Right: infrared spectrum of Mobile Carrier B before and after SO_2 exposure; (b) Left: normalized IR peak intensity at 1460 cm^{-1} during 10% CO_2 absorption. Right: infrared spectrum of Mobile Carrier B before and after CO_2 exposure; (c) Left: normalized IR peak intensity at 960 cm^{-1} during 10% CO_2 and 45 ppm SO_2 absorption. Right: infrared spectrum of Mobile Carrier B before and after mixture exposure; (d) Left: normalized IR peak intensity at 1460 cm^{-1} during 10% CO_2 and 45 ppm SO_2 absorption. Right: infrared spectrum of Mobile Carrier B before and after mixture exposure.

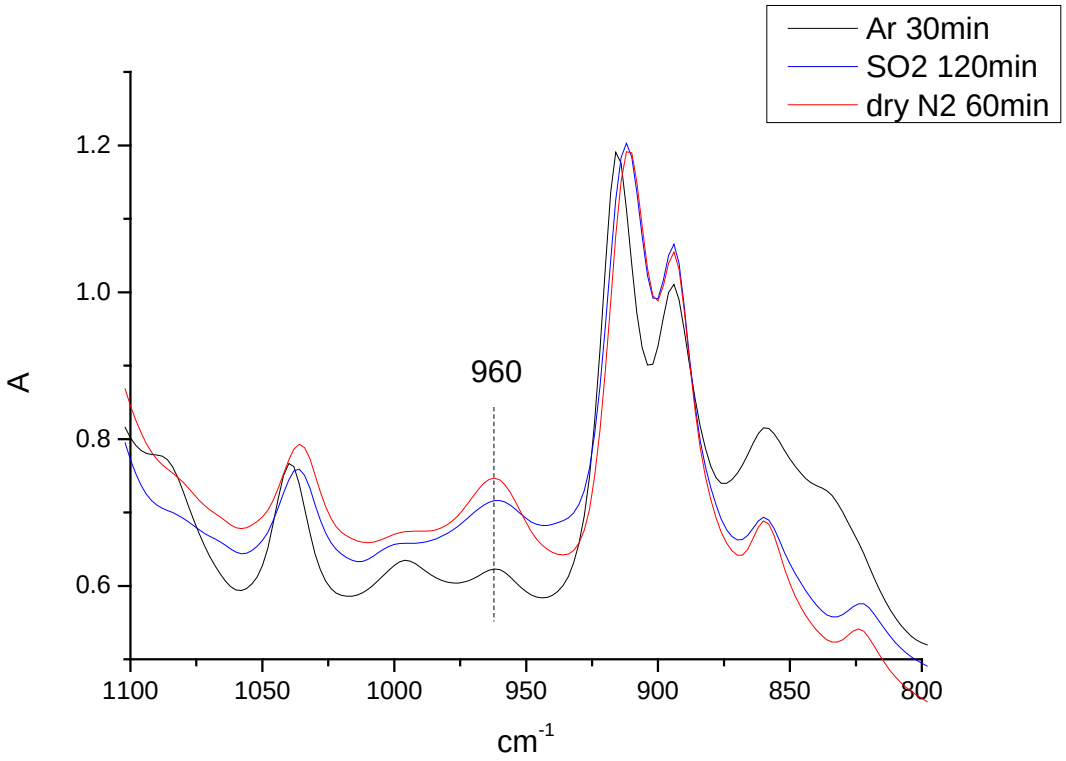

Fig. 37. Infrared spectrum of mixed mobile carriers in Ar (black curve), after 45 ppm SO_2 exposure at 102ºC for 120 min (blue curve), and after N_2 purging (red curve).

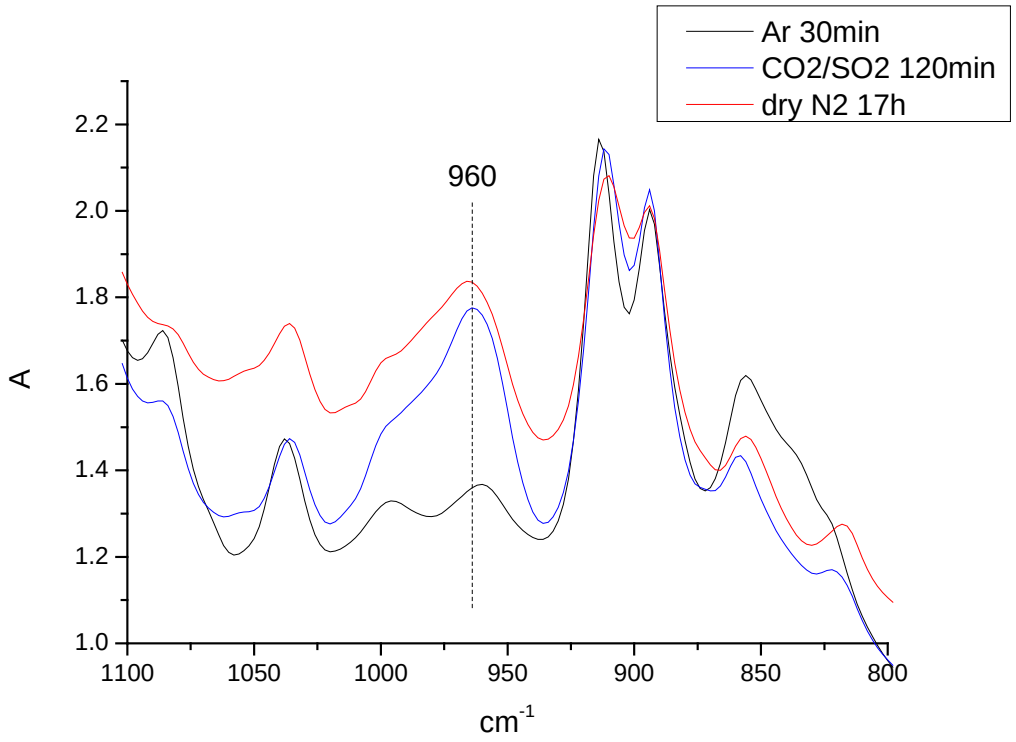

Fig. 38. Infrared spectrum of mixed mobile carriers in Ar (black curve), after 10% CO_2 and 45 ppm SO_2 exposure at 102°C for 120 min (blue curve), and after N_2 purging (red curve).

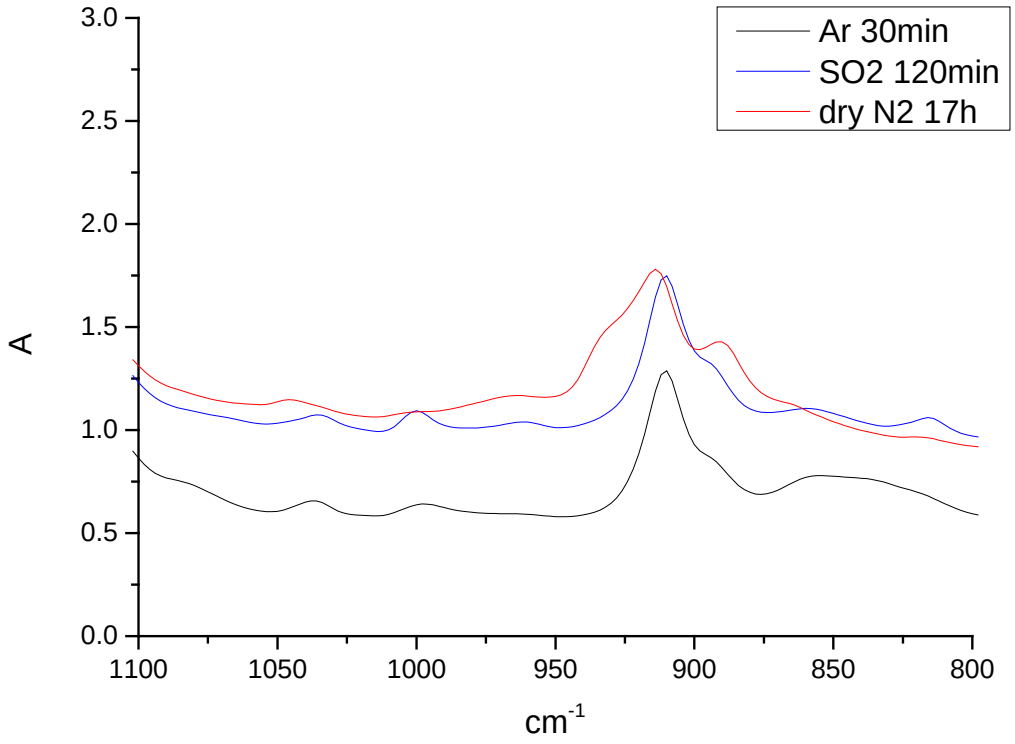

Fig. 39. Infrared spectrum of mixed mobile carriers in Ar (black curve), after 45 ppm SO_2 exposure at 57°C for 120 min (blue curve), and after N_2 purging (red curve).

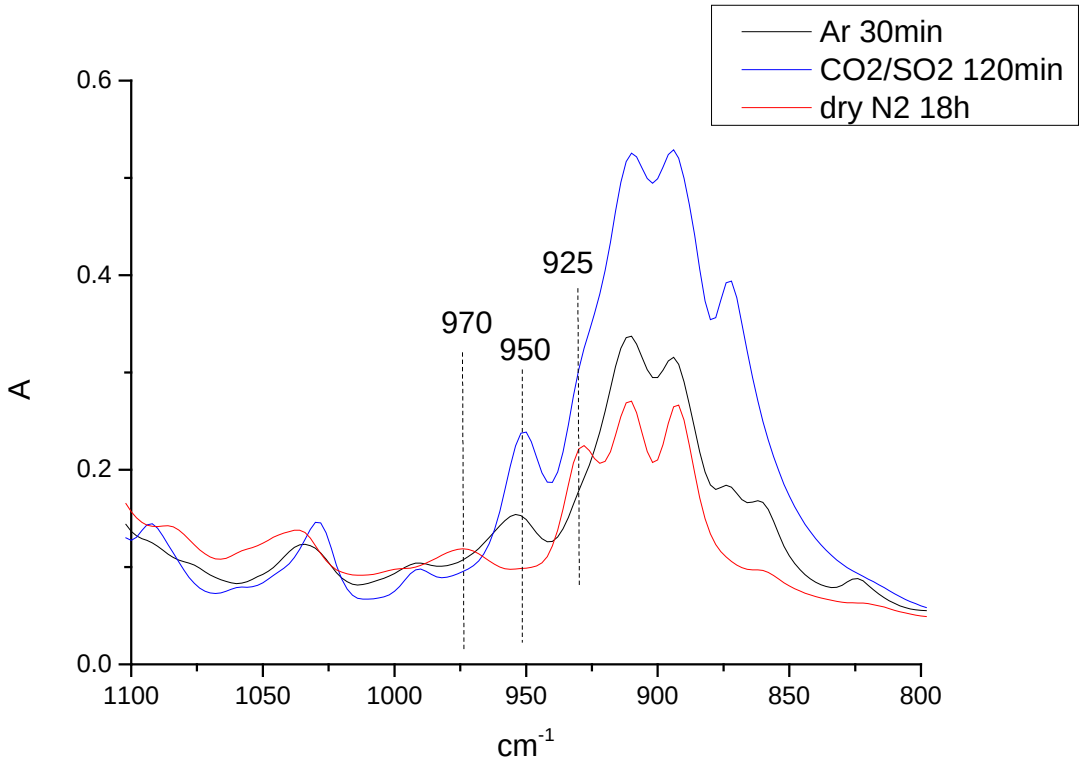

Fig. 40. Infrared spectrum of mixed mobile carriers in Ar (black curve), after 10% CO_2 and 45 ppm SO_2 exposure at 57°C for 120 min (blue curve), and after N_2 purging (red curve).

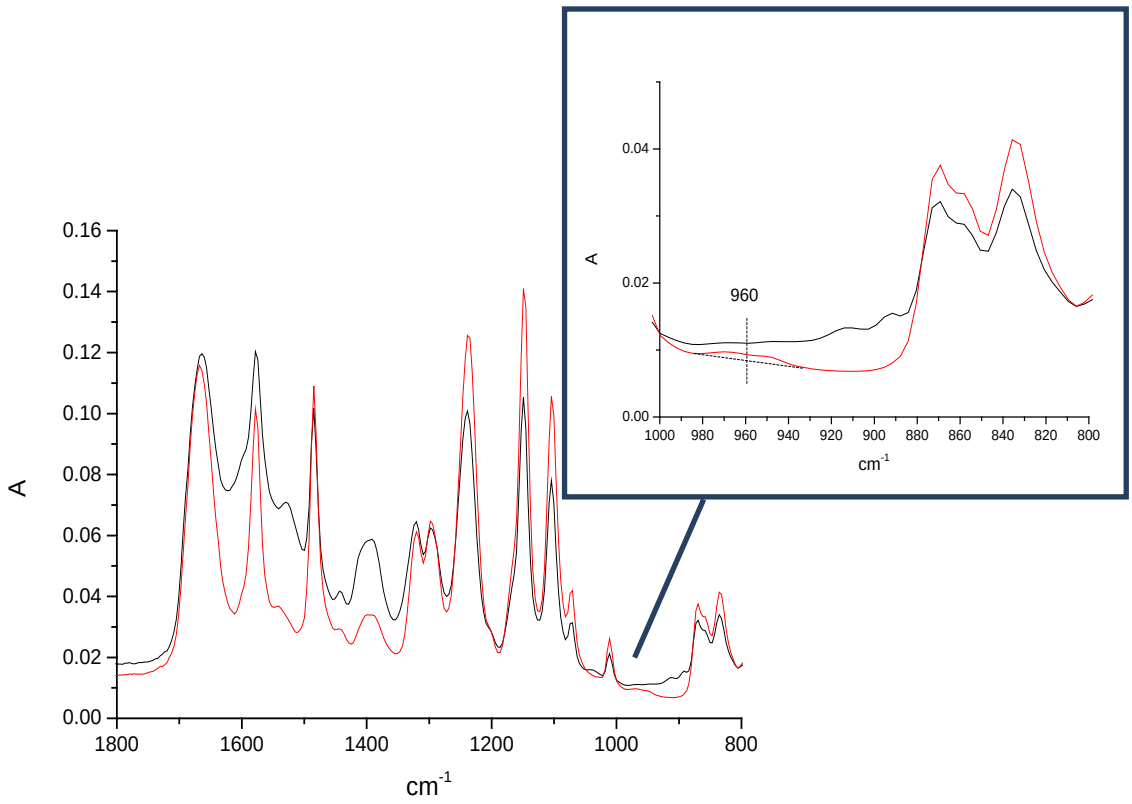

Fig. 41. ATR infrared spectrum of Membrane Sample A: fresh membrane (dashed line); membrane exposed to 0.7 ppm SO_2 at 57°C (solid line). Inset: detail spectrum in 1000 to 800 cm^{-1} region.

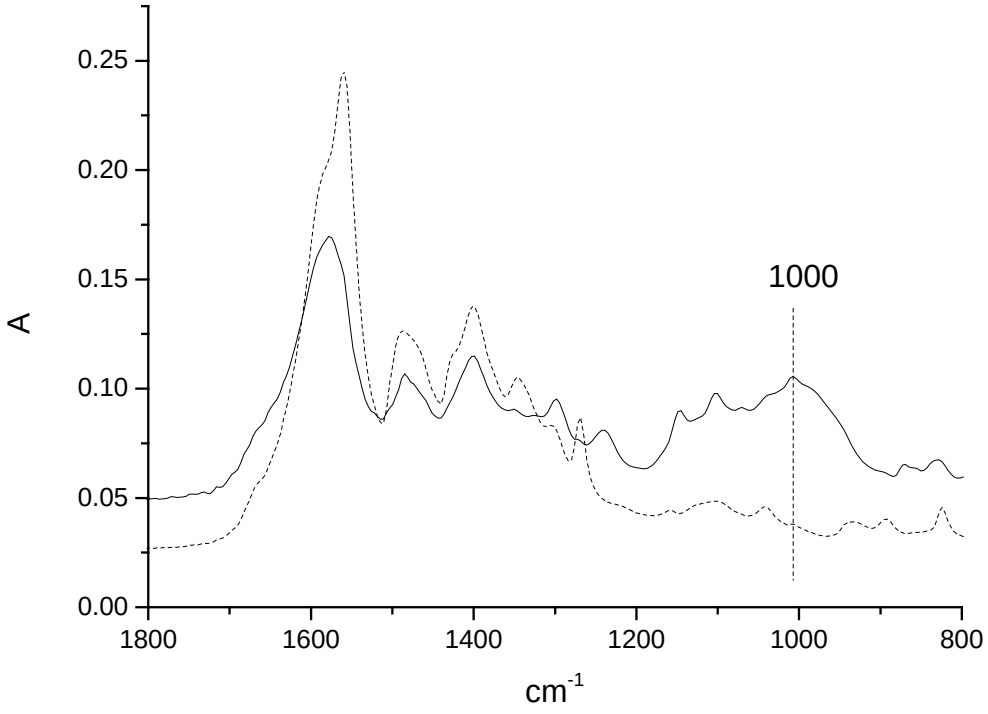

Fig. 42. ATR infrared spectrum of membrane sample B: fresh membrane (dashed line); membrane exposed to 0.7 ppm SO_2 at 102°C (solid line).

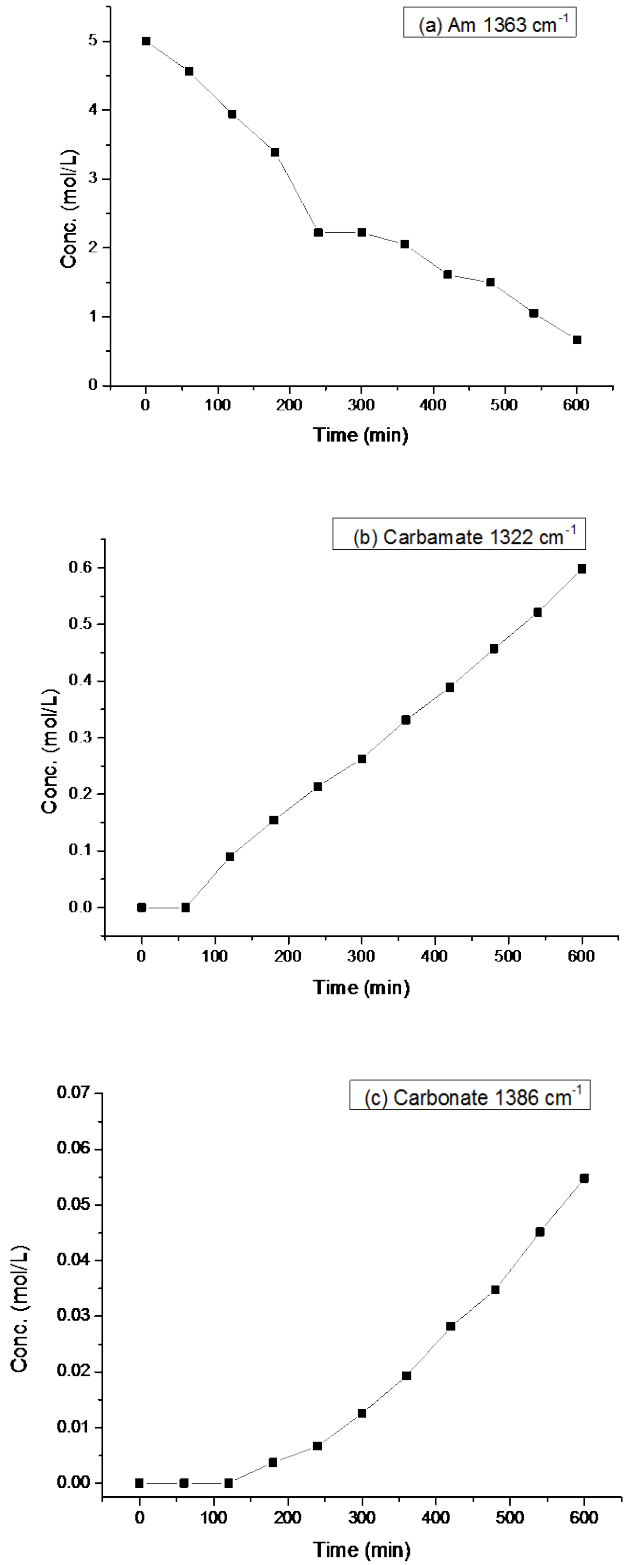

Fig. 43. Kinetic concentration profiles calculated for (a) a primary amine, (b) carbamate, and (c) carbonate.

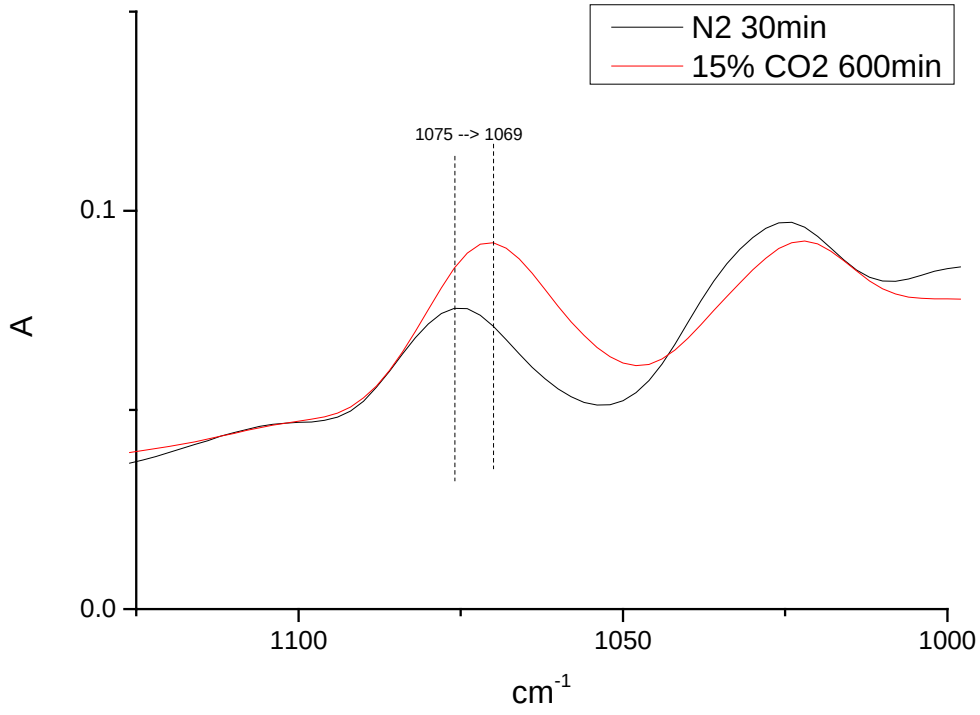

Fig. 44. Infrared spectra of peak shift during amine protonation.

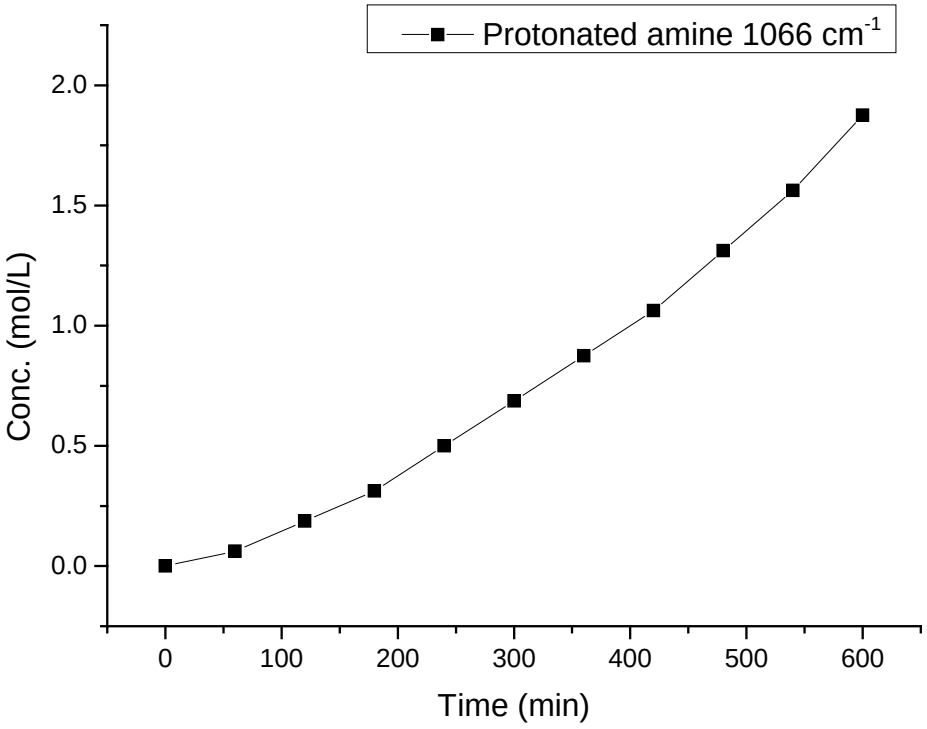

Fig. 45. Kinetic concentration profiles calculated for protonated amine.

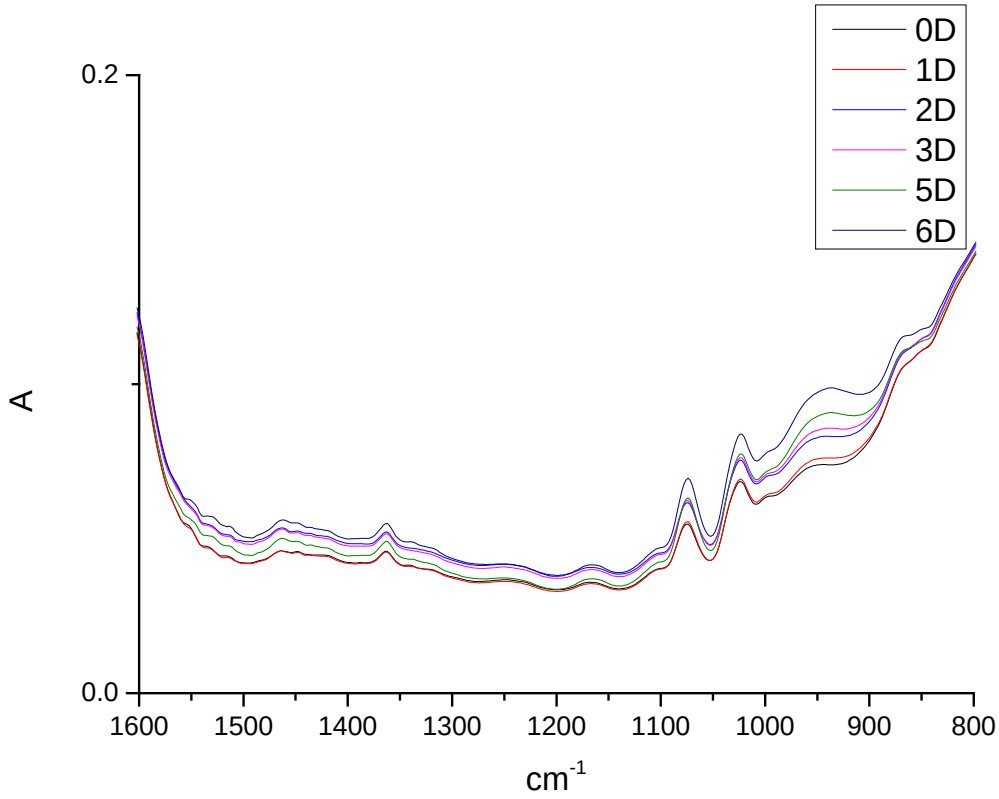

Fig. 46. HATR spectrum of 2.5M MEA solution in the presence of 151 ppm SO_2/6% O_2 at 40°C. (D stands for days.)

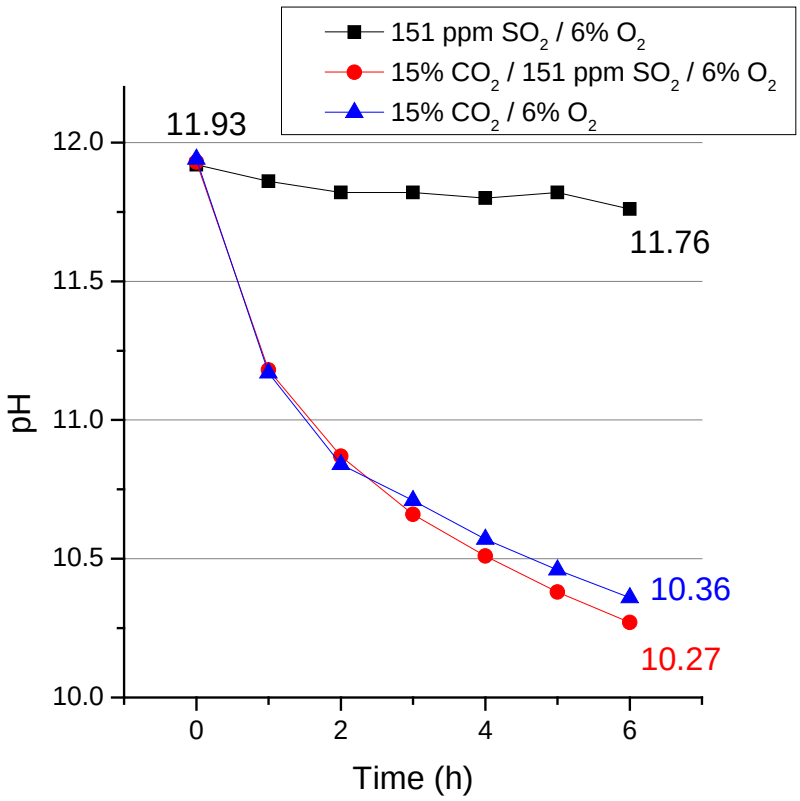

Fig. 47. pH change of 30 wt.% MEA at 57°C.

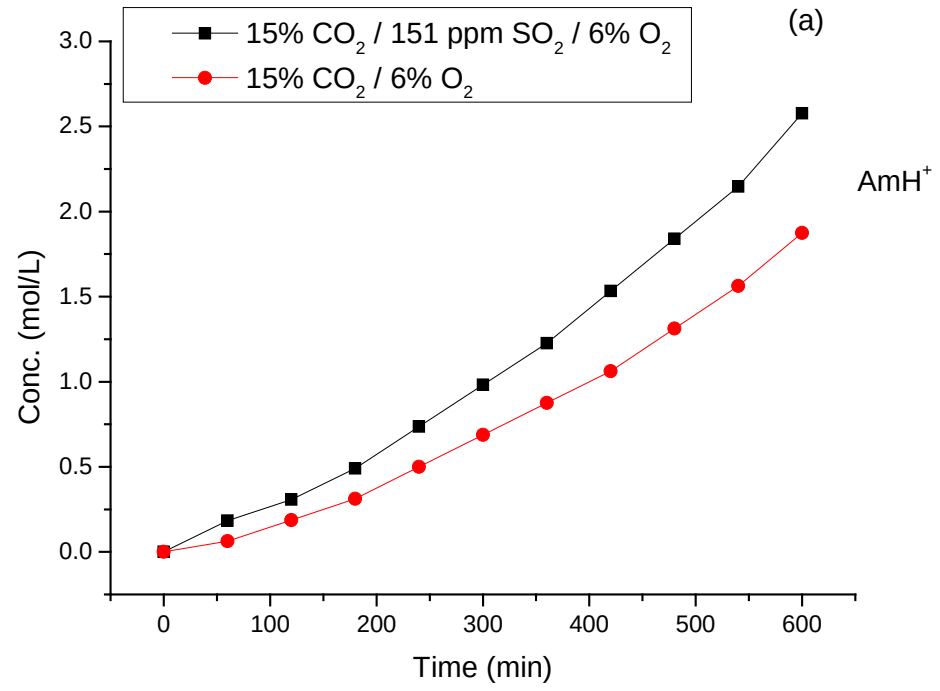
(a)
15% CO_2 / 151 ppm SO_2 / 6% O_2
15% CO_2 / 6% O_2
AmH^+
Conc. (mol/L)
Time (min)
0.0
0.5
1.0
1.5
2.0
2.5
3.0
0
100
200
300
400
500
600

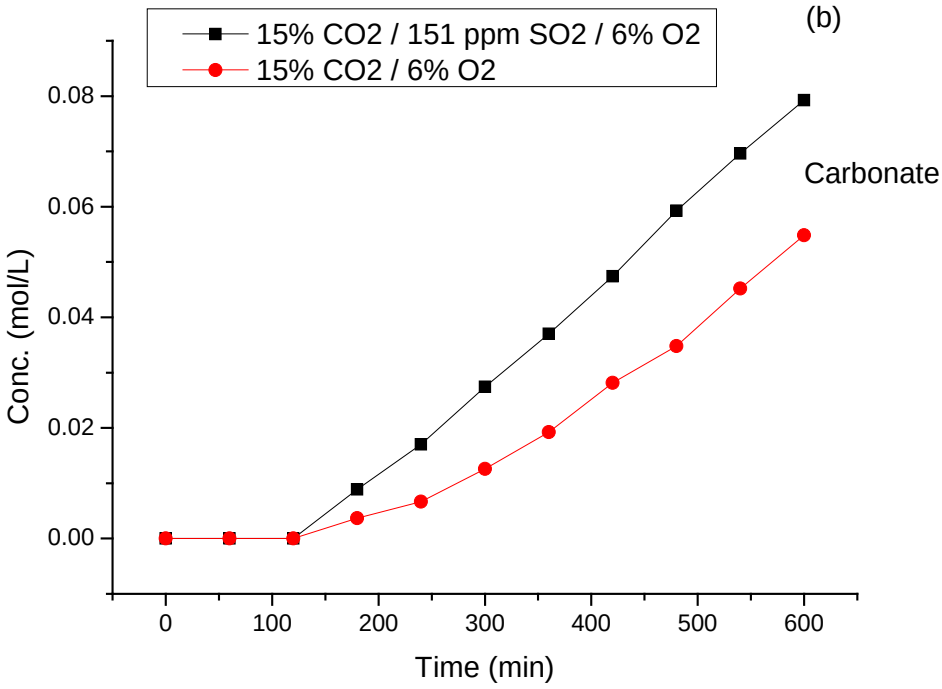
(b)
15% CO2 / 151 ppm SO2 / 6% O2
15% CO2 / 6% O2
Carbonate
Conc. (mol/L)
Time (min)
0.00
0.02
0.04
0.06
0.08
0
100
200
300
400
500
600

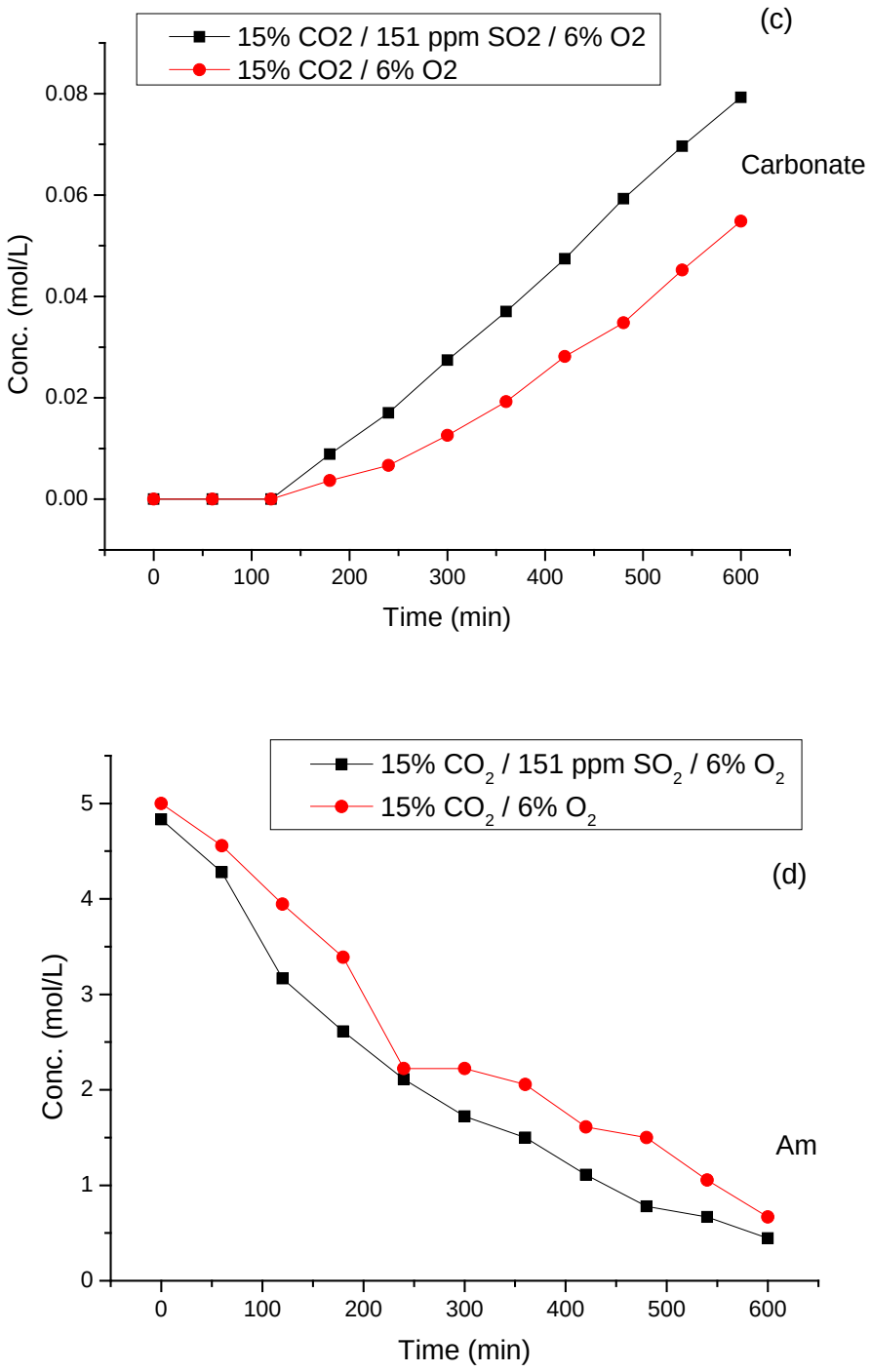

Fig. 48. Kinetic concentration profiles based on the HATR spectra calculated for (a) $MEAH^+$, (b) carbamate, (c) carbonate, and (d) MEA. (Am stands for amine.)

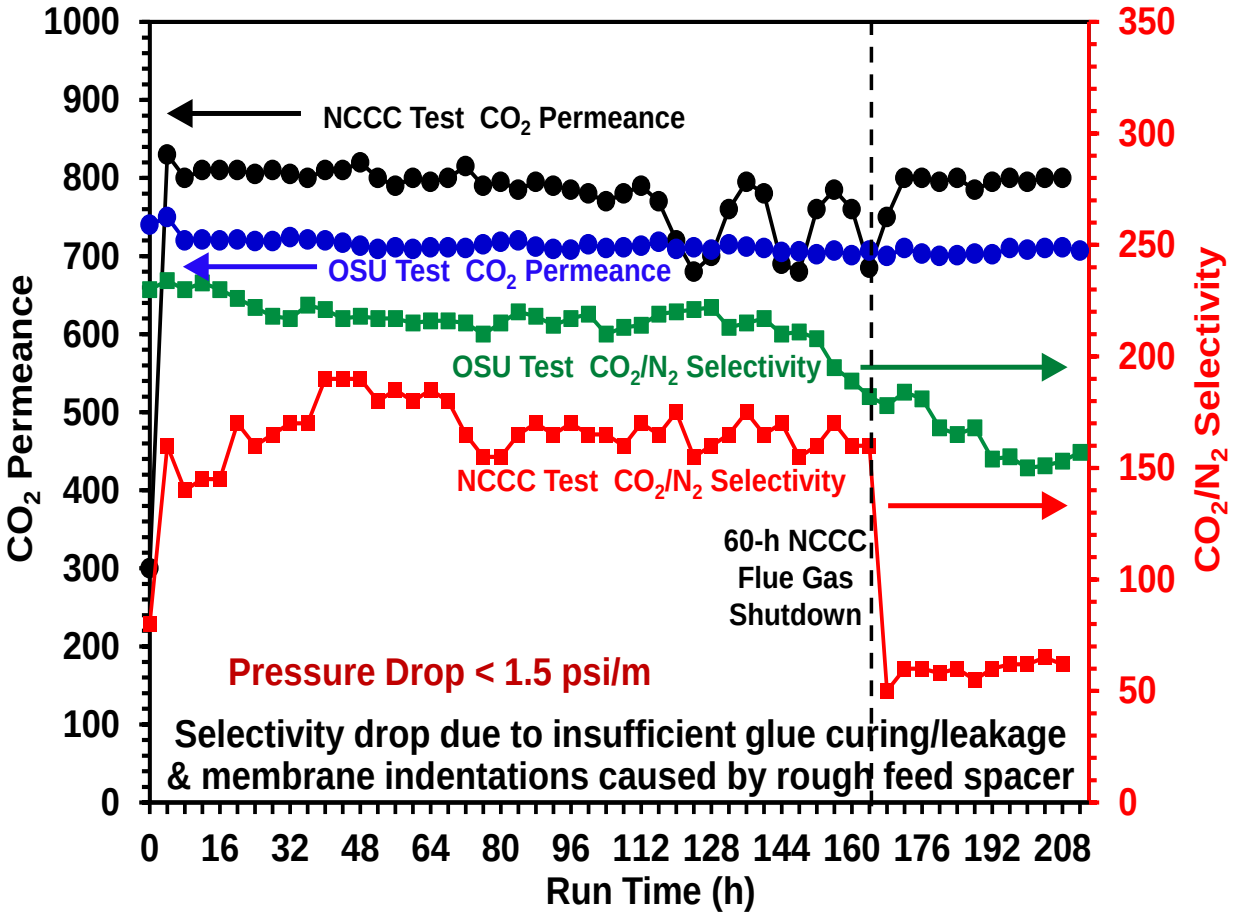

Fig. 49. The stability plot of the spiral-wound membrane module SW-162 tested at NCCC for comparison with that of SW-173 tested at OSU.

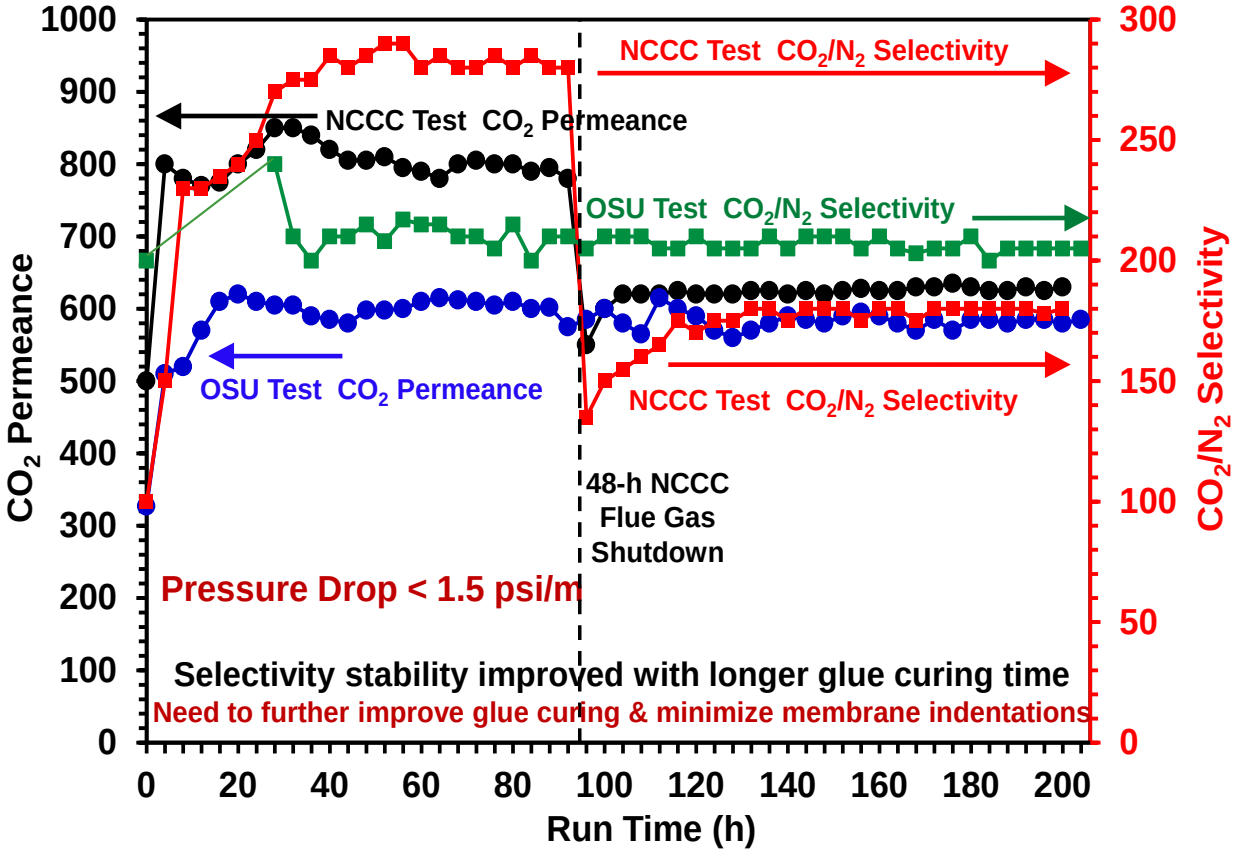

Fig. 50. The stability plot of the spiral-wound membrane module SW-161 tested at NCCC for comparison with that of SW-67 tested at OSU.

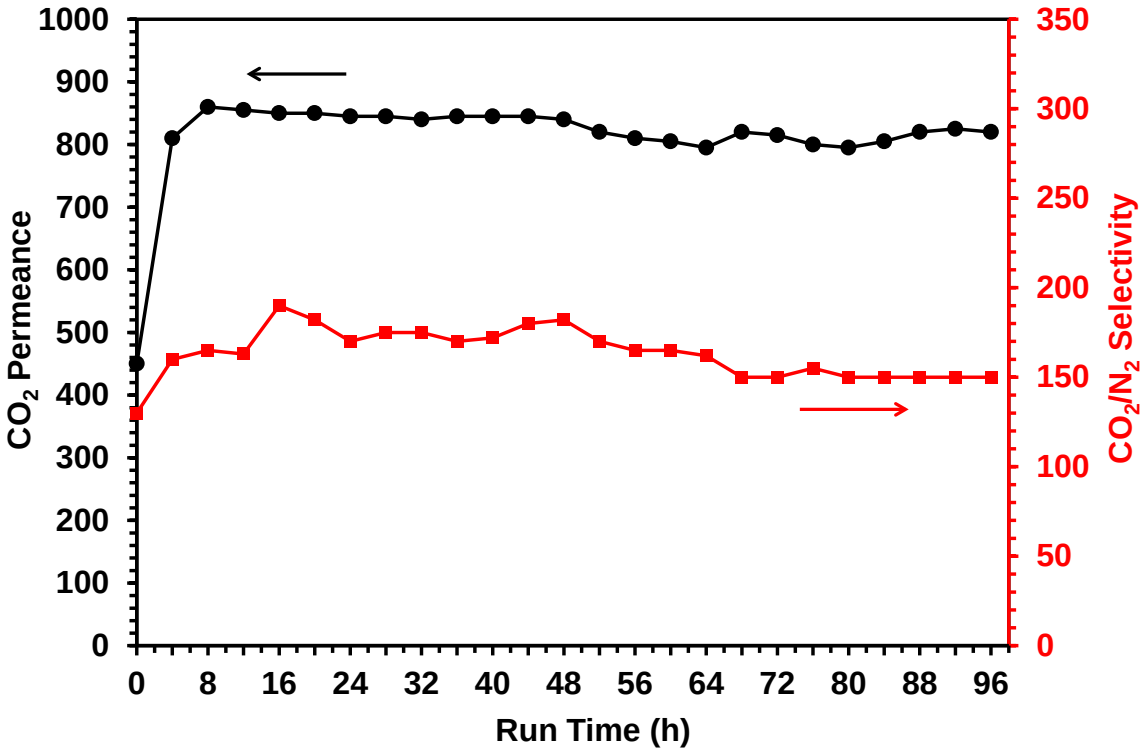

Fig. 51. Spiral-wound module (SW-154) stability test at NCCC.

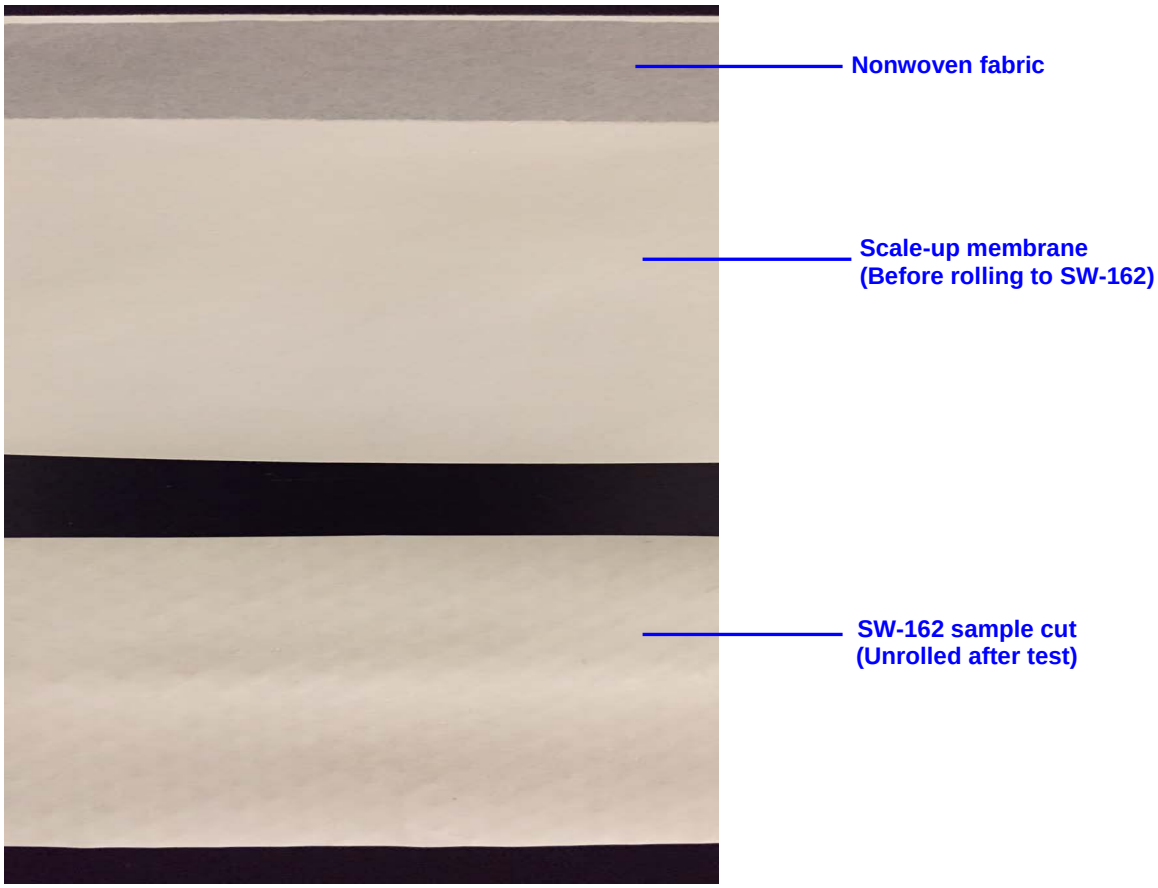

Fig. 52. The images of the membranes: Top: no indentations on the membrane selective layer surface before rolling to SW-162 and Bottom: indentations of the feed spacer on the membrane selective layer surface after the test.

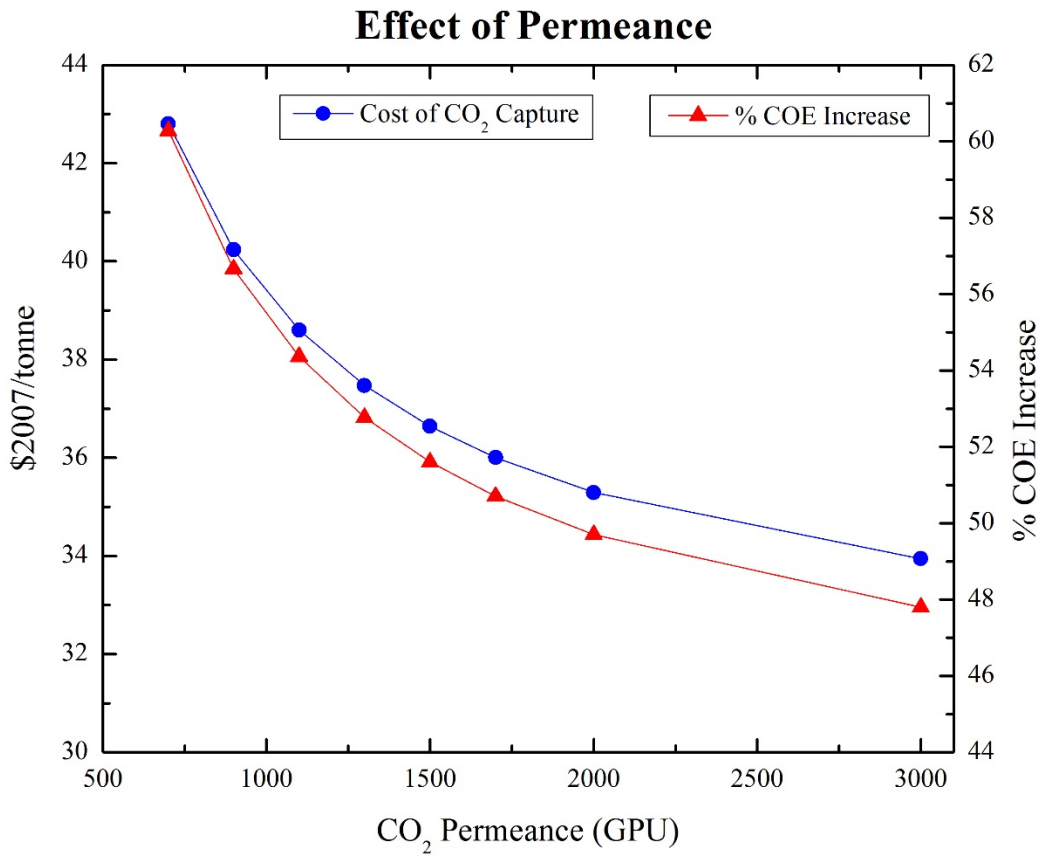

Fig. 53. Effect of CO_2 permeance on cost ($/tonne of CO_2 removed in 2007 dollar) with 1.5 atm feed gas pressure and 150 torr Stage 1 permeate pressure.

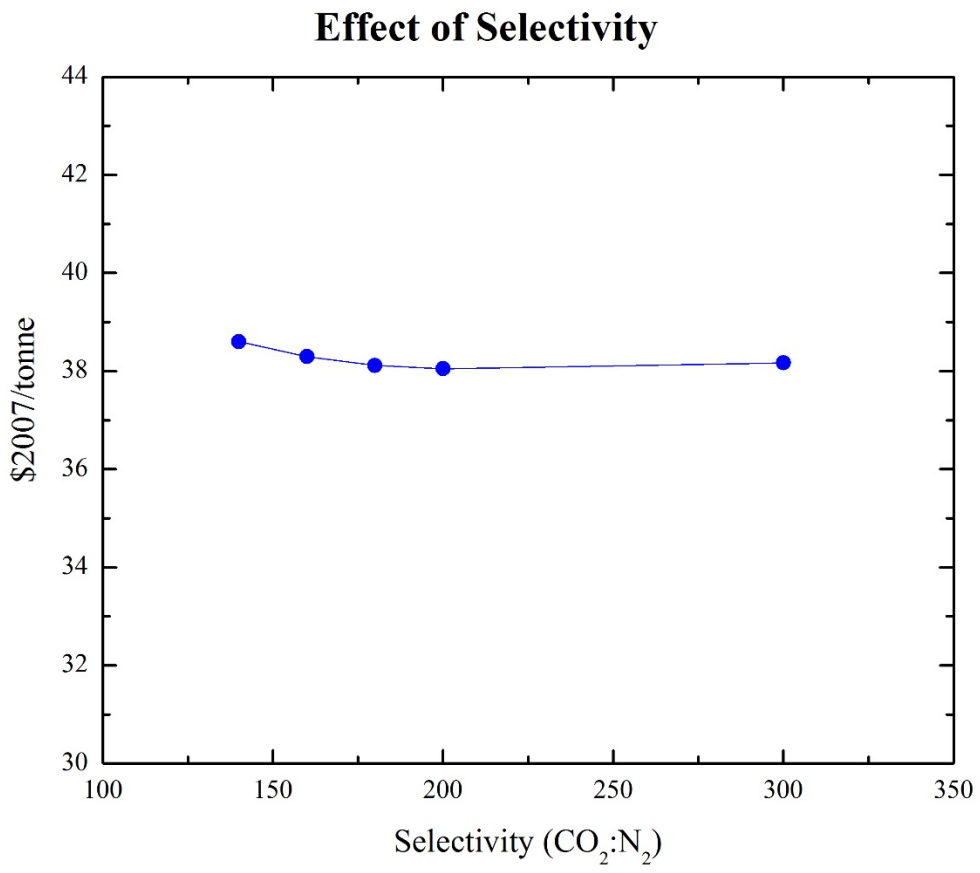

Fig. 54. Effect of CO_2/N_2 selectivity on cost ($/tonne of CO_2 removed in 2007 dollar) with 1.5 atm feed gas pressure and 150 torr Stage 1 permeate pressure.

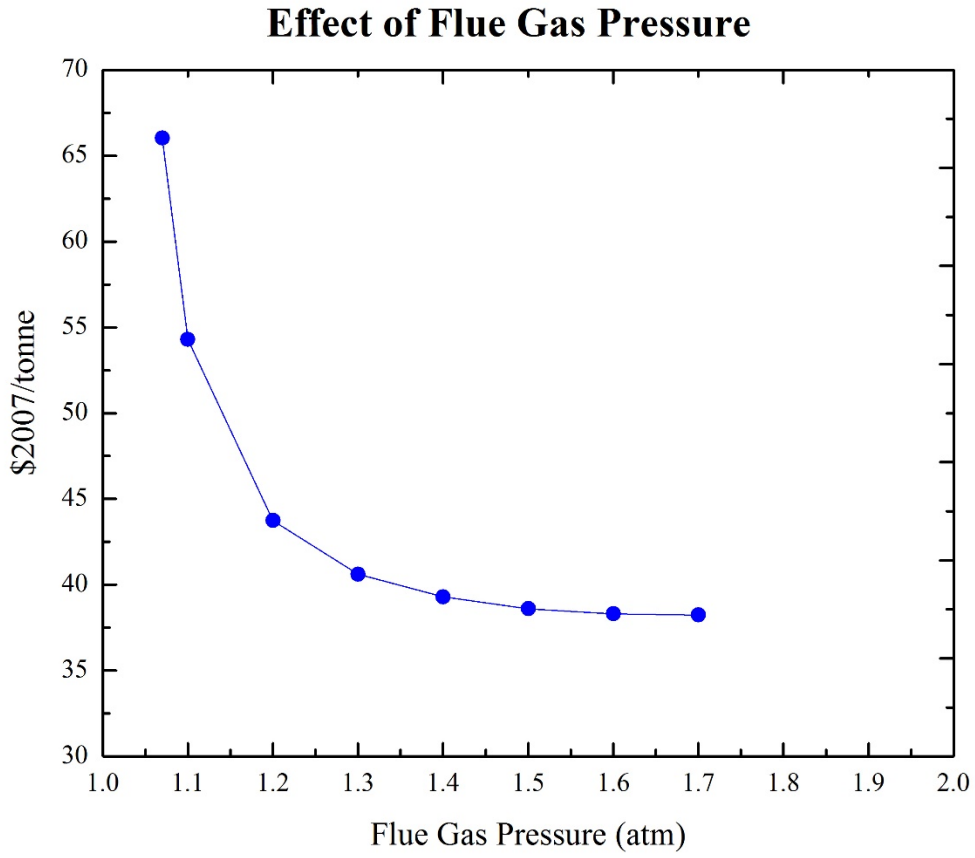

Fig. 55. Effect of Stage 1 flue gas pressure on cost ($/tonne of CO_2 removed in 2007 dollar) with 1100 GPU CO_2 permeance and 140 CO_2/N_2 selectivity.

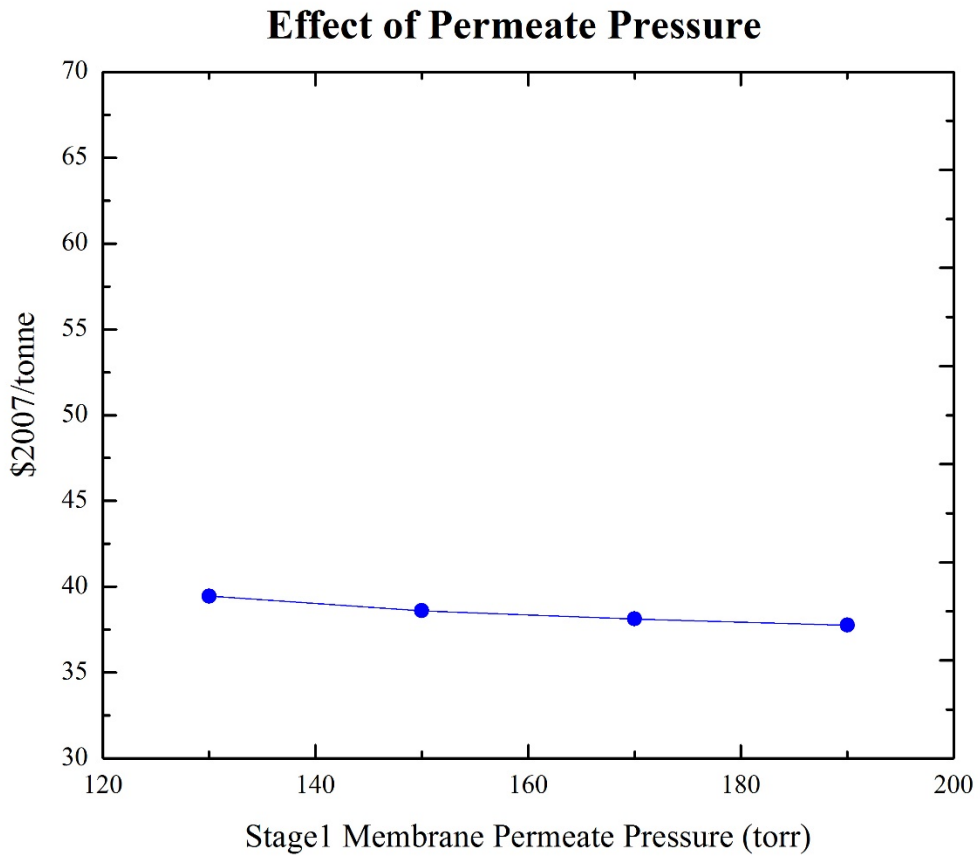

Fig. 56. Effect of Stage 1 Stage 1 permeate pressure on cost ($/tonne of CO_2 removed in 2007 dollar) with 1100 GPU CO_2 permeance and 140 CO_2/N_2 selectivity.

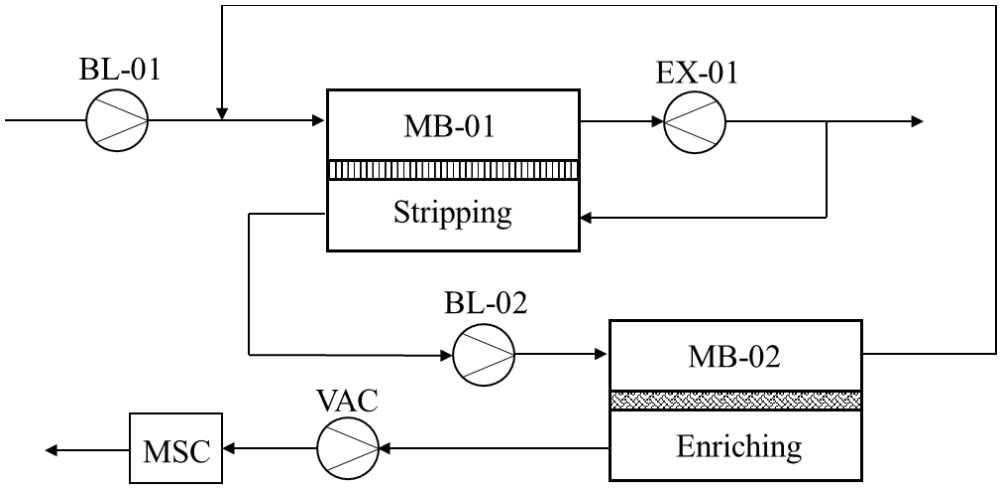

Fig. 57. Diagram of the retentate recycle process.

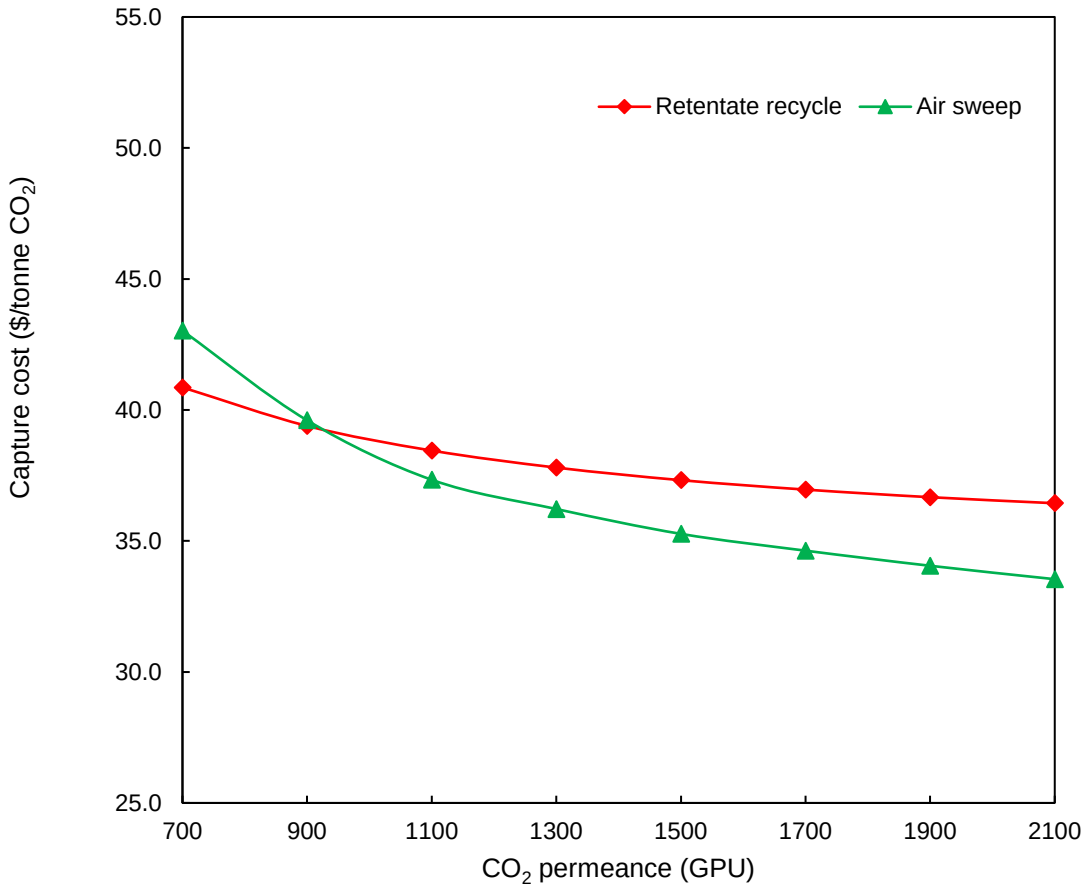

Fig. 58. Effects of CO_2 permeance on the capture costs (in 2007 dollar) of the air sweep and retentate recycle processes.

8 References

1. W. S. W. Ho and K. K. Sirkar, eds., Membrane Handbook, Chapman & Hall, New York (1992), Kluwer Academic Publishers, Boston, reprint edition (2001).
2. W. S. W. Ho, "Membranes Comprising Salts of Aminoacids in Hydrophilic Polymers". US Patent 5611843, (1997).
3. W. S. W. Ho, "Membranes Comprising Aminoacid Salts in Polyamine Polymers and Blends", U. S. Patent 6,099,621 (2000).
4. J. Zou and W. S. W. Ho, "CO_2-Selective Polymeric Membranes Containing Amines in Crosslinked Poly(vinyl alcohol)", J. Membr. Sci., 286, 310-321 (2006).
5. Y.-H. Tee, J. Zou, and W. S. W. Ho, "CO_2-Selective Membranes Containing Dimethylglycine Mobile Carriers and Polyethylenimine Fixed Carrier", J. Chin. Inst. Chem. Engrs., 37 (1), 37-47 (2006).
6. J. Zou, J. Huang, and W. S. W. Ho, "CO_2-Selective Water Gas Shift Membrane Reactor for Fuel Cell Hydrogen Processing", Ind. Eng. Chem. Res., 46 (8), 2272-2279 (2007).
7. J. Huang, J. Zou, and W. S. W. Ho, "Carbon Dioxide Capture Using a CO_2-Selective Facilitated Transport Membrane", Ind. Eng. Chem. Res., 47 (4), 1261-1267 (2008).
8. J. Zou, J. Huang, and W. S. W. Ho, "Facilitated Transport Membranes for Environmental, Energy and Biochemical Applications", in Advanced Membrane Technology and Applications, N. N. Li, A. G. Fane, W. S. W. Ho, and T. Matsuura, eds., John Wiley & Sons, New York, Chap. 28, pp. 721-754 (2008).
9. R. Xing and W. S. W. Ho, "Crosslinked Polyvinylalcohol-Polysiloxane/Fumed Silica Mixed Matrix Membranes Containing Amines for CO_2/H_2 Separation", J. Membr. Sci., 367 (1–2), 91-102 (2011).
10. H. Bai and W. S. W. Ho, "Carbon Dioxide-Selective Membranes for High-Pressure Synthesis Gas Purification", Ind. Eng. Chem. Res., 50 (21), 12152-12161 (2011).
11. K. Ramasubramanian and W. S. W. Ho, "Recent Developments on Membranes for Post-combustion Carbon Capture", Curr. Opinion Chem. Eng., 1 (1), 47-54 (2011).
12. K. Ramasubramanian, H. Verweij, and W. S. W. Ho, "Membrane Processes for Carbon Capture from Coal-Fired Power Plant Flue Gas: A Modeling and Cost Study", J. Membr. Sci., 421-422, 299-310 (2012).
13. H. Bai and W. S. W. Ho, "Carbon Dioxide-Selective Facilitated Transport Membranes for Hydrogen Purification", in Production and Purification of Ultraclean Transportation Fuels, Y. H. Hu, X. L. Ma, E. B. Fox, and X. Guo, eds., ACS Symposium Series, Washington, DC, doi: 10.1021/bk-2011-1088.ch007, Vol. 1088, Chap. 7 (2011).
14. Y. Zhao and W. S. W. Ho, "Steric Hindrance Effect on Amine Demonstrated in Solid Polymer Membranes for CO_2 Transport", J. Membr. Sci., 415-416, 132-138 (2012).
15. Y. Zhao and W. S. W. Ho, "CO_2-Selective Membranes Containing Sterically Hindered Amines for CO_2/H_2 Separation", Ind. Eng. Chem. Res., ACS ASAP doi:10.1021/ie301397, 52, 8774-8782 (2013).
16. K. Ramasubramanian, Y. Zhao, and W. S. W. Ho, "CO_2 Capture and H_2 Purification: Prospects for CO_2-Selective Membrane Processes", AIChE J., doi:10.1002/aic.14078, 59 (4), 1033-1045 (2013).
17. K. Ramasubramanian, M. Song, and W. S. W. Ho, "A Spiral-Wound Water-Gas-Shift Membrane Reactor for Hydrogen Purification", Ind. Eng. Chem. Res., doi:10.1021/ie302424y, 52, 8829-8842 (2013).

18. Y. Zhao, B. T. Jung, L. Ansaloni, and W. S. W. Ho, "Multiwalled Carbon Nanotube Mixed Matrix Membranes Containing Amines for High Pressure CO_2/H_2 Separation", J. Membr. Sci., 459, 233-243 (2014).
19. Z. Tong, V. K. Vakharia, M. Gasda, and W. S. W. Ho, "Water Vapor and CO_2 Transport through Amine-Containing Facilitated Transport Membranes", React. Funct. Polym., 86, 111-116 (2015).
20. V. K. Vakharia, K. Ramasubramanian, and W. S. W. Ho, "An Experimental and Modeling Study of CO_2-Selective Membranes for IGCC Syngas Purification", J. Membr. Sci., 488, 56-66 (2015).
21. L. Ansaloni, Y. Zhao, B. T. Jung, K. Ramasubramanian, M. Giacinti Baschetti, W. S. W. Ho, "Facilitated Transport Membranes Containing Amino-Functionalized Multi-Walled Carbon Nanotubes for High-Pressure CO_2 Separations", J. Membr. Sci., 490, 18-28 (2015).
22. V. K. Vakharia and W. S. W. Ho, "Separation and Purification of Hydrogen Using CO_2-Selective Facilitated Transport Membranes", in "Hydrogen Production from Renewable Resources", Zhen Fang, Richard L. Smith, Jr., and Xinhua Qi, eds., Springer Book Series – Biofuels and Biorefineries, Springer, Dordrecht, Germany, Chap. 12, pp. 315-338 (2015).
23. Y. Chen, L. Zhao, B. Wang, P. Dutta, and W. S. W. Ho, "Amine-containing Polymer/Zeolite Y Composite Membranes for CO_2/N_2 Separation", J. Membr. Sci., 497, 21-28 (2016).
24. B. A., Holmberg, H. Wang, J. M. Norbeck, and Y. Yan, "Controlling Size and Yield of Zeolite Y Nanocrystals Using Tetramethylammonium Bromide", Microporous and Mesoporous Materials, 59, 13-28 (2003).
25. J. C. White, P. K. Dutta, K. Shqau, and H. Verweij, "Synthesis of Ultrathin Zeolite Y Membranes and their Application for Separation of Carbon Dioxide and Nitrogen Gases", Langmuir, 26, 10287-10293 (2010).
26. Hsu, C.; Chiang, A. S. T.; Selvin, R.; Thompson R. W. Rapid Synthesis of MFI Zeolite Nanocrystals. J. Phys. Chem. B 2005, 109, 18804-18814.
27. H. K. Beyer, I. M. Belenykaja, F. Hange. "Preparation of High-Silica Faujasites by Treatment with Silicon Tetrachloride", J. Chem. Soc., Faraday Trans., 81, 2889-2901 (1985).
28. G. T. Kerr, Chemistry of Crystalline Aluminosilicates. V. Preparation of Aluminum-Deficient Faujasites", J. Phys. Chem., 72, 2594-2596 (1968).
29. M. A. Severance, B. Wang, K. Ramasubramanian, L. Zhao, W. S. W. Ho, and P. K. Dutta, "Rapid Crystallization of Faujasitic Zeolites: Mechanism and Application to Zeolite Membrane Growth on Polymer Supports", Langmuir, doi:10.1021/la5004512, 30 (23), 6929-6937 (2014).
30. J. Black, "Cost and Performance Baseline for Fossil Energy Plants", U.S. Department of Energy, DOE/NETL-2010/1397, 2010.
31. W. S. W. Ho and Y. Han, "Methods for the Separation of CO_2 from a Gas Stream", PCT Patent Application No. PCT/US2016/033757 (filed May 23, 2016); U.S. Provisional Patent Application No. 62/168,268 (filed May 25, 2015).
32. J. Black, "Updated Costs (June 2011 Basis) for Selected Bituminous Baseline Cases", U. S. Department of Energy, DOE/NETL-341/082312, 2012.
33. M. Wilf, L. Awerbuch, and C. Bartels, The Guidebook to Membrane Desalination Technology: Reverse Osmosis, Nanofiltration and Hybrid Systems Process, Design, Applications and Economics, Balaban Desalination Publications (2007).
34. R. W. Baker and K. Lokhandwala, "Natural Gas Processing with Membranes: An Overview," Ind. Eng. Chem. Res., 47, 2109-2121 (2008).

35. N. Voutchkov, Desalination Engineering: Planning and Design, McGraw Hill Professional (2012).

9 Acknowledgements

We would like to thank José D. Figueroa for his great inputs and efforts for this project, including coordinating with the National Carbon Capture Center and providing us an opportunity for the field testing of the membrane developed in this project. We would also like to thank Peter Knappe of TriSep Corporation and Dan Duellman, Matt Usher and Indra Bhattacharya of American Electric Power for their helpful discussion and consultation for this project. The smooth membrane testing at NCCC would not be possible without the great efforts of NCCC team members, particularly Tony Wu and Bob Lambrecht. We are grateful for their excellent analytical and mechanical supports including the arrangements of lifting our membrane unit into their analytical lab, setting it up, connecting all tubings and electrical parts outside of our membrane module testing unit, installing air flow to our oven for accurate temperature control, providing an oxygen analyzer to measure the oxygen concentration in the retentate stream, and giving us the concentration data log (including CO_2, O_2, SO_2, NO_2, and NO concentration from the flue gas, and O_2 concentration from the retentate stream). NCCC support and cooperation for our membrane module testing were wonderful and professional, and we truly enjoyed working with the NCCC people.

10 List of Acronyms, Abbreviations and Symbols

$\alpha_{CO2/N2}$:	Membrane selectivity from mixed gas measurement: $\alpha_{CO2/N2} = f_{CO2} / f_{N2}$.
AEP:	American Electric Power.
BP:	Budget Period.
CAS:	The College of Arts and Sciences at OSU.
CBE:	The Department of Chemical and Biomolecular Engineering in CoE.
CHEM:	The Department of Chemistry in CAS.
CoE:	The College of Engineering at OSU.
COE:	Cost of electricity.
DLS:	Dynamic light scattering.
EDS:	Energy-dispersive X-ray spectroscopy.
EDX:	Energy-dispersive X-ray spectroscopy.
f_i:	Permeance of species *i*.
FAU:	Faujasite zeolites.
FCB:	Fischer College of Business.
GPU:	Gas permeation unit for f_i; 1 GPU = 10^{-6} cm^3(STP)/($cm^2 \cdot s \cdot cmHg$).
GT:	Gradient Technology.
IIP:	Industrial Innovation and Partnerships, National Science Foundation.
Lab scale membrane:	Flat sheet membrane fabricated in the lab by hand.
MSE:	The Department of Materials Science and Engineering at CoE, OSU.
MWCO:	Molecular weight cut-off.
NCCC:	National Carbon Capture Center.
NSF:	National Science Foundation.
ODOD:	The Ohio Department of Development.
ONR:	The Office of Naval Research.
OSU:	The Ohio State University in Columbus, Ohio.
p:	Pressure.
PEO:	Polyethyleneoxide.
PES:	Polyethersulfone.
PSF:	Polysulfone.
Q:	Quarter.

Scale-up membrane: Flat sheet membrane fabricated using the roll-to-roll continuous machine.

SEM: Scanning electron microscopy.

Si/Al: Silicone/aluminum ratio.

Si-1: Silicalite-1.

Spiral-wound module: Membrane module (or element) fabricated in the spiral-wound configuration using the scale-up membranes.

TEM: Transmission electron microscopy.

T_{set}: Temperature set point.

USY: Ultra stable zeolite Y.

X: Membrane thickness.

XRD: X-ray diffraction.

ZY: Zeolite-Y.

11 Suppliers

1. Sigma-Aldrich, 3050 Spruce Street, St. Louis, MO, 63103, USA; www.sigmaaldrich.com.
2. Varian Inc., 3120 Hansen Way, Palo Alto, CA 94304-1030, USA.
3. ThermoFisher Scientific. 25 Nimble Hill Rd., Newington, NH, USA. Contact: Greg Vinson, Ph: (800)258-0830, Office: (281)334-0164, Mobile: (281)851-0640.
4. Alfa Aesar, 26 Parkridge Road, Ward Hill, MA 01835, USA; Phone: 1-978-521-6300; Fax: 1-978-521-6350; www.alfa.com.
5. McMaster Carr, P.O. Box 94930, Cleveland, OH 44101-4930, USA; Phone: 330-995-5500; Fax: 330-995-9600.
6. Millipore Corporation, 290 Concord Road, Billerica, MA 01821, USA; Phone: 1-800-MILLIPORE (1-800-645-5476) or 978-715-4321.
7. Pall Corporation, 25 Harbor Park Drive, Port Washington, NY 11050, USA; Phone: (516) 484-5400.
8. TriSep Corporation, 93 South La Patera Lane, Goleta, CA 93117, USA; Phone: 805-964-8003; Fax: 805-964-1235.
9. NL Chemical Technology, Inc., 479 Business Center Drive, Suite 100, Mount Prospect, IL 60056, USA; Phone: 847-824-2888; Fax: 847-824-2898.
10. Arkema Inc., 900 First Avenue, King of Prussia, PA 19406, USA; Phone: 610-205-7252.
11. The Ohio State University Department of Chemistry Machine Shop, 0041 Evans Laboratory, 88 W 18th Avenue, Columbus, OH 43210, USA.
12. Branson Ultrasonics Corporation, 41 Eagle Rd., Danbury, CT 06813-1961, USA.
13. THINKY USA, Inc., 23151 Verdugo Drive, Suite 107, Laguna Hills, CA 92653, USA.
14. Inabata America Corporation, 611 Anton Blvd., Suite 925, Costa Mesa, CA 92626, USA.
15. R. T. Vanderbilt Company, Inc., 30 Winfield Street, Norwalk, CT 06856, USA.
16. Spectrum Laboratories, Inc., 18617 S Broadwick Street, Rancho Dominguez, CA 90220, USA.
17. Sekisui Specialty Chemicals America, LLC, 1603 West LBJ Freeway, Suite 200, Dallas, TX 75234, USA.
18. Pervatech Sales, Rondweg 48, 7468 MC Enter, The Netherlands.
19. Sumitomo Chemical Corp. http://www.sumitomo-chem.co.jp/english/.

20. Sekisui Specialty Chemicals America, LLC, 1603 West LBJ Freeway, Suite 200, Dallas, TX 75234, USA; Phone: (972) 277-2900; Fax: (972) 277-2907. (Distributed by: Brenntag Northeast Inc. Contact: Brian M. Bartashus, 81 W. Huller Lane, Reading PA 19605, USA; Phone: 610-926-4151 x3368).
21. Modular Process Technology Corporation, 2233 Paragon Drive, San Jose, CA 95131, USA; Phone: (408) 325-8640; Fax: (408) 3258649; Website: http://www.modularpro.com/.
22. Ellipsometer, J.A. Woollam Corporation, Inc., 645 M Street, Suite 102, Lincoln, NE 68508, USA; Phone: (402) 477-7501; Fax: (402) 477-8214; Website: www.jawollam.com.
23. BASF Corporation, 1609 Biddle Avenue, Wyandotte, MI 48192, USA; Phone: 734 324-6100; Website: http://www.basf.com.

12 Distribution List

José D. Figueroa, MBA, PMP
Sr. Project Manager/
Carbon Capture Coordinator
US Department of Energy
National Energy Technology Laboratory
626 Cochran Mill Road
Pittsburgh, PA 15236-0940

Prabir K. Dutta
Subhrakanti Chakraborty
Chenhu Sun
Bo Wang
The Ohio State University
Department of Chemistry
140 W 18th Ave, McPherson Chemical Lab 3051
Columbus OH 43210-1106

W.S. Winston Ho
Kai Chen
Yang Han
Witopo Salim
Zi Tong
Varun Vakharia
Dongzhu Wu
The Ohio State University
William G. Lowrie Department of Chemical and Biomolecular Engineering
Department of Materials Science and Engineering
2041 College Road, Watts Hall 291
Columbus OH 43210-1178

Jacqueline R. Hitchingham, Chemical Engineer
Steve J. Schmit, Director of Research and Development
Gradient Technology
11080 Industrial Circle NW
Elk River, MN 55330